Iyer, Subramanian Srikanteswara

DOPANT INCORPORATION IN SILICON MOLECULAR BEAM EPITAXY

University of California, Los Angeles PH.D. 1981

UNIVERSITY OF CALIFORNIA

Los Angeles

Dopant Incorporation in Silicon Molecular Beam Epitaxy

A dissertation submitted in partial satisfaction of the requirements for the degree Doctor of Philosophy in Engineering

by

Subramanian Srikanteswara Iyer

1981

The dissertation of Subramanian Srikanteswara Iyer is approved.

Paul Chaiken

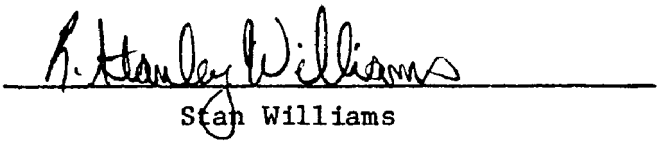

Stan Williams

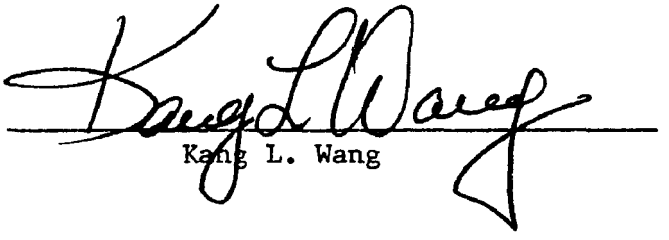

Kang L. Wang

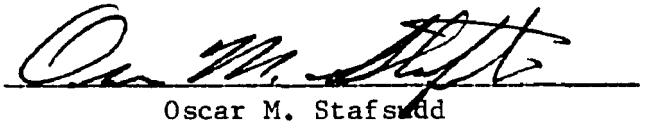

Oscar M. Stafsudd

Frederick G. Allen, Chair

University of California, Los Angeles

1981

DEDICATION

To my parents.

TABLE OF CONTENTS

TABLE OF SYMBOLS USED

A_h	area of base of hemispherical gallium island (cm^2)
A_s	surface species of single dopant atom
A_{2_g}	vapor species of dimer of dopant species
A_{2_s}	surface species of dimer of dopant species
A_{4_g}	vapor species of tetramer of dopant species
c	dummy constant of integration in Equation 2.22
$D_{Ga\|si}$	diffusivity of gallium on a silicon surface (cm^2/sec)
$\left.\frac{dN_{DS}}{dt}\right\|_{inc}$	incorporation rate (atoms/cm^2-sec)
E_{ADS}	activation energy for adsorbtion (eV)
$E_{chemisorption}$	potential well depth for chemisorbed state (eV)
E_D	activation energy for first order desorption (eV)
E_{Dc}	covalent component of desorption energy (eV)
E_{Di}	ionic component of desorption energy (eV)
$E_{diff\ Ga\|Si}$	activation energy for surface migration of gallium on a silicon surface (eV)
E_{Dp}	activation energy for pth order desorption (eV)
E_I	activation energy for incorporation (eV)
E_{Iq}	activation energy for qth order incorporation (eV)
$E_{Physiadsorbed}$	potential well depth for physiadsorbed state (eV)
E_s	sticking coefficient exponential energy factor (eV)
E_{sub_a}	elemental sublimation energy for adsorbate (eV)
E_{sub_s}	elemental sublimation energy for substrate (eV)
F	fraction of electronic charge transferred between adsorbed atom and surface

F	function defined by $$F(\psi,\frac{n_{p0}}{p_{p0}}) = [(e^{-\frac{q\psi}{kT}} + \frac{q\psi}{kT} - 1) + \frac{n_{p0}}{p_{p0}}(e^{-\frac{q\psi}{kT}} - \frac{q\psi}{kT} - 1)]^{\frac{1}{2}}$$
F_D	incident dopant flux (atoms/cm^2-sec)
F_{Di}	design parameter, steady state flux needed to grow ith segment (atoms/cm-sec)
F_{Dmax}	maximum allowable flux for linear regime (atoms/cm-sec)
F_{DS}	dopant flux at which saturation of incorporation begins (atoms/cm^2-sec)
F_{reqd}	design parameter, flux needed for given doping level (atoms/cm^2-sec)
F_{Si}	incident silicon flux (atoms/cm^2-sec)
$G(\theta)$	shape factor used in determining work function
h	Planck's constant (eV-sec)
k	Boltzman constant (eV/'K)
K_D	desorption rate constant
K_{D0}	preexponent for first order desorption (sec)
K_{D0p}	preexponent for pth order desorption ($cm^{2(p-1)}$/sec)
K_{Dp}	desorption constant for pth order desorption ($cm^{2(p-1)}$/sec)
K_I	first order incorporation constant (sec^{-1})
K_I^*	incorporation coefficient for gallium when gallium activity is different from its concentration (sec^{-1})
K_{I0}	preexponent for first order incorporation (sec^{-1})
K_{I0q}	preexponent for qth order incorporation ($cm^{2(q-1)}$/sec)
K_{Iq}	incorporation coefficient for qth order incorporation ($cm^{2(q-1)}$/sec)
ℓ	design parameter, $$\ell = \frac{\text{desired doping}}{\text{maximum allowable doping for linear regime}}$$
L_D	Debye length (cm)

L_{D0}	Debye length at x = 0 (cm)
N	bulk doping (cm^{-3})
N_{DB}	bulk doping (cm^{-3})
N_{DS}	number of adsorbed dopant atoms on silicon surface ($/cm^2$)
N''_{DS}	number of atoms in each hemispherical gallium island
N_{Dsi}	design parameter, required steady state adatom concentration for ith level of doping ($atoms/cm^2$)
$N_{DS_{ss}}$	design parameter, required steady state adatom concentration to achieve required doping level ($atoms/cm^2$)
n_i	intrinsic carrier concentration (cm^{-3})
N_{inc}	number of atoms incorporated on the surface ($atoms/cm^2$)
N_o	atom density of silicon ($atoms/cm^3$)
N_O	bulk doping at x = 0 ($atoms/cm^3$)
n_{p0}	electron concentration in equilibrium in p layer (cm^{-3})
N_{SS}	uniform surface state density in midgap region (states/eV-cm^2)
p	desorption order
P_h	perimeter of base of hemispherical gallium island (cm)
p_{p0}	hole concentration in equilibrium in p layer (cm^{-3})
q	order of incorporation
q	electronic charge (coul)
q_a	valence charge shared for adsorbate (electrons)
q_s	valence charge shared for substrate (electrons)
r	distance of atom from surface (cm)
$R\cos\beta$	effective surface double layer thickness (Å)
r_o	radius of hemispherical gallium island (cm)
s	sticking coefficient, ratio of atoms incorporated to those incident, in steady state.
S_o	preexponent for sticking coefficient

$S\|_a$	sticking coefficient in saturation for a real incorporation.
$S\|_p$	sticking coefficient in saturation for perimetric incorporation
T	temperature of surface (°K)
T_a	temperature of impinging atom (°K)
T_d	temperature of desorbing atom (°K)
T_s	substrate temperature (°K)
U	potential energy of atom due to surface (eV)
v	rate of silicon growth (cm/sec)
$v_{d_{avg}}$	approximate mean velocity of a gallium atom on a silicon surface due to diffusion (cm/sec)
V_f	ionization potential of adsorbate (eV)
V_{hemi}	volume occupied by each hemispherical island (cm^3)
V_i	ionization potential (eV)
$(V/I)_n$	four point probe reading at the nth stage of anodic etching (ohms)
x	thickness of film grown (cm)
x_d	approximate distance moved by a gallium atom on a silicon surface in one residence time(cm)
α	number of hemispherical gallium islands per square cm.
α	electronic polarizability (A^3)
α	accomodation coefficient
β	volume occupied by each gallium atom (cm)
β	defined by $\beta = 2\pi \|\Gamma$
Γ	period of cosine profile (cm)
γ	ratio of peak doping to average doping in a cosine profile
δ	defined as $\delta = (\frac{q^2}{r_0} - V_f)\|\phi_e$

ΔS_a	entropy contribution of adsorbtion process (eV/ K)
Δt	thickness of layer removed by anodic etching (cm)
ϵ	dielectric constant (farads/cm)
θ	coverage of surface by adatoms
λ	equilibration distance (cm)
σ_n	conductivity of nth layer removed by anodic etching (mho/cm)
τ_i	design parameter, equilibration time at temperature at which ith segment is grown (sec)
τ_D	residence time of dopant atom on silicon surface (sec)
τ	equilibration time (sec)
ϕ_e	electronic work function of composite surface (V)
ψ	potential in semiconductor, referred to bulk value (V)
ψ_o	potential at interface at which step change in doping occurs (V)
ψ_s	potential at surface (V)

LIST OF FIGURES

ACKNOWLEDGEMENTS

This thesis is the result of work done over an extended period of time and was possible only because of the cooperation of several people and instructors. It is a pleasure for me to acknowledge their help.

I would, at the outset, like to express my sincere gratitude to my advisor Professor Frederick G. Allen for introducing me to a new and exciting field and actively guiding me throughout. His help has been crucial in the development of this work. I am also grateful to my colleague Bob Metzger for his close association, support and cheer during this project.

My examination committee, Professor O. M. Stafsudd, Professor K. L. Wang, Professor R. S. Williams and Professor P. Chaiken have been especially helpful. I thank them for their interest, encouragement and their useful suggestions. In addition I wish to thank Professor C. R. Viswanathan and Professor D. S. Pan for their help and encouragement. I also thank Moshe Sergeant for his assistance.

Financial support for this project was made available by the National Science Foundation, the University of California, Los Angeles and in part by Hughes Electron Dynamics Division and TRW. I am grateful for this help.

Finally, I would like to thank Dwight Streit for helping me polish up this work and Phyllis Parris for typing the manuscript so carefully.

VITA

July 10, 1954 -- Born, Madras, India

1977 - B. Tech. Indian Institute of Technology, Bombay

1978 - M.S. University of California, Los Angeles

PUBLICATIONS

1) "Sharp Doping Profiles with High Doping Levels in Silicon Molecular Beam Epitaxy", (Co-authors R.A. Metzger and F. G. Allen) to be published in the Journal of Applied Physics.

2) "Dopant Incorporation Studies in Silicon Molecular Beam Epitaxy (Si MBE)" (Co-authors F. G. Allen and R. A. Metzger) to be published in Applications of Surface Science.

3) "Dopant Concentration in Silicon Molecular Beam Epitaxy" , paper presented at 1981 (Third) Workshop on Molecular Beam Epitaxy at the University of California, Santa Barbara (Co-authors R. A. Metzger and F. G. Allen).

ABSTRACT OF THE DISSERTATION

Dopant Incorporation in Silicon
Molecular Beam Epitaxy

by

Subramanian Srikanteswara Iyer

Doctor of Philosophy in Electrical Engineering
University of California, Los Angeles, 1981
Professor Frederick G. Allen, Chair

Silicon Molecular Beam Epitaxy (Si MBE) is a process by which extremely thin films may be grown with the simultaneous incorporation of dopants. In addition growth is conducted at relatively low temperatures and in an ultra high vacuum environment. As a result, good quality films with excellent doping control are possible. It is shown however that long delay times are characterestic of the dopant incorporation process. Further,sticking coefficients for most dopants at useful MBE growth temperatures are quite low.

This dissertation is concerned with the dopant incorporation kinetics in Si MBE. A model is proposed by which incorporation proceeds

from a surface accumulation of dopant atoms. This accumulation arises due to the incident dopant flux, the desorption rate of the adsorbed dopant atoms after a certain dwell time and the incorporation rate. The delay time is related to the time the surface accumulation takes to reach steady state. Desorption and incorporation are assumed to be activated processes. The sticking coefficient is shown to be exponential with respect to inverse temperature with an energy coefficient given by the difference of the activation energies for desorption and incorporation. This was measured to be ~1.6 eV for gallium.

Using isothermal desorption with Auger analysis, desorption of gallium from silicon was found to proceed with an activation energy of~2.9 eV. It is also shown that incorporation proceeds with an activation energy of~1.3 eV.

Although time delays are shown to be appreciable, techniques whereby the concentration of surface dopant is controlled rather than the incident flux may be used to obtain hyper sharp profiles. Such techniques called "pre-build up" and "flash off" have been developed. They have been used to produce doping profiles whereby changes of dopant over four orders of magnitude are possible in about 200 - 300 $\mathring{A}$. Several profiles that may be used in microwave devices, quantum well structures and other novel devices are shown.

CHAPTER I

Introduction

1.1 Description of the Silicon Molecular Beam Epitaxy Process

Molecular Beam Epitaxy (MBE) is a term used to describe the synthesis of crystalline layers of material by co-depositing the elemental constituents of these layers with the help of molecular beams in an ultra high vacuum environment. The growth mode is a layer by layer mechanism and since the molecular beams can be changed in intensity, very abruptly, the elemental constitution of the layers can be controllably changed with almost monolayer resolution.

Under correct conditions of growth, this technique of crystalline film synthesis is known to produce films of excellent structural and electrical quality. The constitutional changes possible over extremely small distances has been used in the synthesis of various semiconducting compound structures. Compound synthesis and the growth of heterostructures has been discussed in great detail in the literature. The reader is referred to a review by Cho [1] and the bibliography therein.

The molecular beam technique can also be used to grow elemental semiconductor films. Figure 1.1 shows a schematic of the process. The doping concentration of these films may be altered by varying the dopant flux. This in principle can lead to very sharp doping profiles. Further, the process is conducted at relatively low temperatures such that auto-diffusional smearing of intended profiles is negligible

This thesis concerns the use of MBE to generate an arbitrary

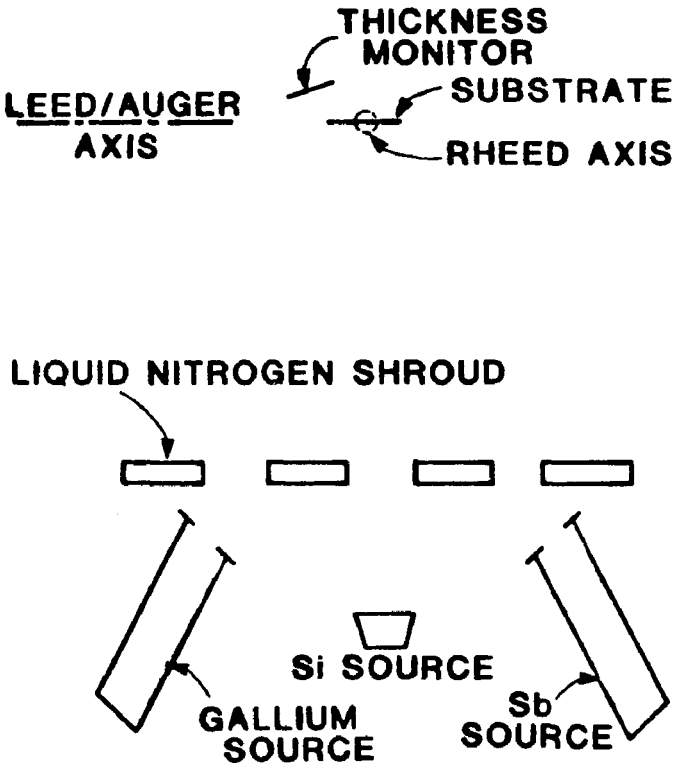

Figure 1.1 Schematic of the silicon MBE process

doping profile in silicon.

1.2 Historical Perspective

Epitaxial growth of silicon means the ordered arrangement of silicon atoms layer by layer such that a single crystal film results. Single crystal films with low defect counts are useful in device fabrication; techniques involving the chemical vapor deposition of epitaxial silicon on silicon substrates have been well developed. However, this is a high temperature process and the need was felt to develop an alternative technique for the epitaxial growth of silicon films at lower temperatures.

One simple way is the vacuum evaporation of silicon onto a moderately heated silicon substrate such that epitaxial growth results.[2 19] The important criteria for epitaxy are: that the incident atoms be sufficiently mobile on the host surface to arrange themselves in single crystal fashion, and that there be few impurities that cause these atoms to be displaced from the epitaxial positions, a condition that influences the crystal quality.

Two principal techniques have been employed to evaporate silicon:

(a) Kilgore and Roberts [88] used flash evaporation from a resistively heated silicon filament.

(b) Most workers used evaporation from a crucible via electron bombardment. This technique is almost exclusively used now.

In efforts made in the sixties, growth was usually performed in pyrex vacuum chambers that were diffusion pumped. The operating pressures were of the order of 10^{-3} to 10^{-4} pascals, (1 pascal = 1

Newton/m^2 ≈ 0.0075 torr). At these pressures, contamination of grown films is a major problem. A monolayer of ambient gas, predominantly oxygen, would be incident on the sample every few seconds. If only a small fraction incorporated, it could lead to formation of crystal faults.

Queisser et al [21] and Unvala et al [5] determined the effect of oxygen on the number of stacking faults. In order to reduce the oxygen content of the films, the growth rate was increased. However, there is a limit as to how high the growth rate may be increased. Sufficient time needs to be given so that atoms can find their epitaxial positions before they are buried by the next incident layer. The growth rates employed in these studies were typically a micron a minute. The mobility of the atoms is related to the surface temperature.

At higher temperatures, higher growth rates may be established while at the same time reducing the sticking of impurities. Booker, et al [10] found that at a 10^{-3} pascal background pressure, the best films were obtained by growing at 1200° C at a growth rate of 1.5 μ/min. It must be noted however, that no doping control is achievable at these temperatures.

With the advent in the early seventies of ultra high vacuum systems, it was possible to reduce the background pressure considerably. As a result, growth rates and temperatures could also be reduced, leading to greater control of the composition of grown films without compromising film quality. Much work has been done on studying the film quality.

It has been shown [26] that proper substrate preparation is important for the growth of good films. Sakamoto et.al [89] have

studied the electrical and crystalline quality of film grown by ionized-cluster-beams of silicon. Sugiura and Yamagachi [98] show that under UHV conditions, unevaporated SiO_2 is a major source of defects and defect formation is an activated process, though ion doping might reduce the stacking fault density due to charge exchange of the dopant ion with silicon, the silicon ion being more mobile than the silicon atom. Such arguments were also used by Itoh et.al. [99]. While we shall discuss the growth mechanism of silicon in chapter two, the various doping techniques employed will be discussed here.

Most of the early workers accomplished doping of the films by using doped silicon sources [19,92]. Bennet and Parrish [92,93] proposed a model to explain how the concentration of dopant in the film varied with the source concentration, growth rate, and substrate temperatures. The doping level could be expressed in terms of partition and sticking coefficients and individual vapor pressures. Kuznetsov et al[95] showed that a low growth temperature (< 500°C) complete transfer of some dopants from the source was possible. More recently, Kuznetsov et al [94] found anomalous doping of their films using this technique due to the presence of defect centers in the incipient stages of epitaxy.

Tolomasov et al[96] used a separate antimony evaporation source to dope their silicon films. They also obtain the Sb sticking coefficient as a function of Sb flux and substrate temperature. Most of this work was done at relatively high pressures, and no attempt was made to intentionally obtain a definite doping profile.

However, Becker and Bean [26] and Bean[27] used varying doping

fluxes to obtain doping profiles. Later Ota [97] used varying substrate temperatures with fixed and varying dopant flux to change the doping level. These probably represent the first systematic efforts to obtain doping profiles of an abrupt nature, utilizing the compositional variation capabilities afforded by MBE.

Other workers have also looked into doped MBE films. König et.al. [80,100] have examined the electrical quality of Si films at different levels of antimony doping. They conclude that electrical quality deteriorates at high Sb flux values.

1.3 Motivation of This Work

As can be seen from the above, the use of silicon molecular beams to grow epitaxial silicon with doping schemes that employ doped silicon sources and separate controllable dopant sources has been demonstrated. In order to be competitive with the existing CVD method of growing epitaxial silicon, silicon MBE must offer marked advantages. Silicon technology is the most mature of all the semiconductor techniques; defect densities of less than 200/cm^2 are routinely possible for device fabrication. However , doping changes are not abrupt enough for many applications. Hence in order to compete, silicon MBE must be able to produce device quality silicon. This means that defect free layers with high "bulk-like" mobilities and long lifetimes,need to be grown and that extreme control of doping profiles, as distinct from uniform doping levels, must be made possible.

Considerable effort has been put into the study of the structure and electrical properties at silicon grown by MBE. These studies have established certain general conditions under which high quality silicon may be grown. In particular, substrate preparation and vacuum level

used have played an important part. In fact, devices have been[24,101] made using these uniformly doped films that have been shown to have comparable if not superior performance characteristics.

However, at the time of this writing, there seems to be no report of a novel device made completely by the MBE process though Goodwin et al[102] have used an MBE grown profile in their microwave diodes. Most devices reported employ MBE grown uniformly doped films and then use conventional processing techniques such as diffusion and ion implantation to fabricate the device.

There are two aspects to the problem of device fabrication. One is the use of MBE as a technique to make films which may be used as starting material for devices used in IC manufacture. It has certainly been demonstrated that this is in fact possible. The other aspect of the use of MBE is in the fabrication of discrete devices, such as microwave devices. These devices would require several layers of doped semiconductor with critical requirements on the transitions between layers often less than 100 A°. It is here that MBE will make an impact because of its unique capability of making these transitions.

In this work, we investigate this second aspect of MBE. We need to review the status of MBE at this point in the area of profile generation. Bean and Becker,[26,27] in a pioneering and to our knowledge, only effort other than ours, investigated the growth of doping profiles. They found that at growth temperatures around 650-700°C, the gallium doping profile followed the flux pulse reasonably closely. The antimony and aluminum profiles did not behave as well, but they seemed to improve somewhat at higher growth temperatures. This lead Bean to

conclude that gallium was "well behaved" and antimony and aluminum operated differently in two regions, which he called the surface segregation region and the diffusion limited region. He postulated that at low temperatures Sb and Al segregated on the surface and stayed there even after the beam was turned off. As a result of this surface scource, doping would continue where not intended. At higher temperatures Bean concluded that the dopant did not segregate and the profile was diffusion limited. As a result of these studies, further work on profile control slowed down and workers began to consider investigation of other methods of doping.

This work arose out of desire to make an abrupt p-n junction. However, initial attempts and previous work indicated that unless further studies were made on the incorporation of the dopants in the growing silicon lattice, this would be difficult to achieve. It was therefore decided to develop a theory of incorporation that could be universally applicable. We believed that since previous workers indicated that gallium was "well behaved" we should first apply our model to gallium. This model is discussed in chapter two, and experiments on its verification are discussed in later chapters.

The objective of this study on gallium was two-fold. One was to see if gallium was in fact a well behaved dopant or, what we suspected, well behaved only in a certain range of temperatures and fluxes. If the latter was true then perhaps other dopants might also be "well behaved" in other temperature and flux regimes.

The second objective was to develop (on the basis of our model) a set of design strategies whereby an arbitrary doping profile could be

generated. Compatibility of these strategies with computer control of the growth parameters at a future date was also desired.

1.4 Contribution of This Work

This thesis addresses itself mainly to the problem of dopant incorporation kinetics. We postulate in chapter two, on the basis of our experimental observations, that the actual incorporation proceeds from a reservoir of dopant that exists as a surface species at a certain rate. Also we derive that this reservoir arises mainly as a result of incident flux and the desorbing flux. In order to verify this model, we obtain experimentally the desorption and incorporation coefficents, including the activation energies for these processes. We also show that there is an inherent time delay in the doping process, and how this delay may be overcome. Finally, a set of design guidelines are set which should govern the choice of growth parameters. We have used these guidlines to grow structures where the profiles are extremely abrupt and can not be achieved in any other way.

CHAPTER 2

Model For Dopant Incorporation

2.1. Introduction

We present in this chapter the details of the kinetics of dopant incorporation in silicon MBE. A brief overview of the mechanism of silicon growth is given. It must be made clear that under certain growth conditions the silicon growth process may be very complex. The kinetic model which will be presented hereafter does not depend on the silicon growth mechanism, though the values of the parameters of the model may reflect the growth mode. The kinetic model we present here will attempt to explain the different effects seen in silicon MBE. Finally some design equations will be developed. Their full impact will be considered later.

2.2. Models for Silicon Growth

Burton, Frank and Cabrera[28] have analyzed the growth of crystals from their vapours and proposed that in the case of atomically clean surfaces, growth occurs via the propagation of steps along the host surface. The source of the steps may be already existing ledges on the more open high indexed surfaces, dislocations or nucleation of terraced structures which grow by step propagation.

The above theory has been verified by Abbink et al[29], at least in the initial stages for atomically clean silicon. However the smallest trace of impurities like oxygen or carbon can cause pinning of steps and ultimately complete arresting of step propagation. Alternatively

the growth might proceed via three dimensional islands. This has been seen by several authors[3,5,7,12]. Cullis and Booker[18] have shown that in UHV deposition of silicon, atom migration to steps and subsequent propagation of steps until a pinning particle(such as SiC) is encountered is the process of homo-epitaxy.

Initially when there are many such pinning sites the steps are curved, although as cleaner and cleaner surfaces are generated the steps get straighter. Regarding the direction of step propagation Cullis et al found there was really no preferred direction on (110) surfaces though Abbink et al imply that steps seem to propagate in the $\langle\bar{1}\bar{1}2\rangle$ direction on surfaces close to (111). Some impurities, such as SiC, influence the growth mechanism. Nevertheless Becker and Bean[26] and our own work here show that smoother surface texture develops after MBE film growth. This leads us to believe that the growth does in fact proceed via step propagation. As we shall show during the course of this work the growth takes place in the presence of a layer of adsorbed dopant impurities. Evidently this layer presents no barrier to the migration of incident silicon atoms to kink sites on steps, and may in fact aid surface transport of silicon in some cases [53]. Several authors have discussed the influence of impurities on surface structures[19] and growth mechanisms[30].

Jona[8] has discussed the temperature considerations for homo-epitaxial growth of silicon by vacuum deposition. The epitaxial growth can occur only if the incident atoms have sufficient surface mobility to migrate to a step. Steps are in most cases sufficiently

slow moving to be considered stationary. It takes about 10^{-7} sec for an impinging atom to diffuse to a step. Step motion depends on the growth rate and is typically several orders of magnitude slower. Surface mobility of atoms becomes appreciable at about one third of the melting temperature. The background pressure during deposition also plays a part in determining the lowest temperature at which epitaxy will occur. Jona describes several phases of the surface structure and concludes that on Si(111) surfaces, epitaxial growth may be achieved at 420°C with growth rates less than 1 monolayer per minute. At these low temperatures epitaxial growth arises from recrystallization of an amorphous layer through an intermediate phase. Jona[73] also concludes that (100) surfaces are more conducive to epitaxial growth than (111) surfaces. This is because the activation energy for recrystallization on a (111) silicon surface is about 2.6 eV while that for a (100) surface it is only about 1.4 eV. This energy difference is due to the surface structure of the two orientations.

2.3. The Adsorbtion-Desorption Incorporation Model

2.3.1. Introduction

We have seen in the above section that the actual mechanism of silicon growth can be quite complicated. However, no matter how complex this is, we may still describe the dopant incorporation mechanism by a model whose parameters do not depend on the microscopic details of the silicon growth. It can be shown that the model used by Wood and Joyce[31] is a special case of the one we have proposed here.

Most dopant/silicon systems exhibit markedly low sticking coeffic-

ients. Our model explains why only a small fraction of incident dopant is incorporated, and why, at most used temperatures, the desorbed flux is substantial.

Further observable delays in incorporation, as evidenced by excessively smeared out profiles, are also explained by our model.

2.3.2. The Model

We consider a silicon host surface, as shown in Figure 2.1, held at a temperature T_s. T_s is greater than the epitaxial temperature, the temperature above which epitaxial growth occurs.

Incident on this surface is a silicon beam of flux F_{Si}. Coincident on this surface is a dopant beam of flux F_D. Since the residence time for silicon atoms on silicon, even at 850°C, is much greater than the time required to incorporate ($\sim 10^{-3}$ and $\sim 10^{-7}$ sec, respectively)[29] every Si atom is incorporated into the growing lattice and contributes to film growth. It is therefore unnecessary to consider the kinetics of silicon incorporation.

The dopant flux is initially entrapped on the surface. (See figure 2.2). This initial entrapment is a result of the potential well created by the host surface. The dopant atoms are completely accommodated thermally; the reason for this is the low difference in energies between the incident atoms and those on the surface. Experimental evidence[32] for indium on Si suggests that this assumption is correct. It is probably true for most of the cases being considered here. The assumption of initial entrapment is also substantiated since the desorbed beam is known to be lambertian. This means that it reached

THE MODEL:

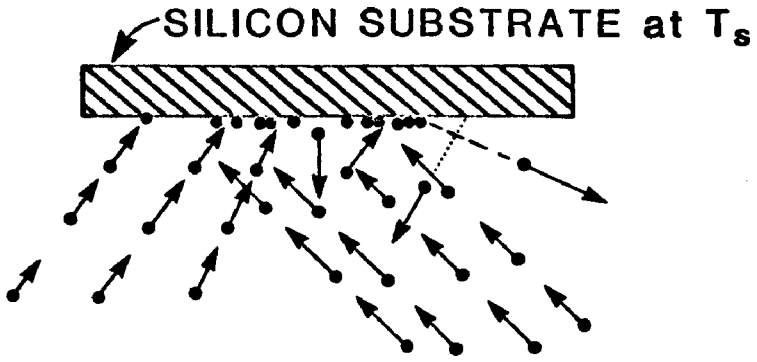

- INCIDENT Si BEAM: FLUX F_{Si}
- INCIDENT DOPANT BEAM: FLUX F_D
- ADSORBED SURFACE DOPANT SPECIES: CONC. N_{DS}
- DESORBED DOPANT ATOMS: RATE $K_D N_{DS}^p$
- INCORPORATED DOPANT ATOMS: RATE $K_I N_{DS}^q$

$$dN_{DS}/dt = F_D - K_D N_{DS}^p - K_I N_{DS}^q$$

Figure 2.1 Schematic of the incorporation model proposed

equilibrium with the surface and was reemittedtherefrom rather than being specularly reflected.

The adsorbed atoms continue to oscillate while in the potential wells at the host surface. This is the chemisorbed state in Figure 2.2. As will be shown in Chapter 4, the physiadsorbed state is usually not important for our analysis. Also in most cases E_{ADS}, the activation energy for adsorbtion,is negligible. They are incident with thermal energy (typically a tenth of an eV or less) and dissipate this energy by launching optical phonons on the surface. It is also possible for the atoms to obtain energy by this process and jump out of the well or desorb. This is a statistical process and may be described by a desorption coefficient K_D and the desorption order p. The desorption order is the order of the rate limiting reaction involved in the various steps in the desorption process. The total desorption rate depends onthe substrate temperature and the concentration of adatoms. The adatoms may also incorporate into the growing lattice at an incorporation rate to be described below. Thus atoms enter the surface phase by the incident flux and they leave either by desorption or by incorporation. Each of these is described in detail below. At any time t, the number of adatoms is given by $N_{DS}(t)$ adatoms/cm^2.

2.3.3. Desorption

The desorption rate may be described by

$$\frac{dN_{DS}(t)}{dt} = - K_D(N_{DS}(t))^p \qquad (2.1)$$

Here K_D is the desorption coefficient and p is the order of desorp-

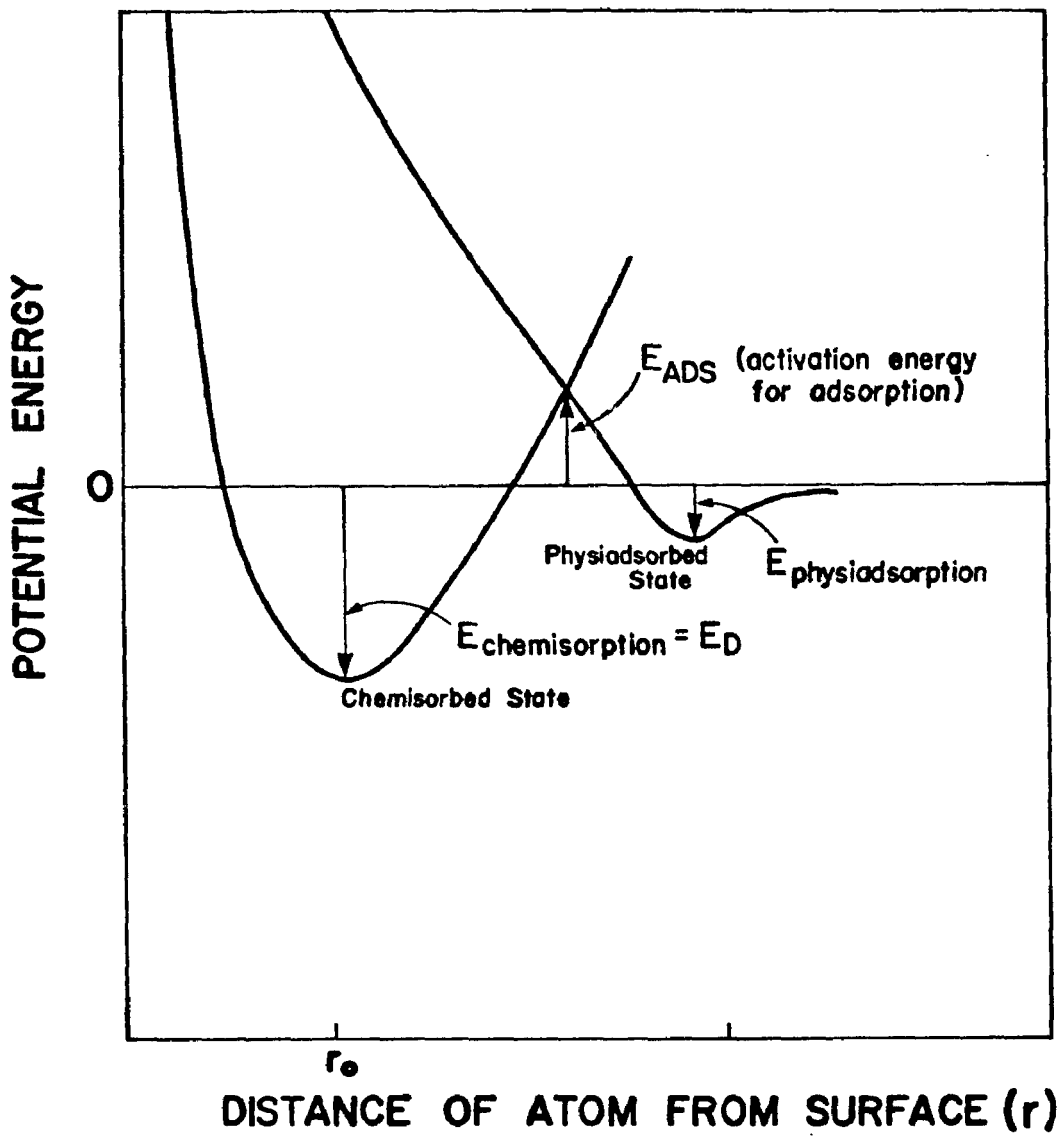

Fig. 2.2 Potential energy of incident dopant atom near surface

tion. That means if they desorb singly $p = 1$ while if they desorb in pairs $p = 2$.

While more details of the desorption studies are reserved for Chapter 4, we shall elaborate on the order of desorption p here. If the desorbing species is a monomer, then $p = 1$. If it is a dimer p is probably 2, as it is expected to be the forward rate order for the following reaction

$$A_s + A_s \rightarrow A_{2_g} \qquad (a)$$

where A_s is a surface species and A_{2_g} a gas species. On the other hand a case where desorption of more than two particles occurs, for example A_4, might proceed by two steps

$$A_s + A_s \leftrightarrows A_{2_s} \qquad (b)$$

and

$$A_{2_s} + A_{2_s} \rightarrow A_{4_g} \qquad (c)$$

with the second one probably being the rate limiting one. In that case the concentration of A_{2_s} is proportional to A_s itself, that is reaction (b) proceeds very fast. Then we may write the order of (b) and (c) combined as second order. If on the other hand there is a competing reaction such as (a), or if reaction (b) proceeds at comparable rate to (c), such that the concentration of $[A_{2_s}]$ is proportional to $[A_2]$, the overall reaction would be close to fourth order.

The absolute desorption rate will thus always increase with N_{DS}. With increasing p, this increase becomes greater. This is be-

cause the probability of desorption increases as a pth power of the surface concentration.

In order to describe the desorption process we must first specify K_D and p. K_D itself may be a function of N_{DS}. It is also a sensitive function of temperature. Frenkel[33] has shown that K_D may be expressed as

$$K_D = K_{DO}\exp(-\frac{E_D}{kT}) \qquad (2.2)$$

This activated curve has a pre-exponent K_{DO} which is related to the vibrational frequency of the atom. The activation energy itself is related to the depth of the potential well the atom oscillates in. The details of determining E_D will be dealt with in a later chapter.

It is possible that the desorption of several orders proceed simultaneously in which case Equation (1) may be rewritten as

$$\frac{dN_{DS}}{dt} = -\sum_p K_{Dp}(N_{DS}(t))^p \qquad (2.1a)$$

where

$$K_{Dp} = K_{DOp}\exp(-\frac{E_{Dp}}{kT}) \qquad (2.2a)$$

Invariably however one process with a single value of p will dominate.

2.3.4. Incorporation

The fact that an adsorbed atom does not promptly incorporate shows that there is a finite rate of incorporation. The actual process of incorporation probably involves a few steps, each being an activated process. Our model presumes that one of these steps is rate determining

and thus the process of incorporation is describable as a process with a single activation energy. We may describe the process by an incorporation coefficient K_I given by

$$K_I = K_{IO}\exp(-\frac{E_I}{kT}) \qquad (2.3)$$

where K_{IO} is the pre-exponent and E_I is the activation energy. Summing up the rates for different orders the total rate of incorporation may be written as

$$\frac{dN_{inc}}{dt} = \sum_q K_{IO_q}\exp(-\frac{E_{Iq}}{kT}) \cdot N_{DS}^q \qquad (2.4)$$

The assumption here is that incorporation may take place by single atoms or in twos, threes and so on, corresponding to different values of q.

In practice one need consider only the $q = 1$ term. This is so because the incorporation of foreign atoms introduces strain into the crystal. The incorporation of larger aggregates would need a higher activation energy. This means that larger aggregates would incorporate more slowly. Thus the incorporation of $q > 1$ may be neglected if single atoms can incorporate.

Further, since we are considering electrically active dopants and can only measure shallow ionization level dopants, it turns out that only the singly incorporated atoms are of importance. For these reasons we will in future analysis retain only the $q = 1$ term in Equation 2.4.

We have made some important assumptions in this section. The adsorbed atom is assumed to incorporate into the slowly moving step.

This process may involve several steps, but we assume that a single one of these is dominant and limits the incorporation rate. For this reason we assume a single activation energy.

2.3.5. Adsorption-Desorption-Incorporation Equation.

We now consider all the processes simultaneously and write down an expression for the increase in the concentration in the surface species of the dopant. In its most general form this is

$$\frac{dN_{DS}}{dt} = F_D - \sum_p K_{Dp} N_{DS}^p - \sum_q K_{Iq} N_{DS}^q \qquad (2.5)$$

Using the arguments regarding p and q mentioned above, we may simplify Equation 2.5 to

$$\frac{dN_{DS}}{dt} = F_D - K_{Dp} N_{DS}^p - K_I N_{DS} \qquad (2.5a)$$

Equation (2.5a) can be solved once a value for p is chosen.

The Case $p = 1$.

The case $p = 1$ is the easiest to solve. It is also very important practically because gallium, the p-type dopant used in this study, satisfies this condition. (See Chapter 4.)

Equation 2.5a reduces to

$$\frac{dN_{DS}}{dt} = F_D - K_D N_{DS} - K_I N_{DS}. \qquad (2.6)$$

2.3.6. Steady State Analysis.

We analyze Equation 2.6 in the steady state i.e., with $\frac{dN_{DS}}{dt} = 0$. Then

$$N_{DS} = \frac{F_D}{K_D + K_I} \tag{2.7}$$

Once steady state has been reached, the number of incident atoms per second is equal to the sum of those that desorb and incorporate per second. Equation 2.7 also shows that there is on the host surface a concentration of the surface species of the dopant atoms. From these a portion incorporate into the growing lattice. This rate is therefore

$$\frac{dN_{inc}}{dt} = K_I \frac{F_D}{K_D + K_I} \tag{2.8}$$

The ratio of the number of atoms that incorporate to those that are incident, on a per unit time basis in steady state, is called the sticking coefficient s. Thus

$$s = \frac{dN_{inc}/dt}{F_D} = \frac{K_I}{K_I + K_D} \tag{2.9}$$

The resultant steady state bulk doping concentration N_{DB} is given by inspection as

$$N_{DB} = \frac{dN_{inc}/dt}{F_{si}} \cdot N_O \tag{2.10}$$

where N_O is the number of silicon atoms per cm^3. Simplifying Equation 2.10 we get

$$N_{DB} = s \frac{F_D}{F_{Si}} \cdot N_0 \qquad (2.10a)$$

The sticking coefficient is an important parameter. When the sticking coefficient is small i.e., $s << 1$ we have $K_D >> K_I$ or the desorption rate is higher than the incorporation rate. Then,

$$s \simeq \frac{K_I}{K_D} \qquad (2.11)$$

i.e., the ratio of the incorporation coefficient to the desorption coefficient.

Since both incorporation and desorption have been assumed to be activated processes we get

$$s = \frac{K_{IO}}{K_{DO}} \exp\left(\frac{E_D - E_I}{kT}\right) \qquad (2.12)$$

s therefore behaves like a simple exponential with respect to inverse temperature. The energy coefficient is the difference between the desorption and incorporation energies and the preexponent is the ratio of the two preexponents.

2.3.7. Transient Analysis

Let us now consider a clean host surface and apply a step flux F_D i.e.

$$F_D = 0 \qquad t < 0$$
$$= F_D \qquad t \geq 0$$

We then have

$$\frac{dN_{DS}}{dt} = F_D - (K_I + K_D)N_{DS}$$

$$N_{DS}(t) = \frac{F_D}{K_I + K_D}\left(1 - e^{-(K_I + K_D)t}\right) \qquad (2.13)$$

This solution closely resembles the behaviour of a simple RC network. The time constant of interest here is

$$\tau = (K_I + K_D)^{-1} \qquad (2.14)$$

The significance of τ, which we shall henceforth refer to as the characteristic dopant incorporation time, is the following: When the Si/dopant system is subjected to a sudden change of flux, the system approaches its new steady state in an exponential manner in time. The initial rate of approach is given by $1/\tau$. For practical purposes we may assume that steady state has in fact been achieved after about four or five time constants.

Large desorption and incorporation coefficients mean smaller characteristic dopant incorporation times, while smaller values mean that steady state will take longer to achieve. A further point to note is that when the sticking coefficient is small τ is equal to the mean time of residence of the dopant atoms on the surface - τ_D.

The incorporation rate follows the surface concentration behaviour. Thus the bulk doping concentration as a function of time is

$$N_{DB}(t) = s\frac{F_D}{F_{si}} \cdot N_0(1 - \exp - (K_I + K_D)t) \qquad (2.15)$$

If the growth rate is constant, as we have assumed here, the temporal variation is easily transformed to a spatial variation by

$$x = vt \tag{2.16}$$

where x is the coordinate of film thickness and v the velocity of growth. This velocity is given by

$$v = \frac{F_{Si}}{N_o} . \tag{2.17}$$

where N_o is the number of atoms per cm^3

$$\therefore N_{DB}(x) = s \frac{F_D}{F_{Si}} N_o\left(1 - \exp - \left(\frac{K_I + K_D}{v}\right)x\right) \tag{2.18}$$

Note that in the above transient analysis we have assumed that K_I and K_D are constants, which means that the temperature is constant and there are no saturation effects.

The quantity $\left(\frac{K_I + K_D}{v}\right)^{-1} = \lambda$ is the spatial counterpart of τ. It represents the thickness of film over which variations in doping density occur in response to sudden changes in doping flux.

We point out at this point that both τ and λ become smaller as the temperature of growth is increased. However the sticking coefficient falls with increasing temperature, and this may impose doping limitations on the abruptness of doping profile changes and on the upper level of which may be achieved with constant temperature growth.

2.3.8. Transient Analysis with Changing Doping Flux.

Let us now relax the condition that the dopant flux be kept constant. Let us however maintain a constant substrate temperature and silicon growth rate.

Let the dopant flux be $F_D(t)$. We have from Equation 6

$$\frac{dN_{DS}}{dt} = F_D(t) - (K_I + K_D)N_{DS}(t) \qquad (2.19)$$

The solution to this equation is

$$N_{DS}(t) = \exp(-(K_I + K_D)t)\left\{\int_0^t \exp((K_I + K_D)t) \cdot F_D(t)dt + c\right\} \qquad (2.20)$$

The number incorporated in unit time is

$$\frac{dN_{inc}}{dt} = K_I \exp(-(K_I + K_D)t)\left\{\int_0^t \exp((K_I + K_D)t) \cdot F_D(t)dt + c\right\} \qquad (2.21)$$

and the doping concentration is

$$N_{DB}(t) = \frac{K_I N_0}{F_{Si}} \exp(-(K_I + K_D)t)\left\{\int_0^t \exp((K_I + K_D)t)F_D(t)dt + c\right\} \qquad (2.22)$$

We now change variables to $x = vt$ as before to get

$$N_{DB}(x) = \frac{K_I N_0}{F_{Si} v} \exp(-(K_I + K_D)\frac{x}{v})\left\{\int_0^{x/v} \exp((K_I + K_D)\frac{x}{v}) + F_D(x/v)dx + c'\right\} \qquad (2.23)$$

Taking the derivative with respect to x we get

$$\frac{dN_{DB}(x)}{dx} = -\frac{(K_I + K_D)}{v} N_{DB}(x) + \frac{K_I N_0 F_D(x/v)}{F_{Si} v} \qquad (2.24)$$

Transposing to obtain

$$F_D(x/v) = \frac{F_{Si}(K_I + K_D)}{K_I N_O} \left\{ N_{DB}(x) + \frac{v}{K_I + K_D} \frac{dN_{DB}(x)}{dx} \right\} \qquad (2.25)$$

and setting

$$K_I + K_D = \frac{1}{\tau}$$

we arrive at

$$F_D(x/v) = \frac{F_{Si}}{K_I N_O \tau} \left\{ N_{DB}(x) + v\tau \frac{dN_{DB}(x)}{dx} \right\} \qquad (2.26)$$

Equation 2.22 shows very clearly that the doping concentration is not directly proportional to flux but rather to an exponentially weighted integral of the flux. The constant c is related to the initial accumulated concentration of surface dopant, and is assumed to be zero.

Equation 2.26 is the inverse relation of Equation 2.22 and is more revealing . It is a design relation for the doping concentration. We note that there is a term related to the derivative of the doping to be achieved. This is an anticipatory term. There is therefore what may be called two term control. The significance of $v\tau$ is as described earlier.

2.3.9. The Design of Particular Profiles

Using Equation 2.21 and inserting the desired doping profiles $N_{DB}(x)$ one may obtain a schedule for the corresponding dopant flux. The significance of terms in these equations can not be obtained until we have reasonable estimates of the actual parameters in the equation. We shall therefore postpone this discussion until the details of our

experimental results are discussed.

2.4. A Comparison of Our Model With the Model of Joyce and Wood.

We consider here briefly the model proposed by Wood and Joyce[31] for the incorporation of tin in GaAs. Based on experimental observation of tin with concentrations much larger than expected on the surface of the semiconductor during growth they have proposed a model similar to ours , except that desorption has been neglected. The implication of this is initially that the steady state sticking coefficient should be unity. However it is easy to see why steady state may not be achieved quickly if the incorporation coefficient is less than unity. Some estimates of K_I for Sn in GaAs are available and they are found to be quite small, implying large delays. It is however mentioned by Wood et al[84], and also by Ploog and Fischer[8], that as the temperature is lowered the surface accumulation decreases.

In this case we have in steady state

$$N_{DS} = \frac{F_D}{K_I} \tag{2.27}$$

$$= \frac{F_D}{K_{IO}} \exp(E_I/kT) \tag{2.28}$$

It is clear from Equation 2.28 that this can not happen if $E_I > 0$. Further, Wood et al claim that $E_I = -1.35$ eV. This means that incorporation proceeds faster for tin in GaAs at lower temperatures. This is an intersting feature which we do not observe in silicon. This also means that at a given Sn flux steady state doping must be the same for all growth temperatures. Experimental evidence[84,34] is not

very clear. Further delay times must be long as a steady incorporation cannot be obtained with constant flux.

To sum up we note that for dopant/silicon systems desorption is an important process, unlike the case of the Sn/GaAs system. Incorporation is an activated process with a barrier in the silicon systems. This does not seem to be the case in the Sn/GaAs system. We therefore expect the silicon behavior to be substantially different from the GaAs behavior, especially with respect to temperature dependence. Alexandre et al[34] suggest that the W-J model may be applicable only over a limited range of temperatures for the Sn/GaAs system.

2.5. Saturation Effects.

We have seen that our model supposes that dopant incorporation proceeds from an accumulated layer of surface dopant species. The incorporation therefore involves transport of the dopant atom from this accumulation, no matter what its form, to a suitable incorporation site. Clearly then, this rate constant could be dependent on the concentration of the surface dopant. If the accumulated layer is uniform, saturation should set in abruptly after a monolayer of surface dopant has accumulated. However, if the surface dopant goes down in clusters a more gradual saturation effect can be expected. We shall discuss this issue further when we present results of saturation experiments.

2.6. Conclusions.

Dopant incorporation in silicon proceeds from a reservoir of surface dopant accumulated on the substrate surface. This accumulation arises as a result of atoms entering the surface phase through the

incident flux, remaining on the surface for a mean time τ_D, and then leaving either via the desorbed flux or by entering the bulk phase via lattice incorporation. Both desorption and incorporation are activated processes, proceeding at increasing rates at higher temperatures.

Our experimental evidence shows that desorption is a faster process than incorporation, explaining the observed low sticking coefficients. At high flux rates saturation effects may be expected. The model does not suppose any details for the physics of incorporation, though using the parameters of the model, it may be possible to infer a physical model. This will be discussed in later chapters. Delays in achieving steady state doping concentration follow directly from the times required to achieve the steady state accumulated surface dopant.

CHAPTER 3

Experimental Details

3.1. Introduction

The present chapter is divided into two parts. The first is concerned with the hardware used in this project. The second part is concerned with the design of our experiments designed to test the model developed in the previous chapter.

While it is now possible to purchase MBE systems with various capabilities, during the initial stages of this project silicon MBE systems were not readily available. It was therefore necessary to design and build our own system. In fact this part of the project occupied a major portion of this work.

3.2. Description of the Basic Vacuum System

The basis for our MBE system was a stainless steel Varian LEED-AUGER vacuum system (See Figure 3.1) that was previously used in photoemission studies. The pumping chamber consisted of a 220 L/sec ion pump controlled by a single power supply (Varian: 921-0066). In addition to the ion pump , there is also a titanium sublimation pump (Varian: 922-0032). There is also a cryopanel to be used with liquid nitrogen or water.

The working chamber contains hemispherical retarding potential 4-grid LEED-AUGER optics. Facilities exist for ion bombardment. The two parts of the chambers may be isolated using a poppet valve. The available working space is cylindrical in shape with a diameter of

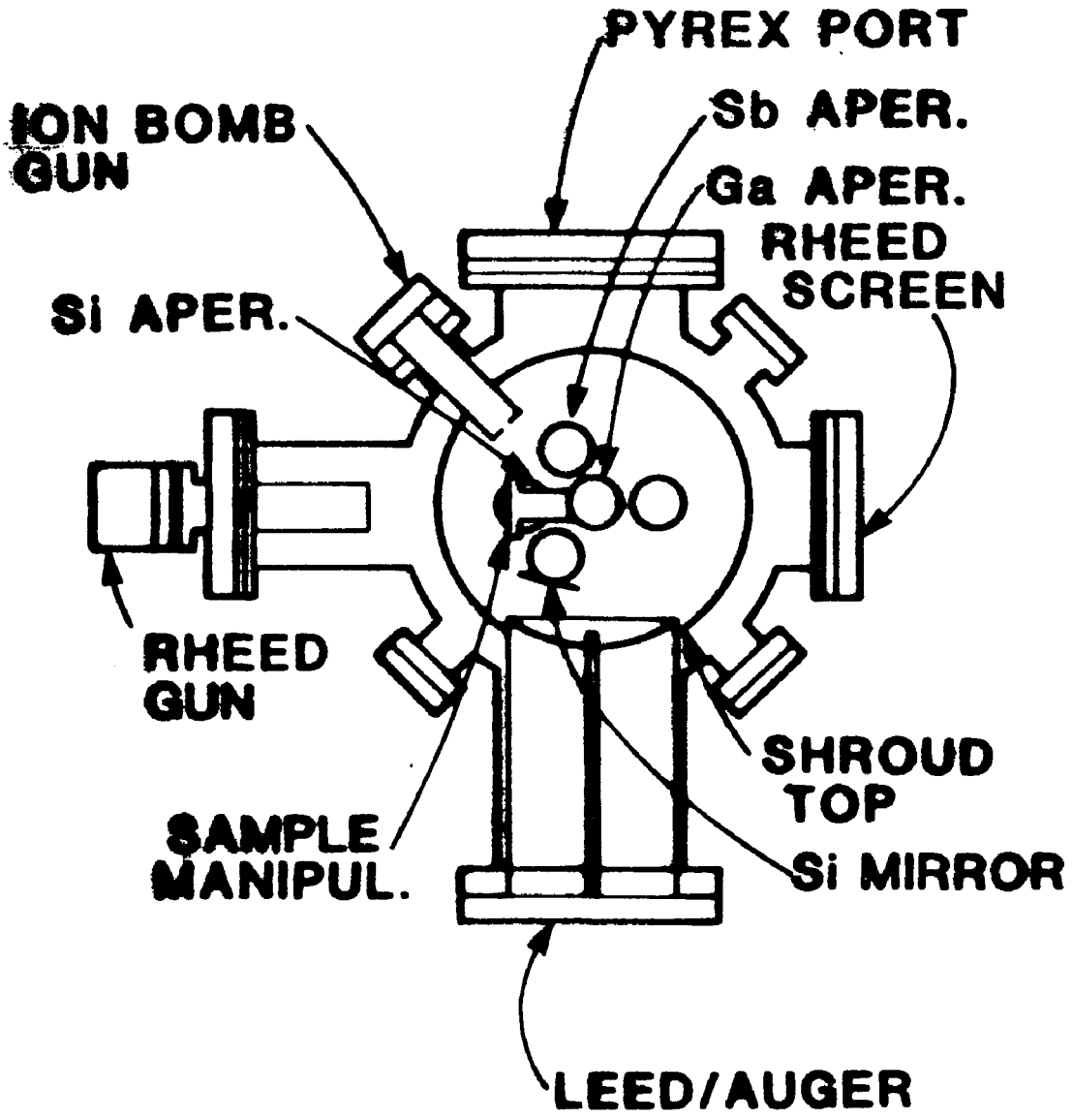

Figure 3.1 Plan of MBE system

about 30 cm. and a height of about 60 cm. Pressure is measured by a Bayard-Alpert type gauge (Varian: 971-1008).

3.3. In Situ Analytic Equipment

1. LEED. Low energy electron diffraction [74], where a low energy electron beam normally incident on a surface is diffracted by the surface atom structure to yield an electron intensity pattern that corresponds to the two dimensional surface reciprocal lattice, is used to characterize the surface structure. The standard Varian 4-grid LEED optics (981-0127) were used. The primary electron beam is generated with a Varian electron gun (981-2125) and is normally incident on the specimen which is held near the focus of the gun. The diffracted beam was accelerated by about 10 keV onto a planar phosphorescent screen. Typically the beam current is a fraction of a microamp and the primary voltage is between 35 and 65 volts.

2. AUGER. Auger spectroscopy [35] uses an electron induced core level transition as a technique for chemical identification of species on the surface, our retarding field auger system utilizes the same optics and electron gun as above, though in a different mode. The gun current can be as high as 60 μA and beam voltage up to 3 kV. Typically we used a beam current on the sample between 5 and 10 μA. with the beam voltage between 2 and 3 kV. The detection system employed retarding fields as a high pass filter, with synchronous detection using a lock-in amplifier. The suppressor grid was modulated at 1000 Hz while both the fundamental and second harmonic could be

measured.

For a clean silicon surface the sensitivity was measured to be about $\frac{i_{auger}}{i_{prim}} \sim 10^{-5}$. Thus for a typical primary current of 10 μA, the measured voltage across a 1 Megaohm input amplifier would be about several tens of μ Volts. This agrees well with calculations of Chatterjee[35].

The typical modulation voltage used was 20 Vpp. This causes some spread in the auger peaks but the sensitivity gained is important. Quantitative information is obtained either by measuring the peak to peak auger height on the second derivative or the area under the characteristic auger hump, the former being a more easily measurable quantity.

3. RHEED.[75] The reflected high energy electron diffraction system consists of a glancing angle incidence electron gun (PHI-04-015). The sample is capable of being flipped down (using a high-precision sample manipulator to be described later) to varying degrees and the beam itself is capable of x and y deflection making possible an incidence angle range of 0 to 90°. The diffracted beam is viewed on a phosphorescent screen. The screen was made by depositing a ZnS film on a pyrex port. The film was deposited using a 1 : 7 suspension of ZnS (Fisher Z-73-phosphorescent grade) in a saturated solution of sodium silicate in water. The water was slowly evaporated without mechanical disturbance at room temperature. Due to the limited distance of the screen and its height from the sample, the angle of incidence was limited to about 5°. Typically we use an incidence angle of 1.5°. Like LEED, RHEED also projects the surface reciprocal

net. Although the incident energy is high, the normal component of the electron momentum is the same in both RHEED and LEED. Both RHEED and LEED yield important qualitative information on the surface structure. They can be used to study the improvement of film structure and also the existence of adsorbed phases on the surface. In our set-up, neither LEED, AUGER or RHEED may be used during the growth process due to distorting magnetic fields. RHEED is advantageous because a RHEED pattern may be viewed momentarily by arresting growth and turning off the magnetic field. RHEED further is more sensitive to the surface morphology. With magnetic shielding RHEED observations could be made, but this has not yet been accomplished.

3.4. Design Considerations for an MBE System

At the point of this writing, several manufacturers offer fairly sophisticated MBE systems[36]. Most of these are production oriented and geared to the III-V and other compound semiconductor synthesis. We shall outline here our design considerations and include details on our MBE system. Figure 3.1 shows a plan view of our system.

We consider RHEED, LEED and AUGER analysis essential for research in MBE , where auxiliary experiments in addition to film growth are to be conducted. In addition to LEED, AUGER and RHEED our experience suggests that SIMS, which would include a mass spectrometer for residual gas analysis, should be made part of the system as well.

3.5. Sample preparation

As discussed earlier proper epitaxial growth cannot proceed in the presence of certain surface impurities, such as oxides and carbides, of

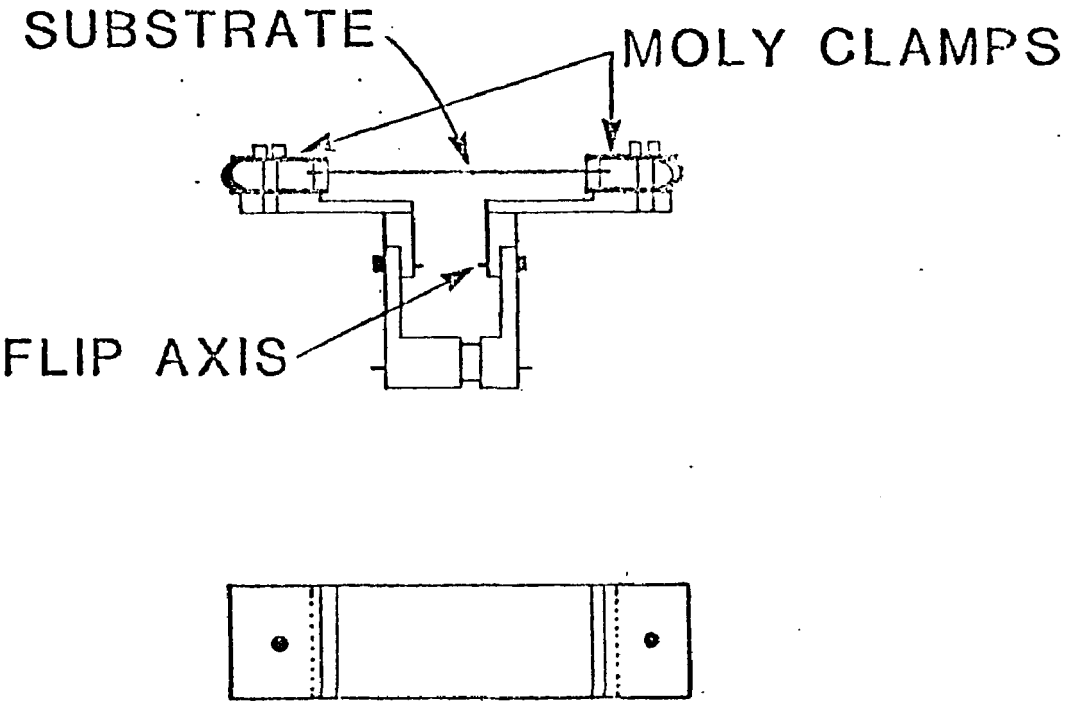

Figure 3.2 Substrate holder

even the smallest concentration. It is imperative therefore to reduce these to a minimal level. Carbon and oxygen can be excluded in several ways. Simplest is the technique of raising the sample temperature to about 1200°C for several seconds and cooling slowly[76]. This is certainly the quickest way but there may be reservations due to the extremely high temperature involved. Alternatively the first several layers may be sputtered away and any resulting crystal damage annealed out. This process needs to be cycled a few times until an atomically clean surface is generated. Argon ions at a few hundred volts are employed. The process is time consuming and the residual damage can be deleterious to the structure of the film grown. Of special interest is the process of galliation[37] in which a gallium beam of about 10^{15} atoms/cm^2sec is made incident on the silicon surface to be cleaned. The silicon itself is maintained at a temperature above 850°C for about 15 minutes. Apparently, the corrosive gallium induces reduction of oxides while the high temperature for the prolonged period causes the expulsion of carbon. The gallium compounds formed are quickly desorbed. The advantage of this technique is the relatively low temperature used.

Heating of the sample is accomplished by passing a current through it. Resistive heating rather than radiative was employed because it is simpler and localizes the heat to the silicon substrate. The sample is held between molybdenum clamps fairly loosely to permit relieving of thermal strains and also minimization of heat loss through the clamps (see fig. 3.2 for details). Nonuniform heating is a problem but can be reduced by adjusting clamp pressure. In the case of high resisti-

vity substrates a fairly high voltage is required to initiate a current through the sample, which increases drastically as the sample temperature rises. As soon as the current reaches a predetermined safe amount the voltage is switched automatically to a lower value and the current controlled via a current amplifier until the required temperature is maintained (See fig. 3.3). The temperature itself is measured by an infra-red pyrometer. (Ircon model 300 LC). The same heating system is also employed to maintain the sample temperature during growth.

3.6. Sample holder

We use a Varian '981-2523) high precision sample manipulator. The vertical motion is limited to 4 cm while x and y translations of 1.25 cm about the central position are possible. In addition full 360° rotation of the holder about the central axis is possible. The sample dimensions acceptable are 2.9 cm x 1.25 cm with a tolerance of 0.1 cm. The actual growth area is 2.2 cm x 1.25 cm. The sample is capable of being flipped through a little over 90°. With the normal to the sample surface horizontal, the sample can be subjected to LEED, Auger and temperature analysis. When flipped down the sample may be moved into the various molecular beams.

3.7. Silicon beam source

Unlike in the case of the group III and V elements, appreciable silicon fluxes may be produced only by electron beam heating. This constrains the molecular beams to move vertically as the molten pool must be kept horizontal. The vertical beam system suffers from the disadvantage that material deposited on the top and walls of the

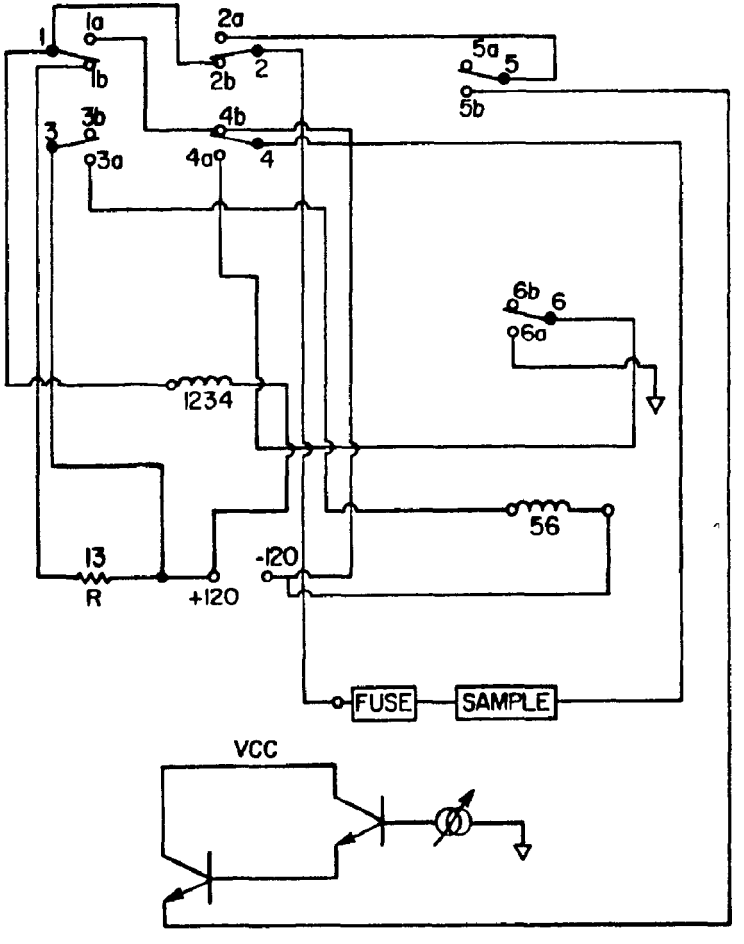

Figure 3.3 Substrate heater switching circuit

system may flake off and interfere with the beam generating mechanisms, causing contamination. Proper maintainence prevents such problems, especially high voltage arcing due to electrical breakdown of silicon on various high voltage conductors.

We use an Airco Temescal (FIH-270) 6 kW electron beam gun. It operates at 10 kV. The electrons emitted from the tungsten filament are turned through 270°C by a magnetic field onto the silicon hearth. The tightly focussed spot is "dithered" to and fro (and laterally also) to obtain an elliptical molten pool of silicon from which the silicon beam is generated. The silicon source is carefully ground to fit a molybdenum crucible. Better thermal contact is achieved by coating the inner surface of the moly crucible with indium. The silicon source is a frustum of a cone with the larger diameter of 2.85 cm and a height of 1.53 cms. The apex half angle is 30°. The moly insert is placed in a close fitting copper crucible that is water cooled with the water rate about 2.2 ℓ/min. During operation power levels are adjusted to ensure that no molten silicon touches the moly insert. (See fig. 3.4)

3.8. Dopant beam sources

Our system is designed for two dopant effusion cells. These cells were fabricated here.[77] Figure 3.5 shows a cut away section. The oven consists of about 48 turns of 0.25 mm tantalum wire spring wound out against four ceramic posts held in place by slots against a tantalum can. The ceramic posts have grooves cut in them to hold the oven winding, and to prevent the winding from touching the can. The upper end of the healing coil is grounded through the can while the

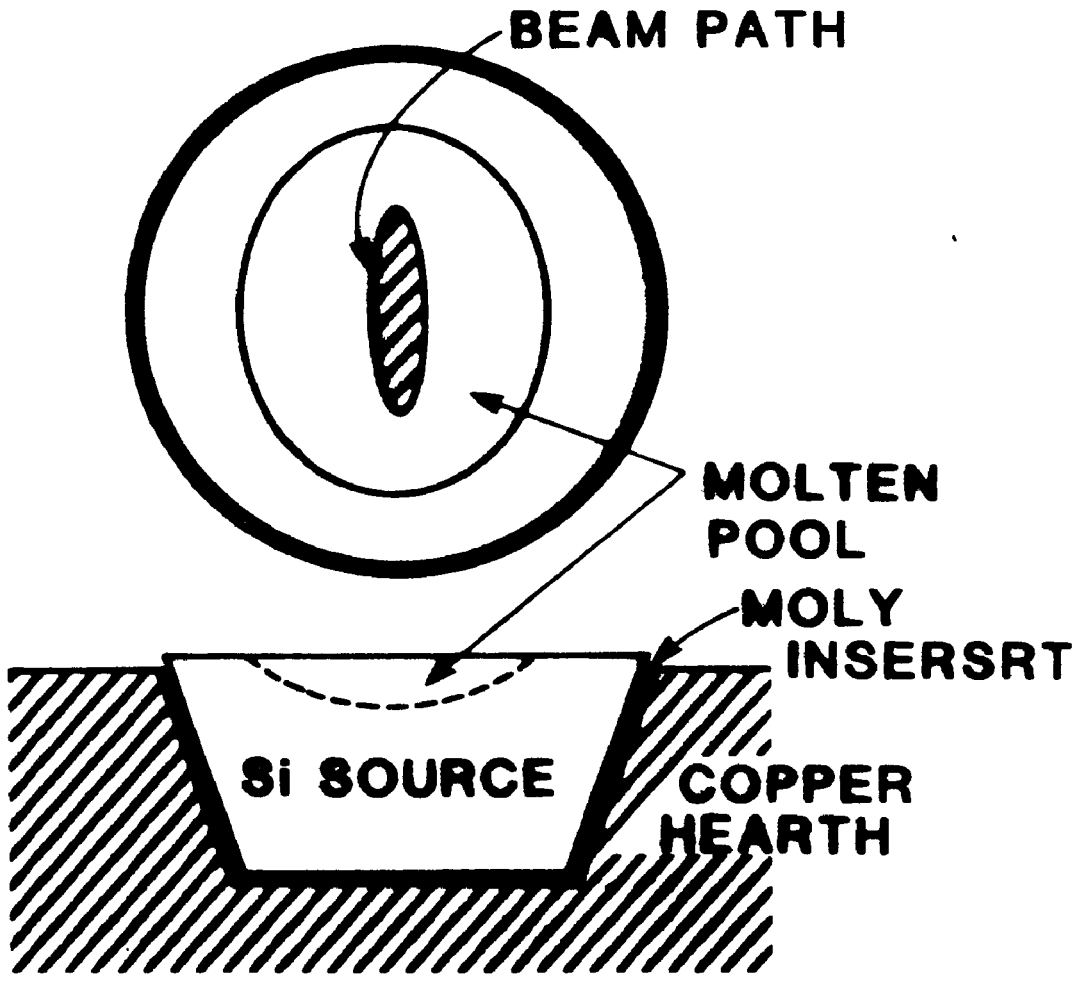

Figure 3.4 Source arrangement

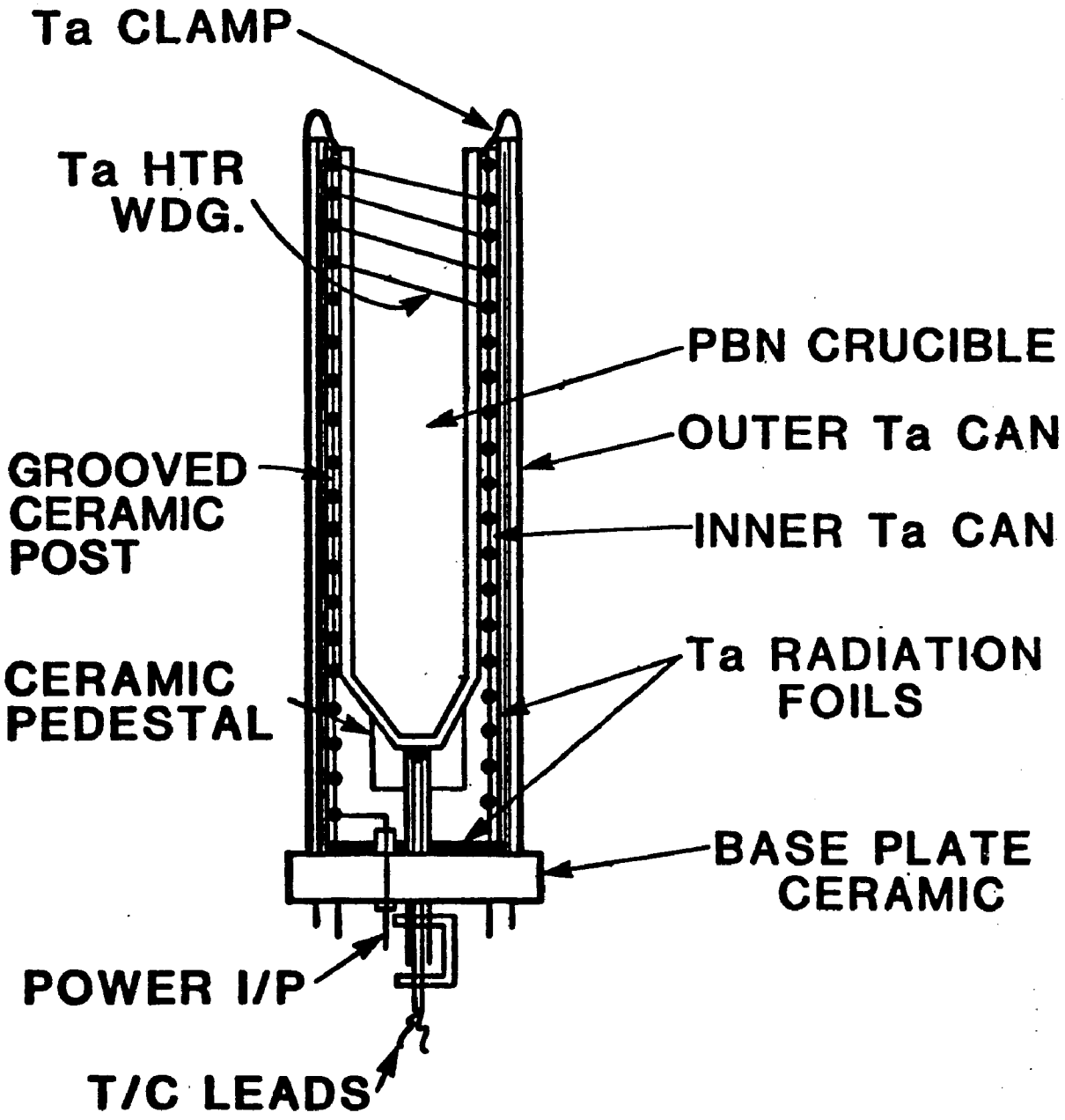

Figure 3.5 Schematic of effusion cell

lower end is fed through a ceramic tube held in a ceramic base plate and forms the power input. The inner tantalum can is held in place by four legs that slide into the base plate. An outer tantalum can is then slipped around the inner. The two cans are separated by 5 layers of perforated tantalum foil, as also the base plate, which serve as radiation shields. We use pyrolytic boron nitride crucibles (Union Carbide H-5110) that slide into the inner can and held in a ceramic pedestal. Through the center of the pedestal a thermocouple is inserted with the junction held by pressure in intimate contact with the crucible. The crucible is centered by means of tantalum spring clamps. The ovens themselves are controlled by PID controllers (LEEDS AND NORTHRUP|EUROTHERM) and the temperatures are controllable to within a fraction of a degree though the absolute temperature of the change is not known to this accuracy. We have used iron-iron constantin thermocouples and are limited to temperatures below 1000°C. The advantage of this system is in the ease with which crucibles may be changed. The overall dimensions of the oven are about 2.5 cm diameter and 9 cm long. We have two such ovens which in this study were used to generate gallium and antimony beams. The beams may be shuttered off when not desired.

3.9 Shroud

The electron beam gun and the two ovens are anchored to a double walled panel shown in fig. 2.1. The shroud also has copper aprons in good thermal contact to it which extend downwards and present a large area. When the shroud is cooled all this area acts as a cold surface and helps keep the pressure low. The function of the shroud, besides

being a cryopanel, is to collimate the molecular beams and ensure that the sample does not see any excess of hot surfaces. It also contains the unused portions of the beams and reduces the indiscriminate deposition on the vacuum chamber walls and other equipment.

3.10. Quartz crystal rate monitor

We use a Sloan digital quartz crystal monitor to monitor the rate of the silicon growth (Sloan model DTM-200). The sensitivity of the unit is about 10^{-9} gms and may be used to measure rates of greater than 0.1 Å/sec. The bakable crystal head is water cooled and suspended rigidly so that it intercepts both the silicon and dopant beams. In principle the life time of the crystal should be enough to grow about 50 μ. In practice however, the crystal needs to be changed after about 10 μ (equivalent to a crystal frequency deviation of 50 kHz), due to the corrosive nature of the gallium beam, which was found to attack the silver electrode on the quartz crystal.

3.11. Other relevant information

The source to substrate distance was 25 cm., while the effusion cell distances from the substrate were 16 cm each. While the silicon beam is normal to the substrate, the dopant beams intercept it at an angle close to 30° from the normal.

3.12. Silicon source characteristics

As mentioned earlier, the silicon source is ground to closely fit the moly insert. We found that a thin layer of indium coated on the inside of the moly crucible played a useful role in limiting the mol-

ten pool size. Indium melts around 156°C and ensures a good thermal fit during system bake-out when termperatures in excess of this are reached. However any sudden change in the beam current caused thermal strains and fracture of the source slug due to extremely good heat sinking by indium. Once this happens the source is rendered non-usable. Hence the practice of lining the silicon moly interface with indium was discontinued, and a good fit of the silicon slug to the moly insert was relied on.

During growth the beam current and dither are adjusted to obtain a desired growth rate, taking care that the molten pool is at all times at least 2 or 3 mm from the sides of the crucible. The source condition is monitored visually with the help of a silicon mirror as shown in fig.3.1. We found that after about 1 μ of film growth the mirror clouded up fairly quickly due to a dendritic growth on the mirror. Hence the mirror would need to be changed every run. The silicon rate and pool size were however sufficiently stable, even during extended runs taking as many as 8 hours.

The material used for the source was typically very high purity (300-1000 Ωcm) P type silicon. The predominant impurity is boron. As boron has low vapor pressures, it was felt that the concentration of boron in the grown film would be negligible. After grinding to size, the source piece was thoroughly degreased, etched in HF, and CP4A (HNO_3: CH_3COOH : HF :: 12 : 2 : 1) for ~ 10 minutes until a shiny polished surface was obtained. The source was then soaked in basic and acidic complexing solutions (see section on substrate preparation) and rinsed well.

Recharging of the source is done either by replacing the source completely or by placing tiny silicon chips of the same type and resistivity as the source in the depression formed by evaporation. These chips are then carefully melted down.

Calibration of the growth rate is easily accomplished, because the moly clamps on the substrate shadow part of the substrate form the beam. The step caused by the film is then measured using a Tolanski interferometer. Typical growth rates for different powers delivered are shown in fig. 3.6. It was found that there were variations of $\sim \pm 15\%$ due to variations in the thermal contact conditions of the source. Typical growth rates used in our work were between 1 and 1.5 Å /sec (0.36 to 0.5 μ/hr).

3.13 Calibration of effusion cells

While it is possible to compute dopant fluxes based on temperature of the effusion cell, it is recognized that such temperature measurements may be inaccurate, depending on good thermal contact between thermocouple and cell and between cell and dopant material. Further, the presence of oxide skins on group V elements causes the evaporation to be retarded. We have followed a more emperical approach in calibrating the effusion rates. We have been able to measure the flux on the quartz crystal monitor at high fluxes ($\geq$ 0.1 A/sec). While under doping conditions such high fluxes are seldom used, these rates versus temperature curves may be extrapolated to lower temperatures. The extrapolation is not arbitrary but is based on the actual behavior of the elemental vapor pressure with temperature. Since measurement of temperature may not be exactly reproducible, the power delivered to the cell at different temperatures was also measured. These have been

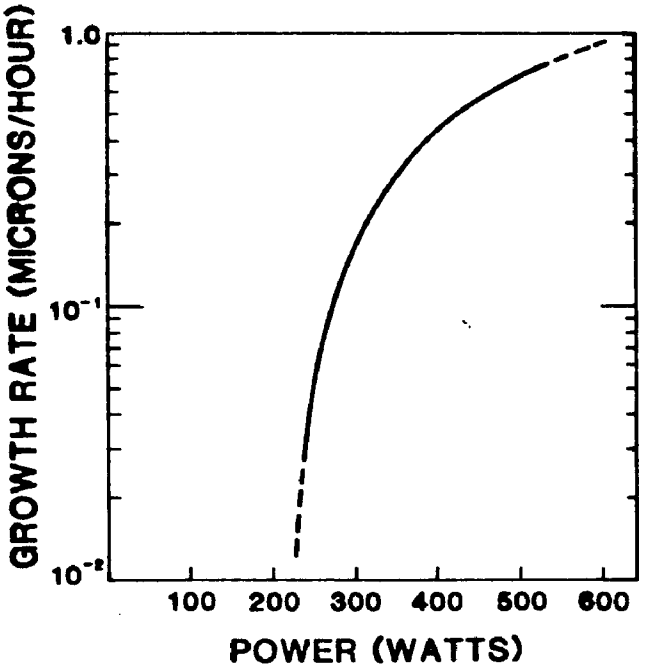

Figure 3.6 Silicon source characterestics

checked and we conclude that the temperature measurements are in fact quite reproducible. These curves are shown in fig. 3.7 and 3.8. The gallium curve (fig. 3.7) shows normal behavior, the experimental curve lies slightly below the predicted curve based on the effusion equation using vapor pressure curves[39]. This is attributable mainly to the gallium temperature being slightly lower than the measured temperature and partly to retardation effects.

The antimony curve (fig. 3.8) is not as straightforward. Firstly, it is believed that the predominant species of antimony effusion from elemental antimony is Sb_4[38] (although Sb_1, Sb_2 and Sb_3 are also found). Secondly, on exposure to air antimony forms an oxide skin that retards evaporation. As a result the curve exhibits hysteresis and the effusion rate depends on the highest temperature attained. Heating it above 425°C seems to be sufficient to disassociate this oxide. Further, the effusion rate seems to be higher than that predicted by the vapor pressure curves, though the agreement is better at higher temperatures. We have been able to reproduce our curves and have therefore used a linear extrapolation of log(flux) vs. 1/T plot to predict fluxes at lower temperatures. We believe that the lower values based on vapour pressure curves[39] may reflect retarding effects. The slopes of the two curves are appreciably different. This we believe is due to changing active area for evaporation. Needless to say, in our experiments the Sb cell was initially heated to 425°C for about 5 - 10 minutes before any experiments were conducted.

3.14. Operating procedure and operating conditions

Initially the silicon samples are cleaned as follows:

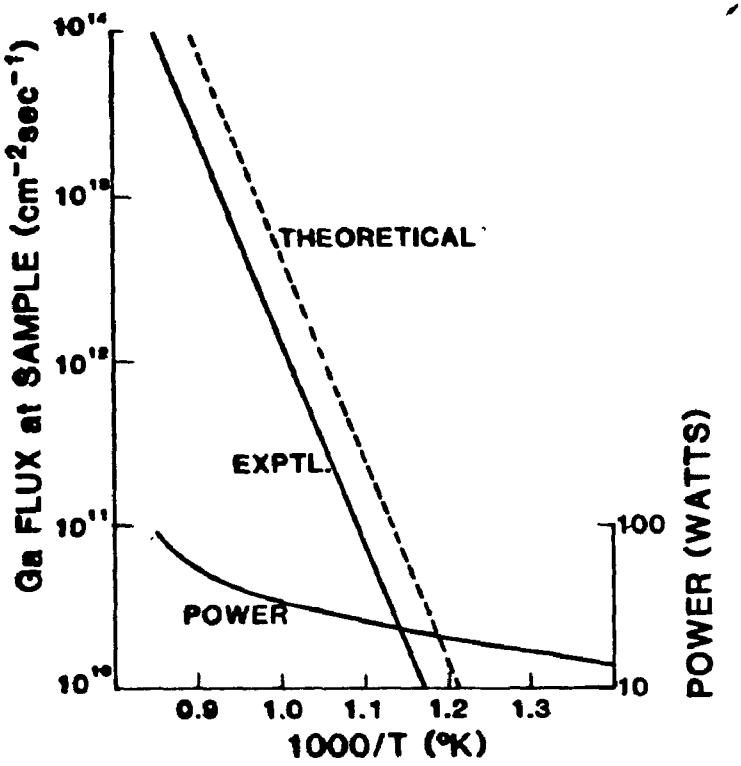

Figure 3.7 Ga effusion cell characterestics

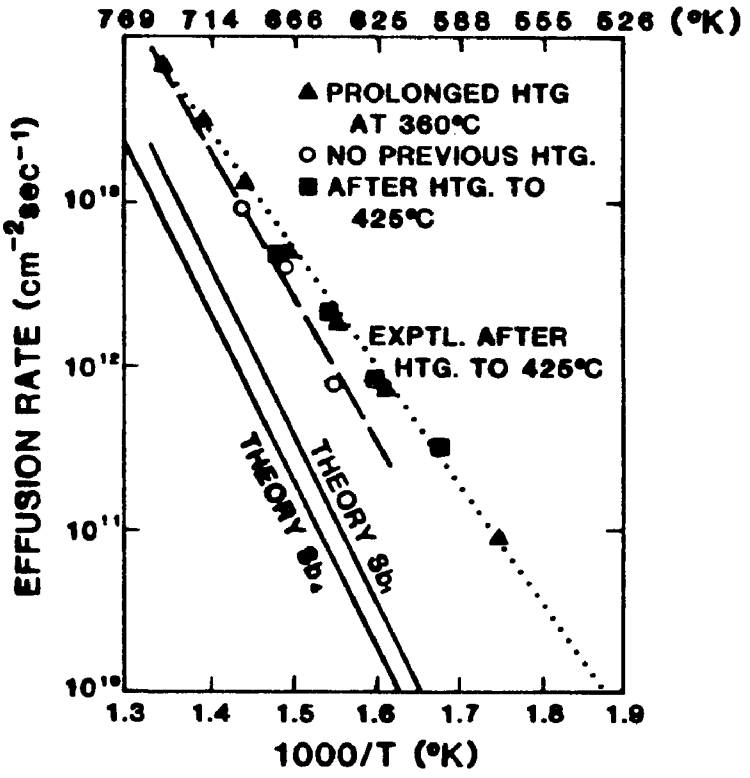

Figure 3.8 Sb effusion cell characterestics

(i) boil in trichloroethylene for 10 minutes.

(ii) rinse in acetone for 10 minutes.

(iii) rinse in methyl alchohol or isopropyl alchohol for 10 minutes.

(iv) rinse in deionized water for 10 minutes.

(v) dip in 10% HF (48%) for 10 sec.

(vi) etch in CP4A (a mixture of 12 parts nitric acid, 1 part hydroflouric acid, buffered with 2 parts glacial acetic acid) for 1 minute with ultrasonic agitation.

(vii) rinse in deionized water for 10 minutes.

(viii) soak in a solution of 5 parts water, 1 part hydrogen peroxide and 1 part ammonium hydroxide (basic soaking solution) for 10 minutes at 60°C.

(ix) rinse in deionized water for 5 minutes.

(x) soak in a solution of 6 parts water, 1 part hydrogen peroxide and 1 part hydrochloric acid (acidic soaking solution) for 10 minutes at 60°C.

(xi) rinse in deionized water for 10 minutes with one minute of ultrasonic agitation.

(xii) blow dry with a nitrogen gas stream.

The sample is then loaded into the vacuum chamber within a few hours. We have determined from p-n junction characteristics that the etching action described in step (vi) is crucial. In some cases the etchant leaves the surface wrinkled (the so-called "orange peel" effect).

It is also believed that the surface is capped by a protective oxide 20 - 30 Å thick which prevents surface contamination.

The system is roughed using a sequence of three vacsorb pumps. The first stage is used to pump from atmospheric pressure down to a few hundred pascals (~ few torr). During this phase of the pump down there is a strong surge of gas into the pump. The noble gas content is entrapped in this flow and enters the pump. However, the molecular sieve is not very efficient in retaining these gases and reemits them (especially helium) into the chamber. Hence the first pump is sealed off at this stage. The pump down is then accomplished with the other two vacsorb pumps in sequence, the second being shut off when the pressure reaches about one pascal and the third being opened. At this stage the filaments of the titanium sublimation pump are degassed by passing a current of 45A through them for a period of 1 minute.

The vacion pump is then started. This is done with the sublimation pump on. At these high pressures sublimation pumps pump about an order of magnitude faster than ion pumps. While pumping the filament current is maintained around 42 A. We have found that this provides for a long filament life with adequate titanium sublimation. Further, depending on the pressure, the sublimation filament is turned on for different fractions of time as shown in Table 3.1.

The system is then baked out. The pressure during bake out is regulated between 2.5×10^{-5} and 2.5×10^{-4} pascals. The Pressure-Temperature plots during bake out are shown in fig. 3.9. Usually it is adequate to continue bake out until a maximum temperature of about 210°C is reached. The initial cycles take a few tens of minutes, due to large outgassing, while the final cycles may take a few hours

as the system becomes cleaner. Typically a 24 to 30 hour period of bake out is used. Throughout the bake-out the sublimation pump filament current is maintained between 25 and 30 A.

After the bake out is turned off the pressure begins to decrease fairly rapidly. While the station is still warm (~ 60°C) it is degassed. This involves heating all filaments and sources to temperatures in excess of those reached during operation. These include the ion gauge, effusion cells, the electron beam gun and silicon source, the LEED/Auger gun, the RHEED gun and the titanium filament.

The pressure then recovers to about 5×10^{-8} Pascals (4×10^{-10} torr) which is the base pressure used in most of our experiments.

The sample is then cleaned, usually by galliation and is checked for a clear well defined LEED/RHEED pattern. It is also checked for any impurity auger signals. We are then in a position to commence growth.

During operation the titanium sublimation pump is kept on for about 10% of the time in 5 minute intervals. Initially when the silicon source is turned on, with water cooling in the shroud, the pressure rises to about 10^{-5} pascals (10^{-7} torr). However, it steadily drops down to about 6×10^{-7} pascals (~ 5×10^{-9}torr) in about an hour of operation. If liquid nitrogen is employed in the cryo panel and shroud, the initial pressure attained is an order of magnitude less, but the final pressure is down only a factor of two or three. Hence most of our runs were made using water cooling of the shroud.

Typically we have used rates between 1 and 1.5 angstroms/sec (0.36 to 0.54 μ/hr). Typical run times are between 5 and 7 hours.

The gallium and antimony fluxes could be well controlled between 10^8 and 10^{15} atoms/cm^{2}sec. at the sample.

While it is possible to use the thickness monitor to control the silicon growth rate, we have relied on the stability of our electron beam gun to provide a uniform growth rate with the help of occasional manual control.

After growth and sometimes during growth the surface may be checked for LEED, Auger or RHEED to ensure that all is proceeding correctly. While the effusion cells are provided with shutters, we have relied on moving the silicon substrate out of the silicon beam or shutting off the source in order to block the silicon beam.

After growth we usually wait six hours before the system is vented with dry nitrogen. The sample is changed and if necessary the sources are recharged. The system is then pumped down.

TABLE 3.1

Percentage of time for which titanium filament is on

Pressure range (Pa)	Pressure range (torr)	%
$< 10^{-2}$	$< 10^{-5}$	100
$10^{-2} - 10^{-3}$	$10^{-5} - 10^{-6}$	50
$10^{-3} - 10^{-4}$	$10^{-6} - 10^{-7}$	25
during run		10

3.15 Design of experiments

We have presented in Chapter 2 a model for the incorporation of dopant atoms in growing silicon by MBE. While we have developed the case of monomer desorption and incorporation, we must bear in mind that desorption with higher orders is also possible. Let us now prescribe the parameters needed to fully quantify our kinetic model.

1. The desorption order - p.
2. The desorption coefficient - K_D. This includes the pre-exponent K_{DO} and the activation energy E_D.
3. The incorporation order - q.
4. The incorporation coefficient - K_I. This includes the pre-exponent K_{IO} and the activation energy E_I.
5. The sticking coefficient - s.

The above quantities may be used to describe the dopant-silicon system as a function of substrate temperature as long as saturation effects do not set in. We may determine from this information:

a) The accumulated surface species of dopant N_{DS} as a function of temperature and dopant flux.

b) The doping concentration N_{DB} as a function of temperature, dopant and silicon fluxes.

c) The delay times needed to achive steady-state values of these quantities.

d) The corresponding film thicknesses needed to achieve steady state values.

We also need to describe the system in the saturation regime. We need to determine:

1. At what level of surface dopant species saturation sets in.
2. Whether this level is the same at all temperatures.
3. What the nature of the dopant adlayer at high levels is [do they from clusters? For example.]
4. How the sticking coefficient behaves with flux and temperature.
5. What possible incorporation mechanisms are in operation in this regime.
6. What the maximum doping levels achievable are.

We have decided to perform a complete study of dopant incorporation in the case of gallium. Our strategy involves first determining the desorption kinetics of gallium from silicon. This is done mainly by thermal desorption studies, using auger spectroscopy and the available surface diffraction techniques.

The details of these experiments will be described in the next chapter. It is possible using these methods to determine p, K_{DO} and E_D. We anticipate our results at this point in order to apply the results derived in Chapter 2. Desorption studies for gallium from silicon, show that p is indeed unity.

If the sticking coefficient is small we recall from equations (2.11) and (2.12) that with a knowledge of K_D we may obtain K_{IO} and E_I. Our next task is to measure the sticking coefficient.

3.16. Measurement of sticking coefficient - s

Measurement of s consists of two parts. Recall that in steady state s is defined as

$$s = \frac{\left.\frac{dN_{DS}}{dt}\right|_{inc}}{F_D} \qquad (3.1)$$

We need to know accurately the flux of dopant and also the number of dopant species in steady state that have been incorporated into the film.

3.17. Measurement of flux - F_D

As the dopant flux is usually a very small quantity, typically 10^{10} atoms/cm^{2}sec to 10^{13} atoms/cm^{2}sec, it is not possible to measure it at all times. We have mentioned earlier in this chapter that the dopant effusion characteristics were studied as a function of temperature. We have repeated this study often and found fig.3.7 to be a reliable indicator of the flux employed. The crucible temperatures are maintained to within 5°C of the desired temperature. At 725°C, a typical oven operating temperature, this could translate into a flux variation between 1×10^{12} and 2×10^{12} atoms/cm^{2}sec. The temperature variation is almost sinusoidal with a time period of about 10 sec. Typically we grow about 10 Å of film in this period and the fluctuation in flux does not pose such a drastic problem. By proper adjustment of the dc power delivered to the cell, the variations may be made smaller. At lower fluxes, the control is better than at higher temperatures.

When making flux changes, it may take up to 5 minutes before steady state is reached. This factor must be considered in all cases, and usually growth is arrested during this interim period.

3.18. Measurement of incorporated dopant

The measurement of doping density N_{DB} may be used to obtain the incorporation rate. Recall that

$$N_{DB} = \frac{dN_{DS}\, dt\big|_{inc}}{F_{Si}} \; N_0 \tag{3.2}$$

which gives, along with eqn. (3.1)

$$S = \frac{F_{Si}}{F_D} \cdot \frac{N_{DB}}{N_0} \tag{3.3}$$

The measurement of doping levels is possible in any one of several ways. These may be catagorized into methods of chemical detection and methods of carrier profiling. The former is considered more fundamental as the carrier profile is always derivable from the chemical element profile while the converse problem does not always have a unique solution. In addition chemical methods are preferred as identification of other incidental impurities may be possible, a capability carrier measurement lacks. Among chemical methods we shall consider secondary ion mass spectrometry (SIMS) while carrier profiling via capacitance-voltage measurements and resistivity measurement will be considered. In addition, other indirect methods of profile measurement will be outlined. The following discussion is also concerned with the depth resolution capabilities of these methods, which is important in the profiling measurements we shall make in order to study the sharpness of the profiles generated.

3.18.1. Secondary Ion Mass Spectrometry (SIMS)[40, 42-44].

SIMS is a technique by which a primary ion beam is used to sputter off particles on the surface and near it, with a subsequent mass analysis of the sputtered ions for their chemical identification. This is done as a function of time, continuously exposing fresh surfaces for analysis. A knowledge of the sputtered ion yields of dopant atoms under the matrix conditions particular to the sample in study, together with a calibration of the ion detector system, enables extraction of profiling information. As the mass detector is tunable to several masses, concurrent detection of different dopant species is possible. A knowledge of the sputter rate while maintaining beam uniformity in space and time are essential for a meaningful interpretation of the data.

As a profiling tool, SIMS is subject to certain limitations. These are:

1. A sensitivity of about 10^{17} atoms/cm^3.
2. An accuracy of 5% in density measurements.
3. Ambiguous interpretation of the initial surface layers (~ 50 - 100 A°).
4. A depth resolution of only 10% - 15% of the depth actually being profiled.

It is seen that SIMS is a useful tool only when considering higher doping levels. The depth resolution is limited by instrumental factors such as a tapering of the analysis crater due to beam non-uniformities and resputtering of material adsorbed from the background. Further, ion-matrix interaction may cause sub-surface mixing, recoil effects,

accelerated diffusion (due to localized heating of the sample and ion induced damage), all of which cause a smearing of the profile. Thus, this smearing must be estimated in order to get a more accurate profile.

In this project the SIMS profiling was done elsewhere[41] and proper calibration of levels of the dopants gallium and antimony in a silicon matrix had to be made using resistivity measurements.

In spite of these limitations, SIMS is a valuable tool and has been used to characterize our grown films.

3.18.2. Capacitance Voltage Measurements[45-49].

Once a certain dopant profile is generated in a semiconductor, it is possible that electronic states are generated in the forbidden gap. If this state has an energy level near the conduction or valence band, a certain fraction of these dopant atoms will be ionized at a given temperature. As a result there is a free carrier density generated in this vicinity. On applying a bias of suitable sign to the semiconductor we may deplete a region of the semiconductor of the free charge, thus leaving a zone referred to as the depletion region. By measuring the depletion capacitance as a function of voltage the free carrier profile may be determined. In one technique both the free carrier concentration and the distance at which this concentration occurs are determined from a single C - V curve, while in other " feedback" techniques they are both determined independently.

We wish to point out here certain limitations of this technique:

1. The carrier profile is not the same as the doping profile. It is a reasonable approximation only if the ionization level is very shallow and there are no abrupt changes in doping. (See below.)

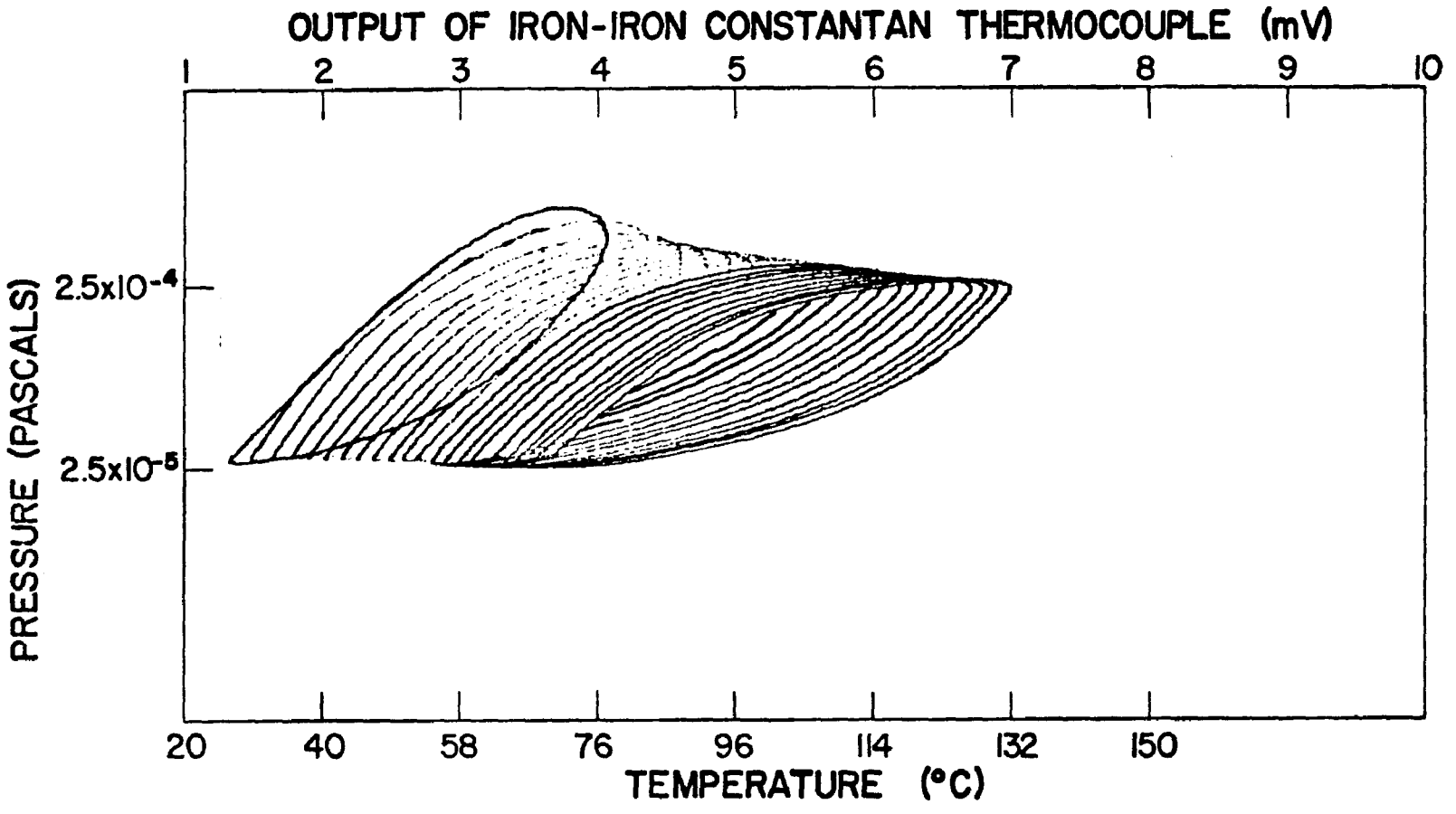

Figure 3.9 Pressure temperature plot of MBE station during bake-out.

2. The carrier profile is smeared by the Debye length, given by

$$L_D = \sqrt{\frac{2\varepsilon kT}{q^2 N_{DB}}} \qquad (3.4)$$

where

ε is the permittivity of the semiconductor.

k the Boltzman constant.

T temperature in °K.

q the electronic charge.

N_{DB} the doping concentration.

Figure 3.9 shows the behavior of Debye length with doping. It is seen that at dopings around $10^{15}/cm^3$ L_D may be several thousands of angstroms. Several algorithms have been developed to obtain the best estimate of the true change profile in the presence of sudden doping changes. Let us now derive a limiting profile where carrier profiling will in fact read the true profile.

Since the profile is smeared by the Debye length, let us assume that the method reads true if the doping level does not change faster than the Debye length, which Schockley[78] shows to be distance over which the electric potential may decay be a factor of 1/e, i.e.

$$\frac{dN}{N} \leq \frac{dx}{L_D} \qquad (3.5)$$

Substituting for L_D we get

$$\frac{dN}{N\sqrt{\frac{2\varepsilon kT}{q^2 N}}} = dx \qquad (3.6)$$

$$\frac{dN}{N^{3/2}} = \sqrt{\frac{2\varepsilon kT}{q^2}}\, dx \qquad (3.7)$$

Using the boundary condition that $N(x = 0) = N_0$ we get an integration

$$\frac{1}{N^{1/2}} = \frac{1}{N_0^{1/2}} - \sqrt{\frac{2q^2}{\varepsilon kT}}\, x \qquad (3.8)$$

This simplifies to

$$\frac{x}{L_{DO}} = \frac{1}{2}\left[1 - \left(\frac{N_0}{N}\right)^{1/2}\right] \qquad (3.9)$$

where x is the distance over which a transition from a low level N_0 to a high level N may be made with confidence that the carrier profile does in fact read the doping profile. L_{DO} is the Debye length at the low doping end. We have plotted the expression (3.7) in fig.10. Typically to achieve a "sudden" change in levels of over a factor of 10^3 we need about $x = \frac{1}{2} L_{DO}$ for carrier profiles to read true. (This is obtained from eqn. 3.9). In case of $N_0 \equiv 10^{14}$ this could be as large as a few thousand angstroms.

Thus C - V profiles suffer a disadvantage when trying to measure very sharp profiles. Further, actually carrying out a C - V profile requires that a method be available to deplete into the semiconductor. This may be done either by a p - n junction with the side not to be profiled much more highly doped than the side to be profiled or by a Schottky diode. The depth to which the semiconductor can be profiled is limited to the depletion width at breakdown. At doping levels of 10^{16} cm^{-3}, this could be as high as $3\ \mu$ while at $10^{18} cm^{-3}$ it could

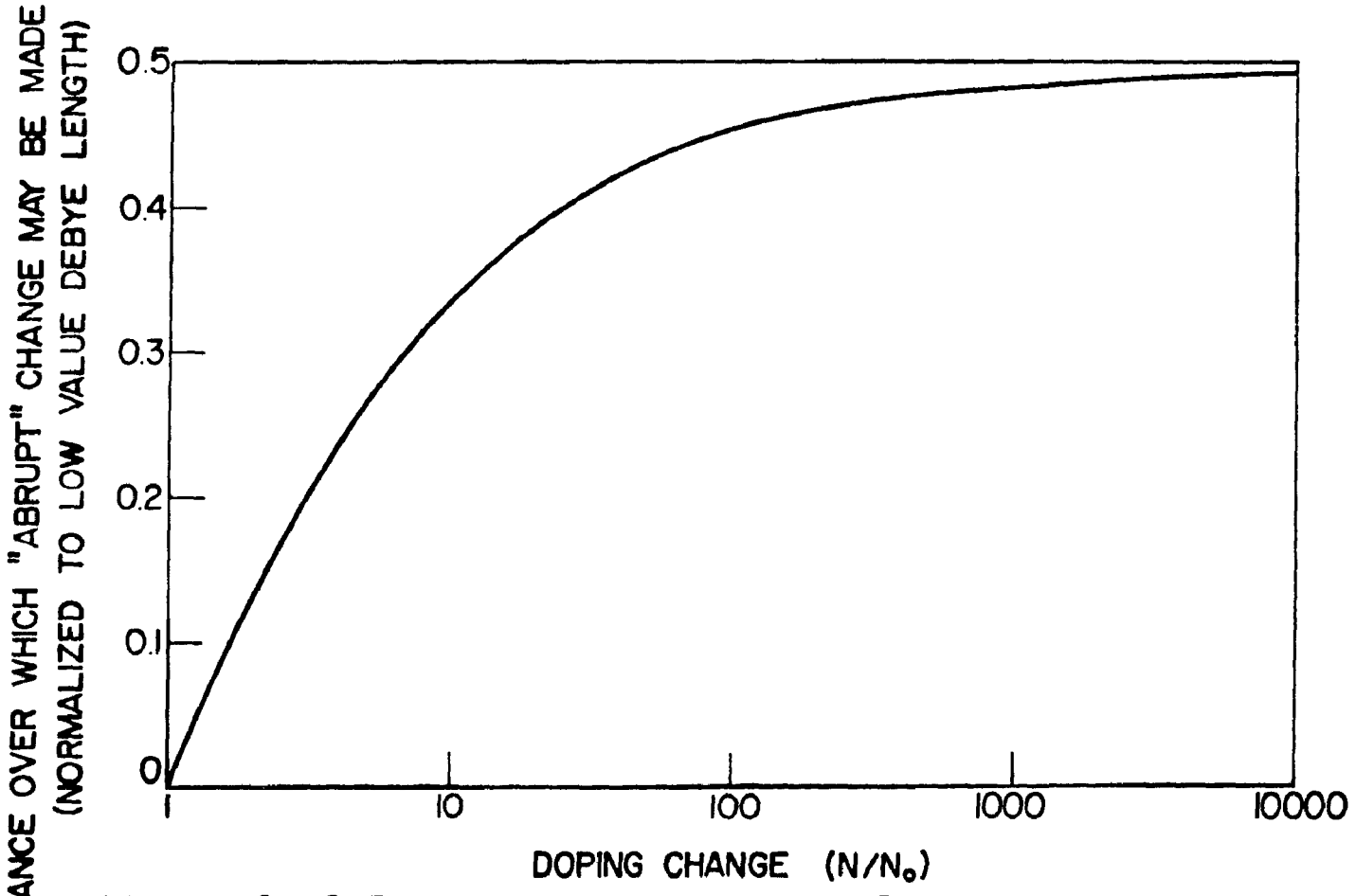

Figure 3.10 Distance over which a "sudden change" in doping may be achieved with carrier profiling. Reading true doping profile distances are in terms of DEBYE length at $a=0$.

be as low as 800 Å in the ideal case. In practice breakdown occurs sooner. In addition, the region near the junction may not be meaningfully profiled on account of the built-in voltage due to which there is a built-in depletion region. When the low doping is about $10^{15}cm^{-3}$ and the high level $\geq 10^{18}$ this unprofilable distance could be a fair fraction of a micron.

3.18.3. Resistivity profiling with anodic sectioning[50]

The theory of oxide growth and removal has been discussed in great detail. We use this technique extensively because of its resolution capability in spite of the Debye length smearing effects discussed above. We stress here that Debye length effects apply here, however certain cases arise which permit the above limitation in resolution to be circumvented. Consider for example the step profile shown in Figure 3.11. Using the notation of S.M. Sze[51], consider the potential at $x = x_0$ where the sudden doping change occurs. This is given by

$$\psi_{x=x_0} = \psi_0 \tag{3.10}$$

Consider the case when the surface potential is fixed at a value ψ_s by surface states. Then the number of free carriers in the region bounded by $\psi = \psi_s$ and $\psi = \psi_0$ is given by (due to a change in ψ from 0 to ψ_s)

$$\Delta p = \frac{q\, p_{p0} L_D}{2KT} \int_{\psi_s}^{\psi_0} \frac{(e^{\beta\psi} - 1)}{F(\beta\psi, n_{p0}/p_{p0})}\, d\psi \tag{3.11}$$

$$\Delta n = \frac{q\, n_{p0} L_D}{2KT} \int_{\psi_s}^{\psi_0} \frac{(e^{\beta\psi} - 1)}{F(\beta\psi, n_{0}/p_{p0})}\, d\psi \tag{3.12}$$

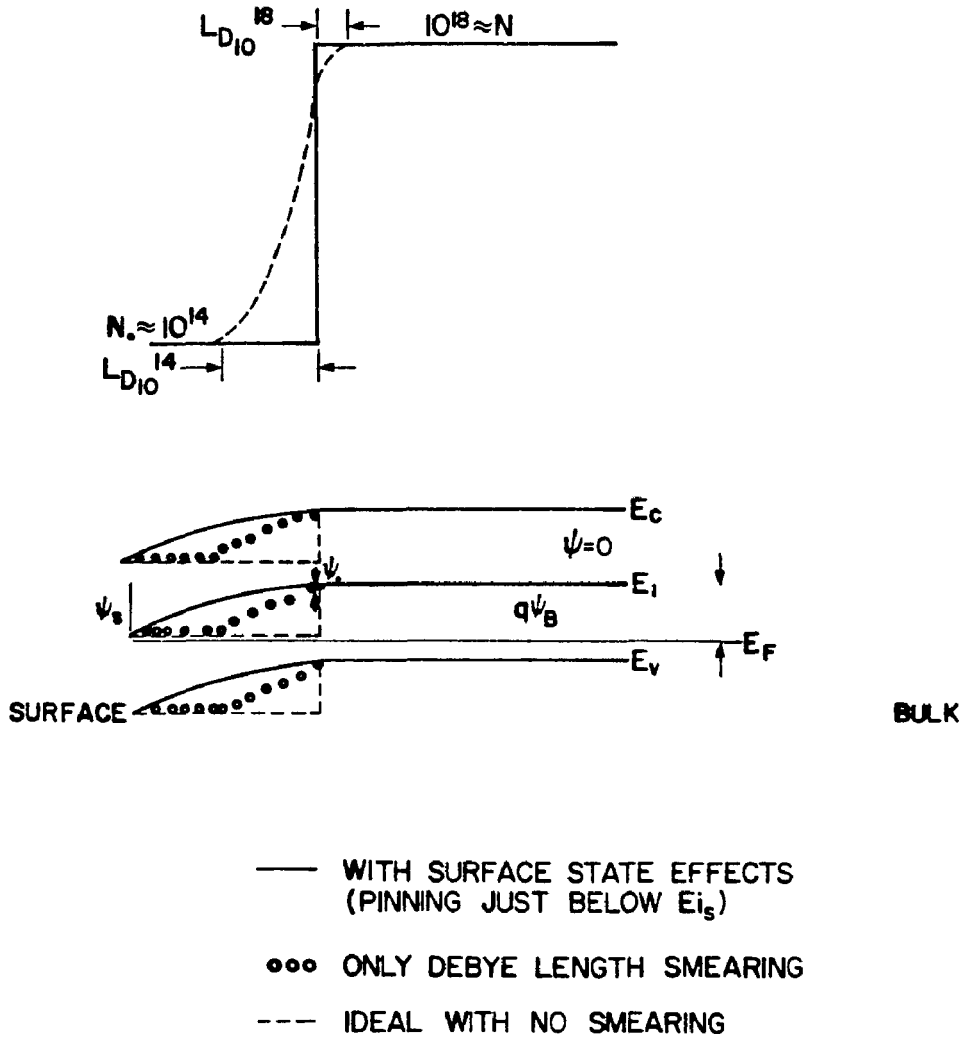

Figure 3.11 Illustrating smearing effects

where $p_{p0} = N$ and $n_{p0} = ni^2/N$ and $L_D = L_D$ for $x > x_0$.

We have shown using a computer program (Appendix II) that for very high surface state densities, where the Fermi level is pinned at the surface almost to the neutral value of these states (which is assumed to be near mid-gap), the value of ψ_0 is such that the integrals in Equations (3.11) and (3.12) are negligible, at least when the low side doping concentration is less than $10^{17}/cm^3$ and the high side doping concentration is greater than $10^{18}/cm^3$. This corresponds to saying that the lowly doped portion of the film is always depleted, a valid assumption for a large surface state concentration. It is clear that the change in conductivity, when the distance over which we have the lower value of dopant N_o is changed, is zero. This will be true as long as the surface potential is pinned at the same value.

During an anodic oxidation process the surface has adsorbed impurities which lead to a very high surface state density, causing the Fermi level at the surface to be pinned at a value probably just below the intrinsic level. Thus the conditions we assumed are true in practice. Typically the surface state density may be as high as $10^{15}/cm^2$. This means that most of the lowly doped film will be depleted and will not contribute to conductivity.

However, as the interface is reached significant changes in the band bending occur in the highly doped section of the film. These changes will contribute to changes in the conductivity. This bending takes place in distances comparable to the Debye length of the highly doped side and will therefore lead to some uncertainity in determining the exact location of the interface by an amount L_{D_N} (high doping Debye length), but this is a much smaller quantity.

We have computed by means of a computer program that this is in fact the case. The program which is listed in Appendix II, computes the change in free carrier concentration for the case where we have a step profile. We assume a uniform surface state density N_{ss} around the center of the bandgap (typically between $10^{13}/cm^2ev$ to $10^{15}/cm^2ev$) and compute (a) the Fermi level at the surface and (b) the total free carrier concentration for different depths x_0. This simulates the conductivity readings we would get on anodic etching of the surface layers. We find that in all cases where N_o lies between $10^{14}/cm^2$ and $10^{17}/cm^2$ there is no significant change in conductivity until we actually reach the boundary. It is only after we go through the doping discontinuity that the change is seen. Further, the resolution is limited to the Debye length in this highly doped segment.

This program thus confirms the qualitative arguments that we have presented. Also we find that for the surface state densities we have assumed the Fermi level pins to within 0.05 eV below the mid-gap. This of course depends on the neutral level assumed. We have assumed it to be mid-gap. Thus anodic sectioning has some advantages.

In general the film conductivity is given by

$$\sigma_n = \frac{(V/I)_n^{-1} - (V/I)_{n-1}^{-1}}{4.53\,\Delta t}$$

where $\frac{V}{I}$ is the 4 - pt probe reading, the suffix is the reading number and Δt the thickness removed. This can be measured to within 50Å. An accurate plot of resistivity versus depth can be obtained, and this may be translated into a doping profile if mobility data is available. The details of the experiment and the calibration used are discussed

elsewhere[50].

To sum up we conclude that in cases where abrupt transitions in doping are made one can, in spite of Debye length limitations, obtain spatial resolution of up to 100Å as long as it can be assumed that the Fermi level pins at the surface to a near mid-band value. The 100Å resolution is the limit of accuracy to which reproducible oxide films may be anodically grown in one setup.

3.19. Other Measurements.

Electrical measurements will also be made. These include deep-level trap measurements using transient capacitance techniques[52,53] and mobility measurements using Vaner Paw techniques[54].

3.20. Conclusions.

In this chapter we have described the system capabilities. We have also outlined the techniques we have used to obtain the information necessary to fully describe the incorporation characteristics of Ga in Si. We have not described the details of desorption studies; this will be the subject of the next chapter.

CHAPTER 4

Desorption Studies of Gallium From Silicon (111) Surfaces

4.1. Introduction

In a previous chapter we described the adsorption - desorption-incorporation model in detail. We study in this chapter the details of the desorption of gallium atoms from the silicon surface. The mean residence time τ_D, which is the average time the atom spends on the surface, is seen to have an important bearing on the doping profiles achievable in silicon MBE. This is so because τ_D is also the time the system takes to reach steady state when responding to a step change in dopant flux. Further, a detailed study of desorption yields useful information on the activation energy for desorption and the order of desorption. Using this information one can present models for the adsorption bond and comment on the amount of charge transferred.

In this chapter we first present a model for the silicon surface and indicate how the desorption may proceed. We then review available literature on desorption from silicon surfaces. Finally we present our results and deduce the parameters of desorption for our case.

4.2. The Model.

We consider a gas molecule (with thermal energy $\sim \frac{1}{20}$ eV) approaching a solid surface. As it approaches the surface (See Figure 4.1) it begins to feel the influence of the surface potential. We have assumed that the molecule is normally incident, and that there is no activation energy for adsorption. As the molecule approaches the surface it is drawn towards it via the attractive potential and begins to

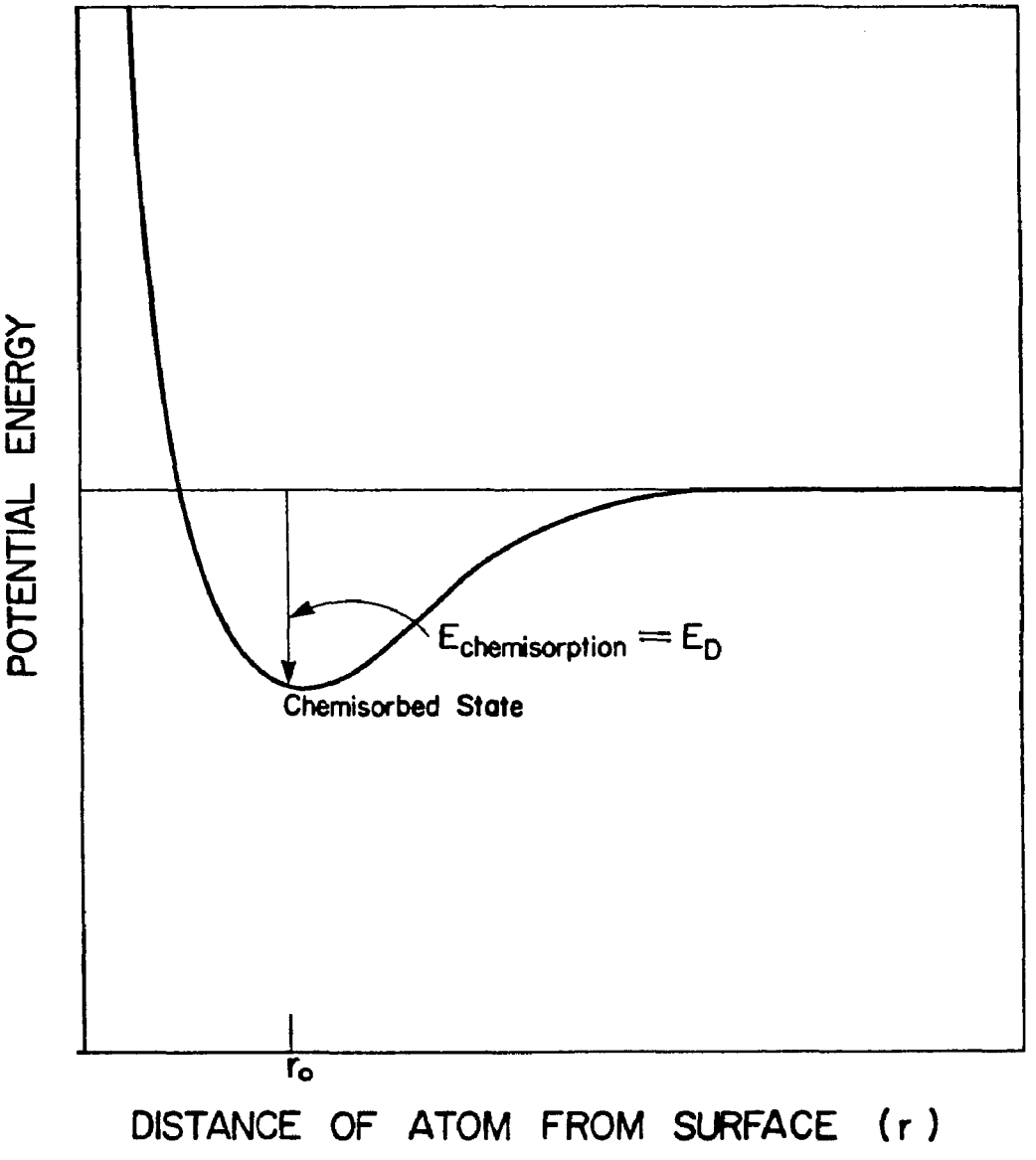

Figure 4.1 Potential energy of incident dopant atom near surface

lose potential energy. As this happens the molecule also gains kinetic energy and soon finds itself at the bottom of the surface potential well at r_0 with a kinetic energy equal to E_D. This kinetic energy causes the molecule to vibrate in the potential well, and it is obvious that the molecule could very well escape. In fact, the higher entropy associated with the molecule being in the gas state would tend to favor its desorption.

While vibrating in this potential well the molecule can launch optical phonons into the lattice (primarily in modes characteristic of the surface) and lose energy. The time it takes for this energy dissipation to occur is very short, and in most cases the process may be considered instantaneous. (Typically it is one time period or about 10^{-13}sec).

It is possible, under certain special cases, that the incident atom may not transfer its excess kinetic energy to the solid. It may bounce back without coming to equilibrium with the surface. This is commonly referred to as incomplete accommodation.

The incident atom/molecule is in general of different temperature than the surface. Let us call the surface temperature T_s and the atom temperature T_a. The temperature of the atom that desorbs is in general T_d. If the atom has been completely accomodated it comes to equilibrium with the surface and acquires a temperature T_s. Now if for some reason it acquires energy to surmount the potential well it escapes with a temperature T_s. If on the other hand the accomodation is not complete, the temperature of the desorbed atom will in general be different from T_s i.e.,

$$T_s \leq T_d \leq T_a$$

The quantity

$$\alpha = \frac{T_a - T_d}{T_a - T_s} \qquad (4.1)$$

is called the accommodation constant and is unity for complete thermal accommodation.

In the case of atoms which accommodate completely with the surface, the desorbed flux is totally random. This is because the atoms have no memory of their incident directions. This is obviously not the case when $\alpha \neq 1$. In fact for $\alpha = 0$ $(T_d = T_a)$ the atoms are specularly reflected.

In most cases which we will encounter complete thermal accommodation takes place. This may be verified in several ways. The desorbed flux at higher surface temperatures may be tested for being lambertian or more simply, if a residence time in excess of that needed for achieving thermal equilibrium is measured, this is proof that the accommodation is complete.

In the case of non-activated adsorption, the heat of adsorption is also the desorption activation energy E_D used in Chapter 3. The order of magnitude of E_D gives a clue to the nature of the physical processes that lead to the surface potential well. Generally if E_D is below about 0.5 eV the process is one of physical attraction, such as Van der Waals forces, while values in excess of this are usually ascribable to chemical interactions. The latter is more important and also in most situations the real case[79].

Levine and Gyftopoulos[59] have considered the case of surfaces covered by metallic adsorbates. Starting from the premise that the adsorbate surface bond may be decomposed into an ionic component and a covalent component they proceed to obtain expressions for these contributions. Thus

$$E_D = E_{Di} + E_{Dc} \tag{4.2}$$

where

E_{Di} is the ionic component

E_{Dc} is the covalent component.

Now E_{Di} can be expressed as

$$E_{Di} = F\phi_e(1 + \delta) \tag{4.3}$$

where

$$\delta = F(e^2|r_0 - V_f)|\phi_e \tag{4.4}$$

Here F is the fraction of charge transferred to the substrate. r_0 is the internuclear distance between the substrate and adsorbate. This is slightly different than the internuclear distance of two atoms in the gas phase a_0. Ponec, Knorr and Černy[60] show that $r_0 = 0.765a_0$. This is because of the effect of subsurface layers.

Also V_p is the ionization potential of the adsorbate and ϕ_e is the electron work function of the composite surface.

In the common case where δ is small

$$E_{Di} \approx F\phi_e \tag{4.5}$$

ϕ_e, the work function of the composite surface, is given by the following expression[60]

$$\varphi_e = \phi_{si} - (\varphi_{si} - \phi_d)(1 - \mathcal{G}(\theta)) \tag{4.6}$$

where θ is the coverage in monolayers, and $\mathcal{G}(\theta)$ in the shape factor usually taken to be

$$\mathcal{G}(\theta) = 1 - 3\theta^2 + 2\theta^3. \tag{4.7}$$

The covalent contribution to the desorption energy E_{Dc} arises from mutual pairing of the valence electrons of the substrate and adsorbate atoms. We can only estimate the value of E_{Dc} as the problem is very difficult to solve exactly. A semiemperical estimate uses the sublimation energy of both the materials, the angular strength of their valence orbitals (which depends upon angular orbital quantum number), and the valence charge that is shared.

Thus we get

$$E_{DC} = \left\{ \left[E_{sub_s} \cdot E_{sub_a} \right] \cdot \left[\frac{4S_s^2 S_a^2}{(S_s^2 + S_a^2)^2} \right] \cdot \left[\frac{4q_s q_a}{(q_s + q_a)^2} \right]^{\frac{1}{2}} \right\} \tag{4.8}$$

Here the subscript s refers to the substrate and a refers to the adsorbate.

E_{sub}	is the elemental sublimation energy
S	is the angular strength of the orbitals
q	is the valence charge shared.

The values of the quantities of interest are available in the literature and have been tabulated in Table 4.1.

TABLE 4.1

DATA USED IN CALCULATIONS FOR DESORPTION ENERGY

Element	E_{sub} (Sublimation energy)	ϕ (electron wk. ftn.)	S (orbital strength)	q
	eV	eV		
Si	4.63	4.6	2.67	4
Ga	2.87	4.2	1.58	3

We are now in a position to calculate the desorption energy for gallium from silicon as a function of coverage. We note that the variation of E_D with coverage will be large only if the ionic component of E_{Dc} is dominant. Variation of the ionic component occurs because of changes in the work function and charge showed as a function of coverage. It is assumed that the covalent component does not change with coverage.

We now compute the covalent component of E_D for gallium as

$$E_D = \left[(E_{Sub})_{si} (E_{Sub})_{ga} \cdot \frac{4 S_{si} S_{ga}}{(S_{si}^2 + S_{ga}^2)^2} \cdot \frac{4 q_{si} q_{ga}}{(q_{si} + q_{ga})^2} \right]^{\frac{1}{2}} \qquad (4.9)$$

$$= 3.11 \text{ eV. (independent of coverage).}$$

The fraction of charge transferred is a function of the surface coverage and may be estimated from

$$F = \frac{M_2}{eR\cos\beta} \tag{4.10}$$

where $R\cos\beta$ is the surface double layer thickness e is the electronic charge . M_2 is the dipole moment of the surface structure and has been shown by Gyftopolous and Levine (Ibid) to be

$$M_2 = \frac{2.03 \times 10^{-18} \cos\beta(\phi_{si} - \phi_{ga})\mathrm{C}(\theta)}{(1 + \alpha|R^3)} \tag{4.11}$$

where α is the electronic polarizability. We thus deduce

$$F = \frac{0.422(\phi_{si} - \phi_{ga})\mathrm{C}(\theta)}{R(1 + \alpha|R^3)} \; . \tag{4.12}$$

Using appropriate units (R in angstrons, α in angstrons^3, ϕ in eV) F is a dimensionless number which is a fraction of the electronic charge.

The ionic component to the desorption energy may be written as

$$E_{di} = F\phi_e - F^2V_i + \frac{F^2e^2}{R} \tag{4.13}$$

$$\simeq F\phi_e \tag{4.14}$$

when the fractional charge transferred is small.

TABLE 4.2

ADSORPTION ENERGY AS A FUNCTION OF COVERAGE

θ	$\zeta(\theta)$	ϕ_e	F	E_{Di}	E_{DC}	E_D
10^{-3}	1	4.6	.025	0.12	3.11	3.23
10^{-2}	1	4.6	.025	0.12	3.11	3.23
0.1	0.97	4.58	.025	0.11	3.11	3.22
0.2	0.90	4.56	.024	0.11	3.11	3.22
0.4	0.65	4.46	.017	0.08	3.11	3.19
0.6	0.35	4.34	.004	0.02	3.11	3.13
0.8	0.1	4.24	.003	0.001	3.11	3.11
1.0	0	4.2	0	0	3.11	3.11

Table 4.2 shows our calculations for E_D as a function of coverage. It shows a slight decrease in desorption energy (about 4%) with coverage . We also see that the amount of charge transferred when gallium is adsorbed on silicon is extremely small (less than 0.025 electron). This is understandable for the following reason:

The ionization energy V_i for Ga is 6.0 eV from the vacuum level. The silicon band edge is about 4.5 eV from vacuum. There will be atomic level displacements of these energy levels on adsorption, but in general these will be less than a few tenths of an eV [103]. Thus the Ga level is still in the continuum valence band of silicon and would therefore be quite stable in a neutral condition.

4.3. Experimental Techniques

4.3.1. Isothermal desorption spectroscopy.

Several methods have been developed to measure the desorption kinetics of adsorbates. Very versatile is the earliest proposed by Redhead[62] called temperature desorption spectroscopy. Here the surface temperature is ramped after predepositing the adsorbate, and the desorbing flux is observed as a function of time. One may determine the activation energy for desorption from the temperature at which the peak desorbing flux occurs. Kawazu and others [55-58] have used this technique to study different phases of bismuth on silicon. One does need, however, to assume the vibrational frequency of the adsorbed atom.

4.3.2. Modulated beam desorption spectroscopy.

This technique used by Arthur[64] and Nguyen[32] employs pulsing the beam and observing the rise and decay of the desorbing flux with time. Using this technique one can obtain kinetic coefficients for desorption orders that are greater than unity provided one can detect the desorbing species as clusters (for example, by using a mass spectrometer).

4.3.3. Isothermal desorption with Auger Electron Spectroscopy.

All the techniques mentioned so far look at the desorbed beam to deduce the desorption kinetics of the system. It is also possible to observe the portion of the undesorbed adatoms and deduce the desorption kinetics - the method used by Florio and Robinson[66] and

also by Davis et al [67]. We have used this method extensively to determine the desorption kinetics of gallium from silicon.

In this technique, as in others, an accurate calibration of the dopant flux is obtained first. The sample is then submitted to this flux at a rather low temperature, such as room temperature, for a given period of time. At the low temperature used all of the incident flux sticks to the sample surface. As will be seen later it is thus possible to obtain silicon surfaces with different concentrations of dopant on each surface. This surface concentration N_{DS0} is then the initial dose for subsequent desorption experiments. The surface concentration itself is measured from the peak-peak intensity of the Auger signal characteristic of the element being desorbed.

The sample surface is then quickly elevated to a desired temperature at which the desorption studies are to be made. It is important that this step take very little time compared to the residence time of the surface species at the temperature of interest.

Several considerations dictate the maximum heating rate permissible. These include the programmability of the substrate heater and the maximum bearable thermal strain. We have used a step current to heat our sample. As the activation energy for desorption is high (> 2.0 eV) the temperature sensitivity is also appreciable. Thus for an experiment performed at 620 °C, the time spent by the sample at temperatures up to about 600 °C may be neglected. The time spent at temperatures close to the temperature of interest can be minimized by causing the current pulse to overshoot slightly and then retract to the steady state value. We have used this technique.

It is our observation that as long as the residence times are in excess of 30 seconds or so this method of heating works very well. Even in other cases the method may be applied, though interpretation becomes difficult. We need to have a plot of temperature versus time and obtain the desorption coefficient by an iterative process from the expression

$$N_{DS} = N_{DSO}\exp[-\int K_D dt] \qquad (4.15)$$

where a reasonable value of activation is assumed and the time dependence of $K_D(t)$ is deduced from the temperature dependence and temperature-time plot. Such a process is no doubt laborious and also approximate.

The considerations for bringing the sample temperature down are similar, though less controllable. Fortunately the thermal loss mechanisms are quite rapid and the cooling rates are fast. Figure 4.2 shows a typical temperature plot using a non-linear scale to accent the region of interest. We have estimated that this pulse is equivalent, with respect to the total desorption it produces, to a one minute pulse at $T_S = 600\,°C$.

We have been able to obtain fairly consistent results in the temperature range between 500 and 700°C. At temperatures in excess of these we can get only estimates by a combination of other techniques to be described in due course.

It should be noted that in the case of extremely long time constants in excess of few hours it may not be possible to desorb all the gallium. In such cases only a partial desorption is effected and

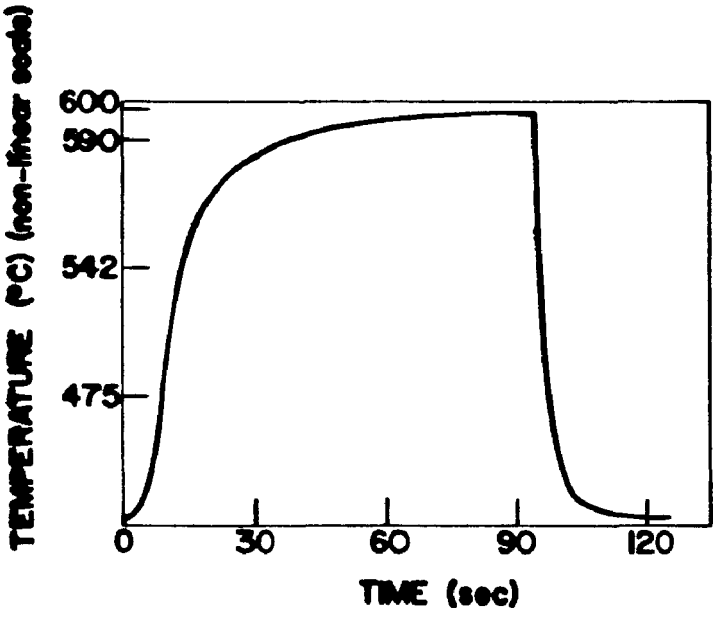

Figure 4.2 A typical substrate temperature verses time characterestic. This profile can be considered equivalent to a one min. pulse at 600°C.

the slopes deduced therefrom.

4.4. Results.

We show in fig. 4.3 the results of our auger peak-peak heights as a function of the gallium deposited on the silicon surface. The silicon surface (111) was cleaned by the process already described in Chapter 3. It was cleaned in situ using the technique of galliation also described earlier. The gallium flux was callibrated using fig. 3.9. We have assumed that a monolayer is about 10^{15} atoms/cm^2. This is rather arbitrary but is only slightly different from the widely accepted value of 8×10^{14} atoms/cm^2 based on the unsatisfied bands on a (111) surface.

4.4.1. Room temperature studies

The sample was held at room temperature and a gallium beam directed towards it. At this low temperature the desorbed beam is negligible and one can assume that every gallium atom incident on the silicon surface sticks.

We have measured the gallium peak at 48.6 volts, which corresponds to $L_1L_2M_2$ transition. The silicon peak was measured at 92 V, which is an LMM transition. The escape depth of electrons for most materials at this energy is on the order of 3 to 5 Angstroms[69], or typically 1 monolayer. Hence on deposition of a uniform layer of gallium one would expect the silicon signal to decrease exponentially with a characteristic distance of about 3 - 5Å, and almost completely extinguish after 4 - 5 monolayers of gallium have been deposited. The gallium auger signal should also rise and achieve its saturated value

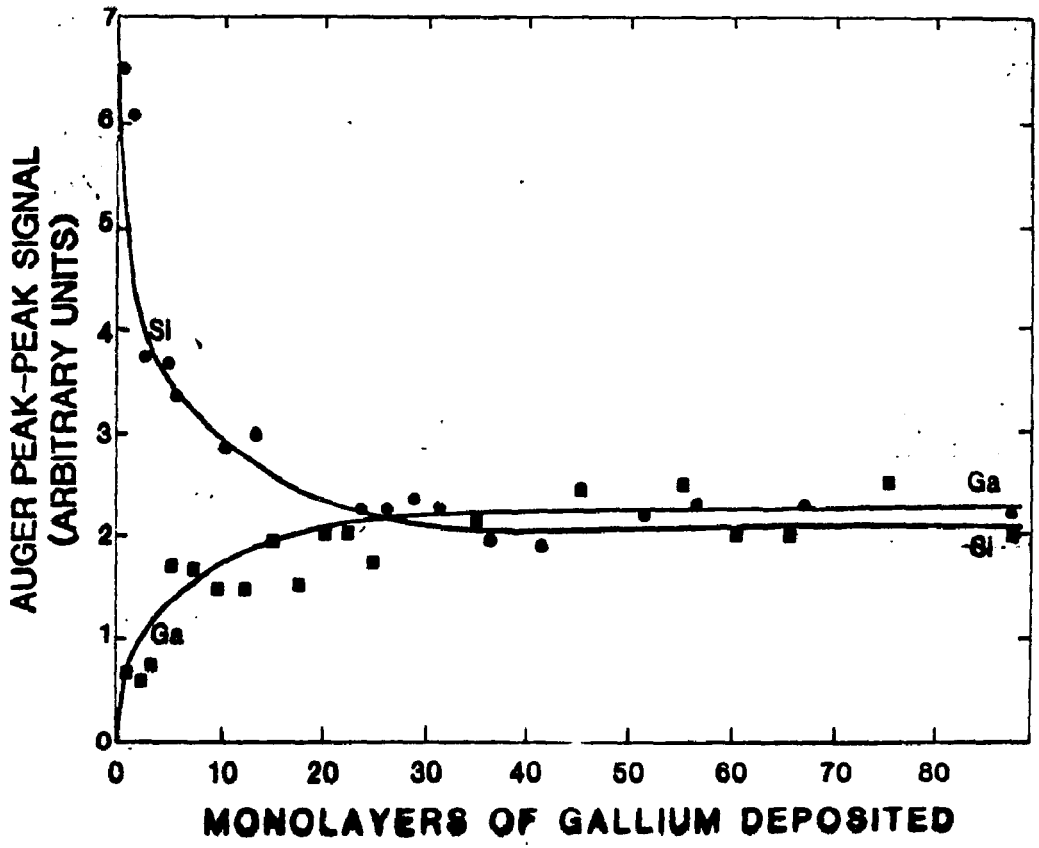

Figure 4.3 Gallium and Silicon auger strengths as a function of Gallium dose at room temperature

with about the same dose.

Fig. 4.3 shows that nothing of this sort happens. The silicon signal does drop initially to about a third of its initial value but very slowly with a characteristic distance of approximately 30Å . The gallium signal also saturates at about the same rate.

It is clear then that the gallium does not go down as a uniform monolayer over the silicon. It appears from fig. 4.5 that the silicon auger signal might be decreasing but this is not unambiguous.

These results may be explained in one of two ways:

The gallium may be clustering on the silicon surface, causing a good portion of the silicon to be exposed at the surface. This sort of heterogeneous clustering has been seen in several systems[70,71], and is a common feature when metals are deposited on dissimilar surfaces.

Alternatively, the gallium forms a phase with the silicon such that a third or so of the phase surface consists of silicon atoms. Wright[84] indicates that the surface morphology does improve and smoother surfaces (as evidenced by streaked RHEED patterns) are generated after prolonged galliation with no silicon growth. This may indicate the occurance of some silicon regrowth, similar to liquid phase epitaxy where silicon dissolved in a silicon-gallium phase is transpated across the surface in this melt and then deposited to obtain smoother surfaces.

However, this does not preclude island formation as the process could also occur with island formation. If islands do form, we expect them to be about 1000Å across. (This has been seen in SEM pictures, though this evidence is not totally reliable due to the fact

that the gallium deposited surface was exposed to air in the process.) Further, the process of galliation would permit the clusters, if they do in fact form, to move. Knuth[72] shows that this is possible in some cases. If clusters do form, they move or form continually at different locations, otherwise the entire surface would not be reduced as we know it to be.

There is another piece of evidence to support island formation that we shall anticipate at this stage. Incorporation of gallium atoms, as we have mentioned, proceeds from the adsorbed surface gallium layer. The behavior of the incorporation rate with respect to the gallium flux may indicate the nature of the surface layer. First of all, we expect that if the gallium formed a uniform monolayer on the surface the incorporation would completely saturate at the gallium flux that produces this monolayer coverage. This is not observed. We find that saturation sets in even before this coverage is reached and appears to obey an $F_D^{-2/3}$ power law with flux. This is consistent with a rate determining step where the atom supply comes from the perimeter of the base of a hemispherical island. We shall discuss this in more detail when we discuss the subject of saturation.

During the deposition of the gallium at room temperature the LEED and RHEED patterns blur out and completely fade away when about 4 or 5 monolayers of gallium have been deposited. They do not reappear with their original sharpness until all of the gallium has been removed from the surface by heating.

4.4.2. Desorption studies.

We have shown in the above sections that it is possible to relate the Auger peak-peak intensity of the gallium signal to the amount of gallium present on the surface. If we assume now that this calibration chart is valid even after the surface has been cycled to a higher temperature, then we can use it to determine the amount of gallium left undesorbed on the surface after heating it to a particular temperature for a specified time. As an example, we show in figure 4.4 the time evolution of the gallium auger signal translated into monolayers of gallium left on the surface after being heated to a nominal temperature of 600°C (the temperature uncertainty being about 10°C).

Fig. 4.5 shows the same data on a log plot of the gallium surface concentration. One can see that the fit to an exponential decay with time is very good. Similar experiments were performed between 500°C and 400°C. In all cases the coverage used was between 0 and 10 monolayers and the fit to a single exponential decay in this range was good, proving the first order nature of gallium desorption from silicon.

Fig. 4.6 shows a plot of this data. Here we have plotted K_D in equation (2.2) versus reciprocal temperature. We find that we can fit this data to a straight line as shown.

These data points were also verified by measuring the time required for the LEED pattern to reappear after heating at the temperature of interest. This time period is approximately four residence times. The results of this test corroborated our Auger results.

The data points at about 800°C were determined by estimation of the time required to obtain a clean silicon surface by heating to that

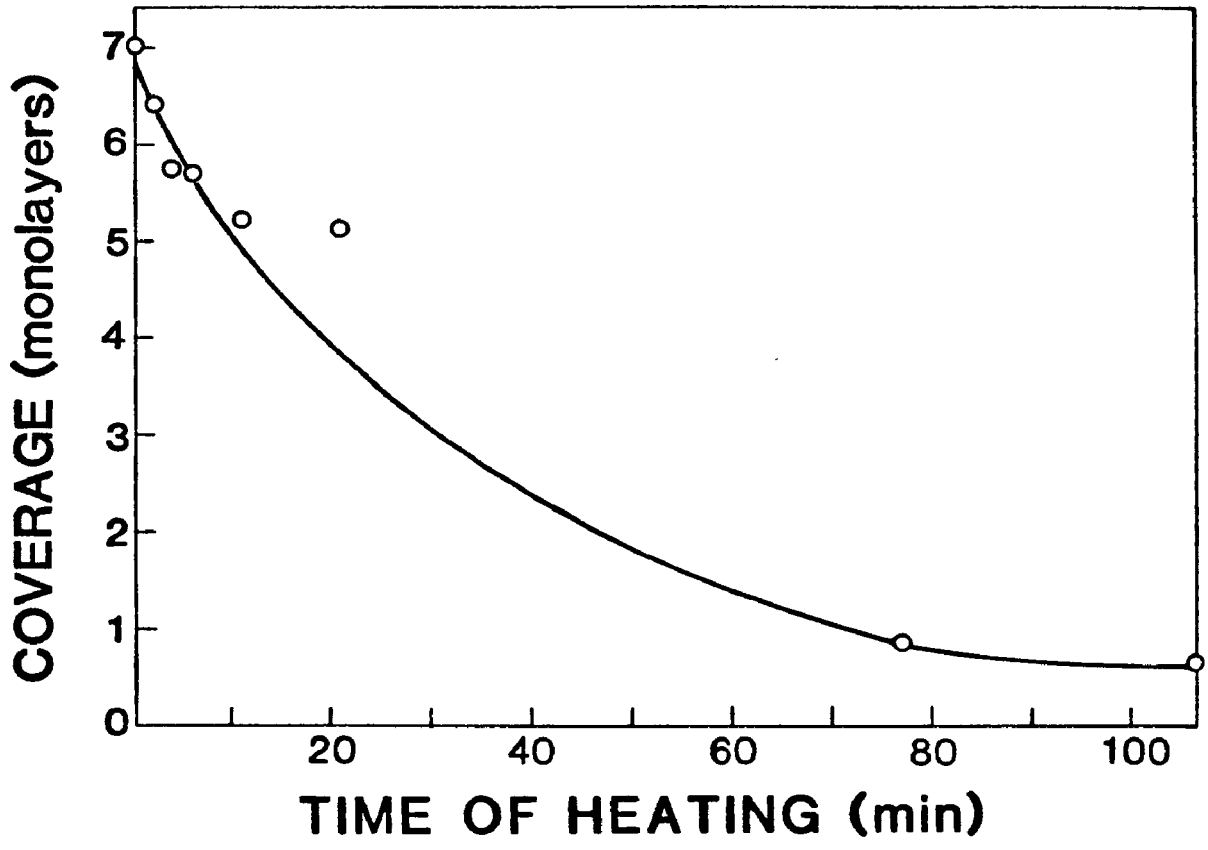

Figure 4.4 Coverage verses time of heating at 600°C. Coverage varies between 7 and 0.5 monolayers.

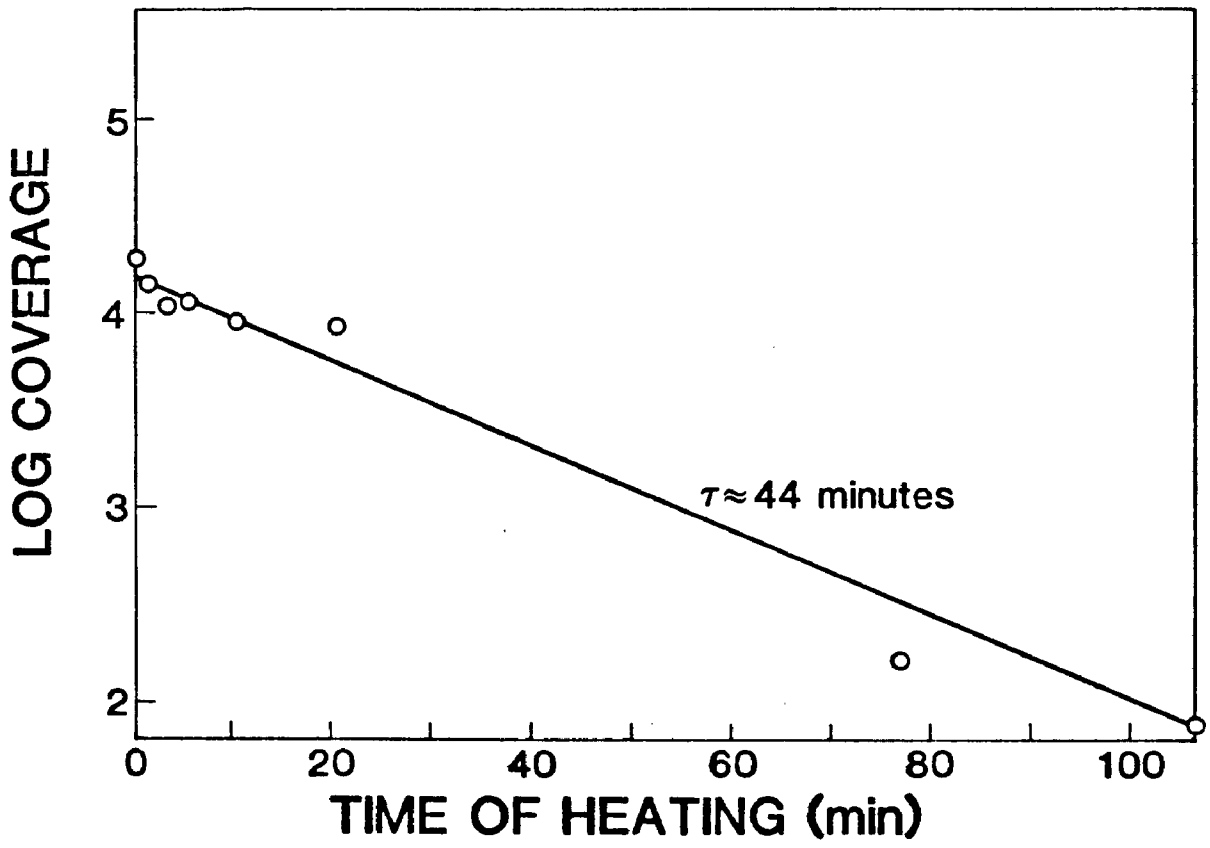

Figure 4.5 Log coverage verses time of heating at 600°C. Coverage varies between 7 and 0.5 monolayers.

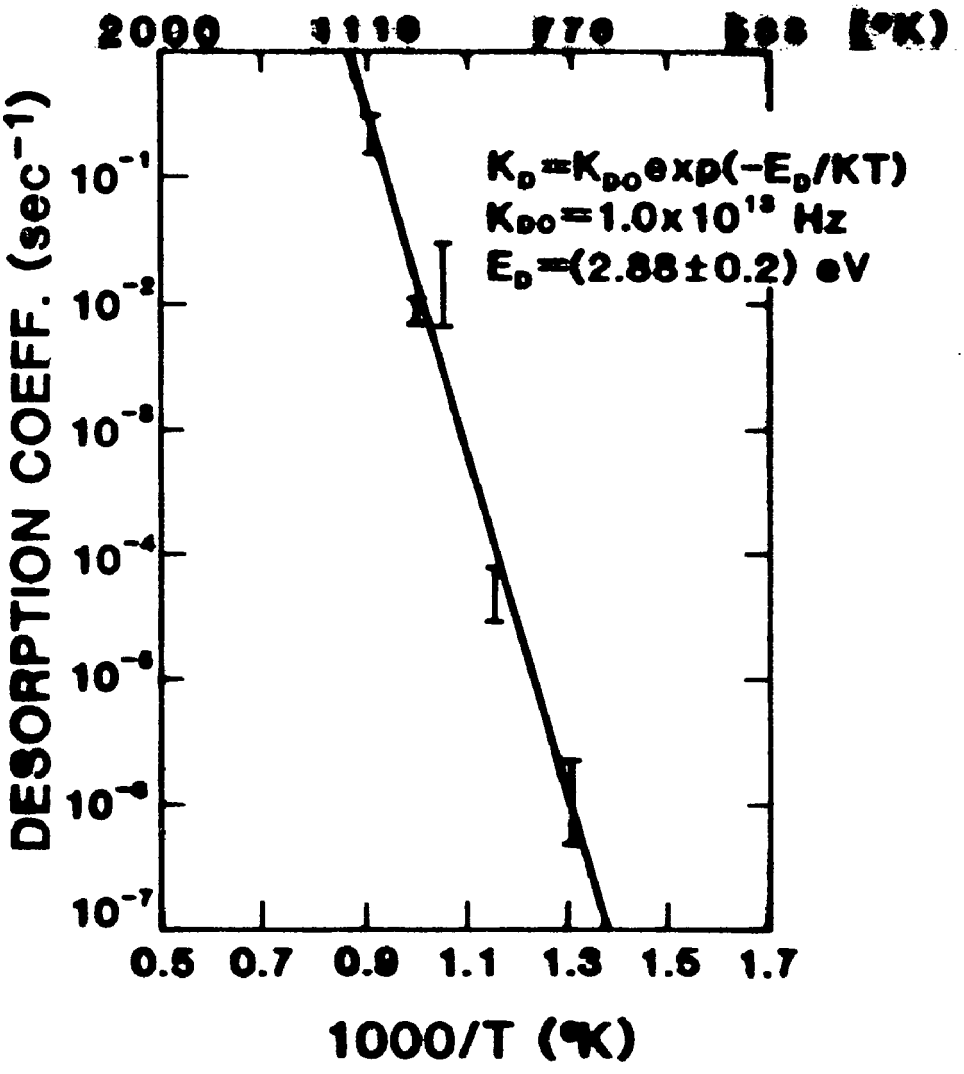

Figure 4.6 Desorption coefficient as a function of temperature

temperature (~ 3 sec) after depositing gallium.

We find that K_D may be expressed as

$$K_D = K_{D0}\exp(-E_D/kT) \qquad (4.16)$$

with the preexponent $K_{D0} = (1 \pm 0.9) \times 10^{13}$Hz and

$$E_D = (2.88 \pm 0.2)\ \text{eV}. \qquad (4.17)$$

Figure 4.7 shows the reciprocal of K_D, which is the residence time of the gallium atoms on the silicon (111) surface, plotted versus $1/T$. The equilibration distance λ may be ignored at this stage.

4.5. Discussion of Results.

The preexponent K_{D0} is determined to have a value close to the optical phonon vibrational frequency at the surface. This is to be expected. However, the value of K_D is difficult to estimate as it is very sensitive to small changes in E_D. As such there may be an order of magnitude uncertainty in this value.

The value of E_D obtained above is quite informative and gives us an idea of the nature of the Ga - Si adsorption bond.

Referring back to Table 4.2 we have computed that E_D should be between 3.1 and 3.2 eV for the coverage ranges considered here. Our value differs from this by less than 10%. This verifies that indeed the Ga - Si bond has very little ionic content and the electron transferred is certainly less than 0.025. This would imply that the adsorption energy would change very little with coverage - an observation we have made.

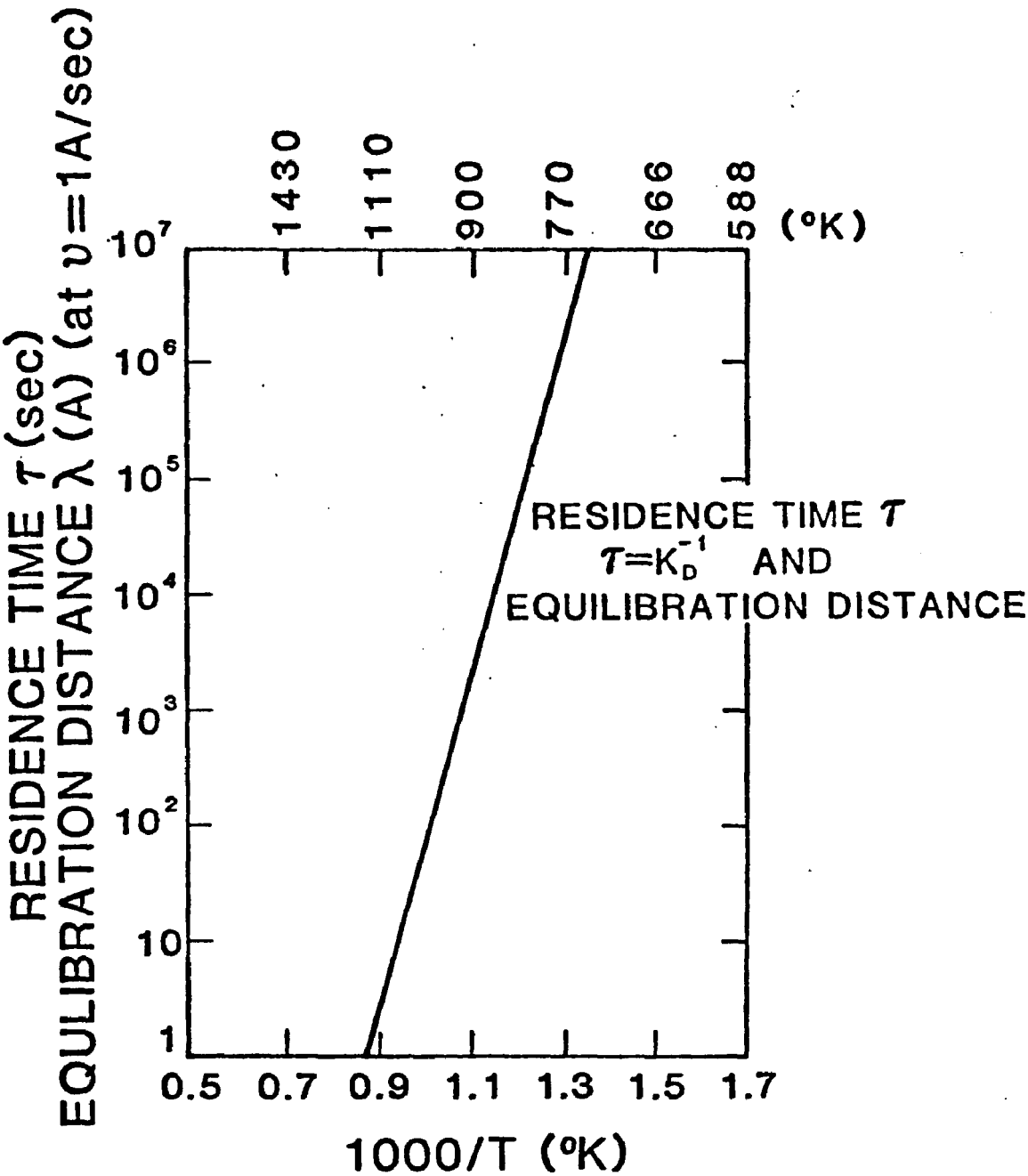

Figure 4.7 Residence time and equlibration distance as a function of temperature

Nguyen[32] has pointed out that in the case of predominantly covalent systems the dependence of K_D on coverage is a consequence not so much of the adsorption energy behavior but rather the behavior of the preexponent. The preexponent may be written as

$$K_{D0} = \frac{kT}{h} \exp(\frac{\Delta S_a}{K}) \qquad (4.18)$$

where

k is Boltzmann's Constant

h is Planck's Constant

ΔS_a is the entropy of adsorption

ΔS_a is the ratio of the partition functions of the initial and final states in the desorption reation.

4.6. Desorption Energy and Vapor Pressure Activation Energy.

We show in Table 4.3 the vapor pressure activation energy and the desorption energy of different elements from silicon. The results show that the two energies are very close in the case of certain elements. This might indicate that the desorption process for these elements takes place via the breaking of the dopant-dopant bond on the silicon surface rather than the dopant-silicon bond.

This would lend credence to the hypothesis that gallium does in fact form clusters on the surface. The difference in the two energies may be attributable to the effect of the silicon substrate.

4.7. Antimony Studies

Before concluding we mention that desorption studies were attempted on the Sb/Si system. The room temperature Auger plots for Sb on silicon are shows in fig. 4.8. The results are very similar to the gallium case. Both the Sb auger peaks (at 465 V and 395 V) increase exponentially and seem to saturate around 5 monolayers. The silicon peak shows the reverse behavior, but does not go down completely to zero.

The ratio of the two Sb peaks remains constant with coverage. This would imply that all the Sb is on the surface and no Sb is buried under the silicon, for if this were the case the lower energy signal would attenuate more.

Desorption studies on the Sb/Si system were not possible, as the residence time of Sb on silicon is extremely short at most useful temperatures. This is understandable because Sb has a very high vapor pressure, even at fairly low temperatures.

We do know however from the limited experimental evidence obtained that the desorption order is not unity. In fact we have deduced that p for Sb from Si may lie between 2 and 4. This is expected because Sb does exist in the form Sb_2 and Sb_4, predominantly the latter[38].

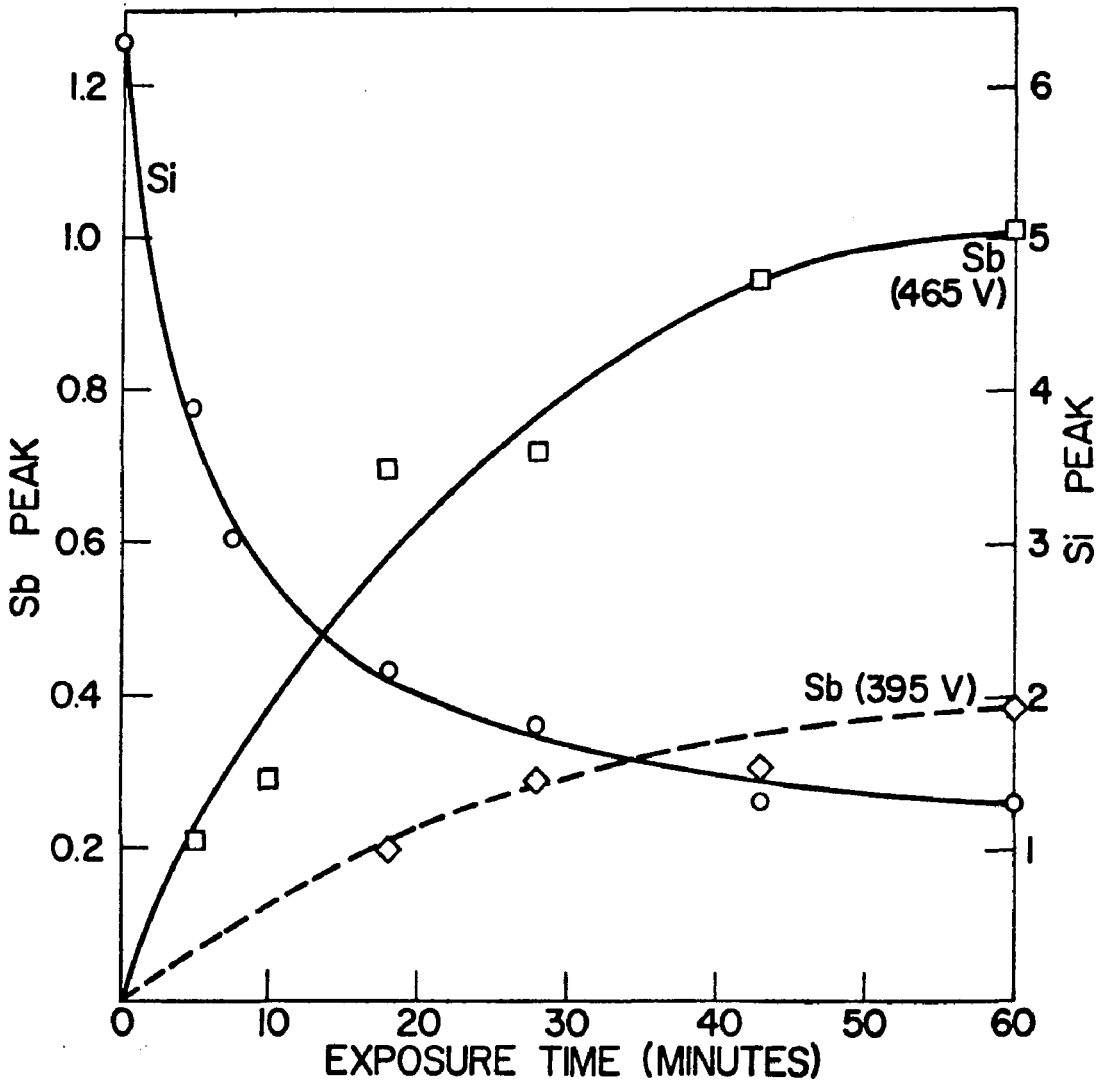

Figure 4.8 Antimony and Silicon auger peaks as a function of coverage at room temperature (10 min. of exposure produces a monolayer of antimony)

TABLE 4.3

VAPOR PRESSURE ACTIVATION ENERGIES AND

DESORPTION ENERGIES FROM SILICON

Element	Vapor Pressure[39] activation energy (eV)	Desorption Activation energy (from Si) (eV)
Si	4.52	4.52[39]
P	0.284	2.90[67]
Ga	2.66	2.88 (this work)
In	2.49	2.48[63]
Au	3.59	3.3[85]
Ag	2.92	2.87[86]

4.8. Conclusions.

We have discussed in this chapter the experimental details of gallium desorption from silicon (111) surfaces. The desorption energy of 2.88 eV is consistent with that predicted by the theory of Gyftopolous. Our indications are that the gallium probably clusters on the silicon surface. The desorption order for gallium from silicon is unity.

CHAPTER 5

Sticking Coefficient, Incorporation, Films and Profiles

5.1 Introduction

In the last few chapters, we have developed a kinetic model for dopant incorporation. We have explained the experiments designed to investigate the validity of this model. This chapter presents the results of these experiments which justify the model. We will also discuss in this chapter application of the process to various profiles We shall show how excessive lag times alluded to in chapter 4 may be reduced. We shall also discuss the electrical properties of our films and some of the devices, mainly p-n junctions, that we have made.

5.2 Sticking Coefficient:

The sticking coefficient has been introduced in Chapter 2 as the ratio of the incorporation rate for dopants to the incident flux once steady state has been reached. We have discussed that in the strict case a chemical rather than electrical identification of the concentration of the dopant species is required. However, such a method is costly and may be resorted to as a calibration check on electrical methods.

We shall discuss later that our mobilities are "bulk-like". We are therefore justified in using the Sze-Irvin curves to correlate the carrier concentration with resistivity measurements. This correlation is also corroborated by carrier profiling (C-V), which looks only at the carrier concentration without regard to mobilities.

There is the consideration that there may be incomplete ionization of dopants. Up to the highest gallium levels we have encountered ($<3 \times 10^{18}/cm^3$) this does not pose a serious problem. However, at very high Sb concentration ($\geq 10^{19}/cm^3$) incomplete ionization and bandtailing effects do take place. In these cases, the assumption that carrier concentration is equal to the doping level breaks down.

We now consider sources of error in the measurement of our sticking coefficient:

5.2.1 Error in Flux Measurement:

We have shown in chapter 3 that in the worst case, the flux may vary by a factor of 2. At unity sticking coefficients, this would translate into a 50% error. However, at lower sticking coefficients, the absolute error is down by the same factor as the sticking coefficient differs from unity. The absolute effect of the flux variations is therefore not as drastic.

5.2.2. Error in Carrier Concentration Measurement:

This arises from two parts: (1). from the error in mobility, which may be estimated to be $\sim$ 20%, and (2). from the uncertainty in resistivity measurement done using the 4-point probe technique [104]. The latter in turn depends on the resolution of the instrument, which in most cases of interest is as low as 1%, and also on the ability to obtain the same measurement repeatedly after raising and resetting the 4 probes. This we have seen to be about 5%, in the worst case. In most cases, we get identical readings. The variation may be caused by spatial variation, though this is a rather negligible effect. The more important reason for this variation is the damage the repeated

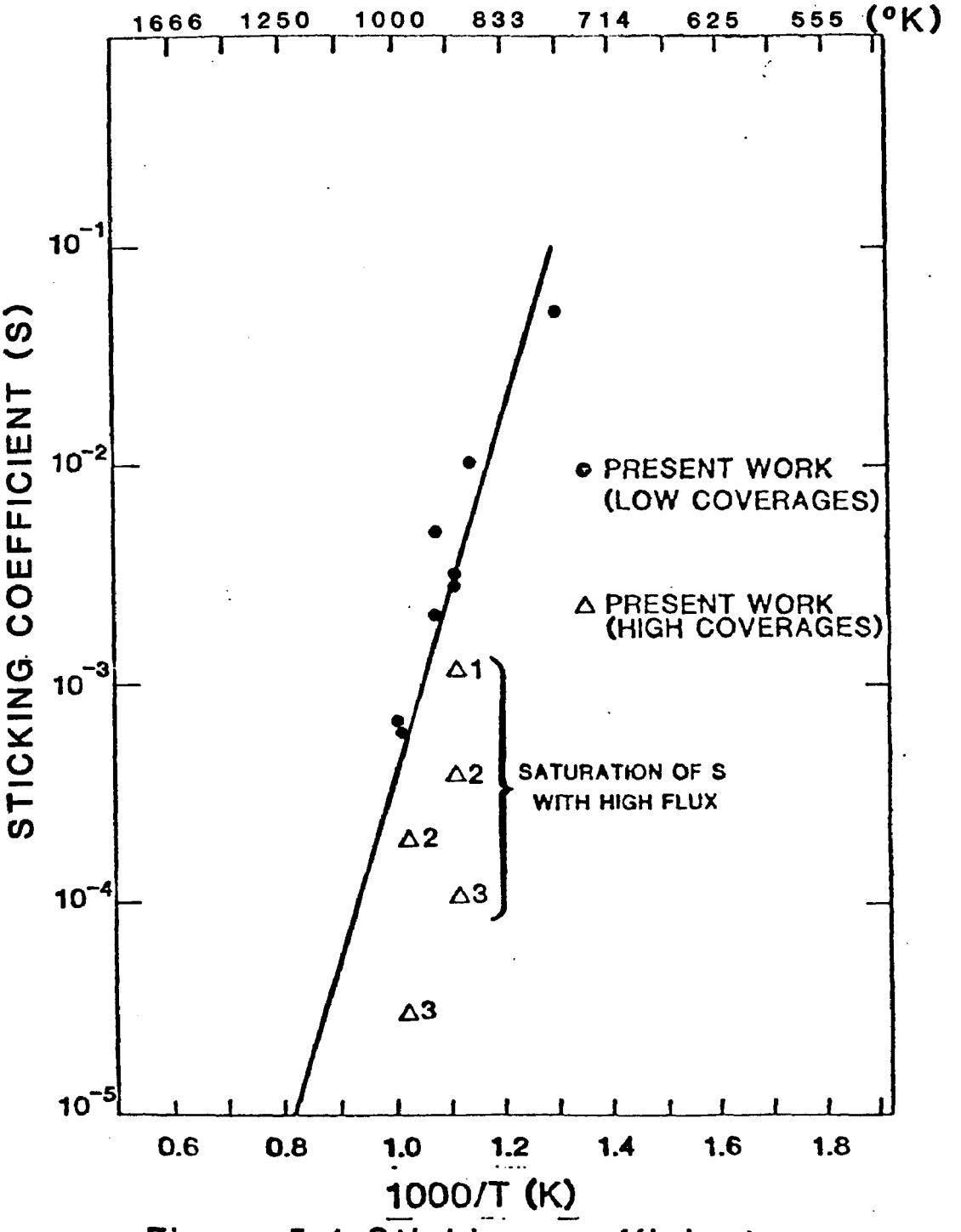

Figure 5.1 Sticking coefficient as a function of temperature

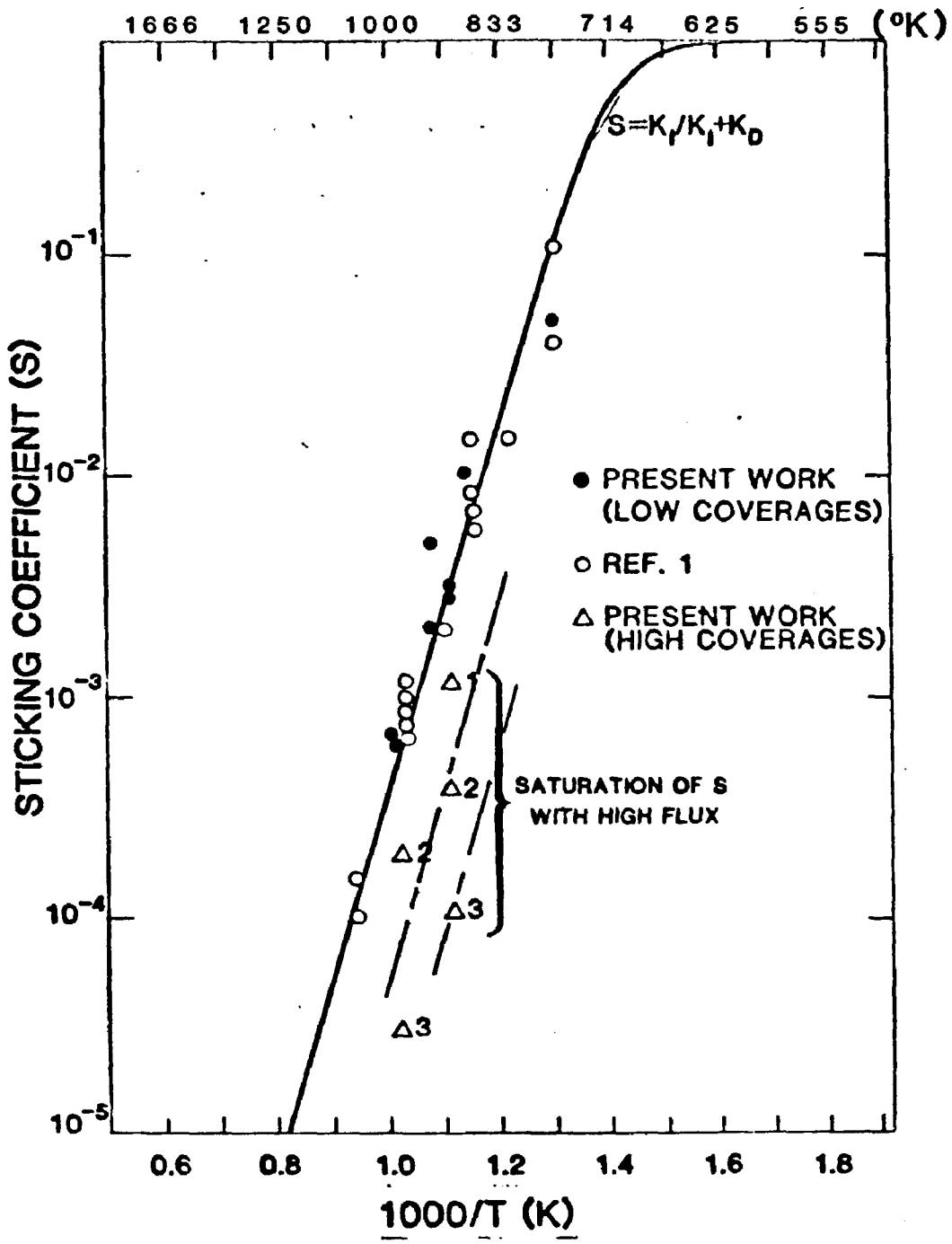

Figure 5.2 Sticking coefficient of Gallium as a function of temperature

resetting of the probes may cause. For this reason, it is advisable not to take too many readings at the same spot. In view of the above considerations, it is estimated, the error in the sticking coefficient curve should be less than a factor of 2. Since we expect these errors to be random, a least square fit to the experimental data points will in fact provide a good estimate of the sticking coefficient behavior with respect to temperature. Figure 5-1 shows a plot of sticking coefficient measured for gallium at different temperatures. The fluxes used in this experiment ranged between 10^9 atoms/cm^2 sec at lower temperatures to about 10^{13} atoms/cm^2 sec at higher ones. Typical doping levels obtained range from 10^{15}/cm^3 to about 5×10^{17} /cm^3. These conditions are important because they ensure that these experiments were performed such that the equilibrium surface coverage was substantially less than a monolayer. This is the low flux regime. The temperature range over which these experiments were performed was between 750° C and 500° C. Figure 5.1 also shows the best fit curve to these points, as well as those obtained by Becker and Bean, which are shown in figure 5.2 along with out points. The curve in the low sticking coefficient regime may be represented by the straight line type plot with an exponential energy factor of 1.6 eV and a pre-exponent of 2.0×10^{-11}. The uncertainty in the energy factor is about 0.1 eV

Thus

$$S = S_o \exp(\frac{E_s}{RT})$$

with

$$S_o = (2 \pm 1) \times 10^{-11}$$

$$E_s = 1 \cdot 6 \pm 0.1 \text{ eV}$$

5.3 Incorporation Coefficient:

We showed that when the sticking coefficient is small (S<<1) it could be represented by

$$s = \frac{K_I}{K_D} = \frac{K_{IO}}{K_{DO}} \exp\left(\frac{E_D - E_I}{KT}\right)$$

$$= S_o \exp\left(\frac{E_s}{RT}\right)$$

We thus have

$$S_o = \frac{K_{IO}}{K_{DO}}$$

and

$$E_s = E_D - E_I$$

which give

$$E_I = E_D - E_S$$

$$= 1.28 \text{ eV} \pm 0.3 \text{ eV}$$

and

$$K_{IO} = S_o K_{DO}$$

$$= (2 \pm 1) \times 10^{+2} \text{Hz}$$

Our values for K_{IO} and E_I seem quite reasonable if one assumes that the incorporation rates are limited by surface diffusion processes, in which the adsorbed gallium atom is transported to a kink site where it is

incorporated. We shall discuss this in more detail later.

5.4 A Complete Representation of the Sticking Coefficient

Now that we have values for both K_I and K_D we may plot a complete representation for s given by

$$s = \frac{K_I}{K_I + K_D}$$

for all temperatures, including low temperatures where s is not very much less than unity. This is shown in figure 5.2. Note also that we have plotted sticking coefficient information for (100) planes as well. The results show that there seems to be no distinguishable orientation dependence for the sticking coefficient. It is seen that s approaches unity within a factor of two for temperatures below 440° C. However, the crystalline quality of the films grown at these low temperatures is not very good.

5.5. A Design Chart For Achieving Steady State Values of Doping:

We now address the problem of achieving certain steady state doping levels. We have in our process the following variables:

(a) Silicon growth rate

(b) Dopant flux

(c) Substrate temperature.

The silicon growth rate and the operating pressure are usually fixed to some optimal value, and in any case cannot be varied over more than a modest range. The operating pressure is usually the lowest possible permitted under the available pumping system and growth rate.

A typical growth rate which is reasonable for our system is

1 to 2 Å per second. Thus our only variables are the substrate temperature and the dopant flux. In addition, we must not have the substrate temperature below about 450° C to ensure epitaxial growth, nor may it be above 850° C for extended periods of time in order to prevent possible diffusional smearing. The dopant flux may be varied from between 10^{9} atoms/cm^{2}-sec to about $5x10^{14}$ atoms/cm^{2}-sec.

Another consideration is whether the growth mode be in the linear or the saturation regime. While we have not yet discussed saturation effects, we mention for the present that the incorporation rate slows down when the equilibrium coverage of surface dopant atoms gets close to a monolayer. Further there is some question [80] regarding the electrical quality of films grown under the influence of heavy surface coverage by dopant atoms. The behavior of the sticking coefficient in the saturation regime is different from that in the linear regime and will be considered later.

For the present, we consider growth in the linear regime. We show in figure 5.3 the maximum doping level obtainable in the linear region at different temperatures. While it is not clear as to exactly when saturation sets in, we have, based on experimental evidence, chosen this limit to be when the surface concentration of dopant reaches 10^{14} atoms/cm^{2}. The flux required to obtain this doping level is also shown.

Two things are clear from this chart. First, it is possible to obtain doping levels as high as $3 \times 10^{17}/cm^{3}$ for fluxes of 10^{14} atoms/cm^{2}-sec at a temperature of 815° C. Second in the linear regime one may get higher doping levels at higher temperatures. This needs to

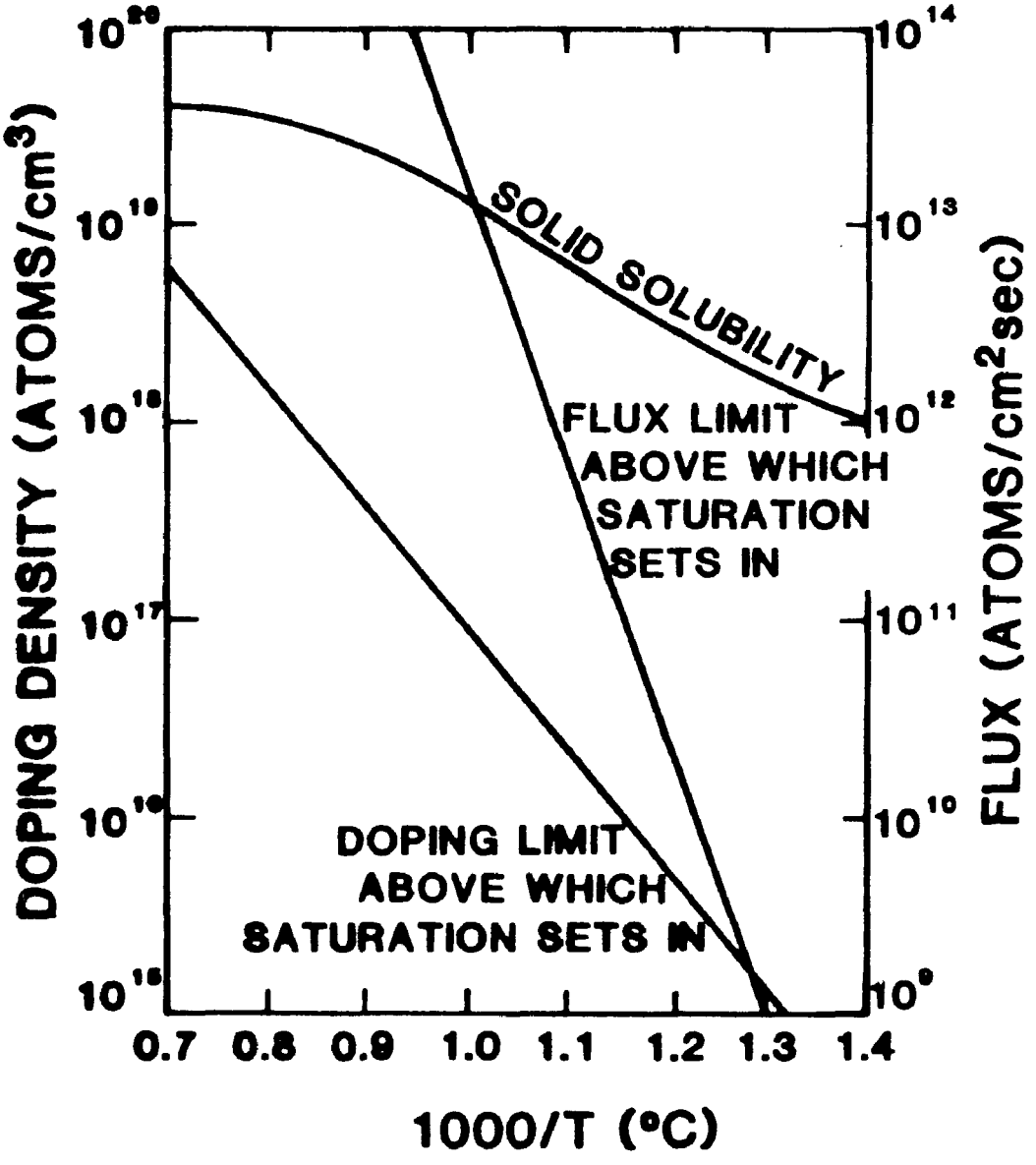

Figure 5.3 Design chart for use in the linear doping regime

be clarified: While it is true that the incorporation rate increases at a fast rate at higher temperature, so does the desorption rate. In fact, the desorption rate increases at a faster rate. This results in lower sticking coefficients at higher temperatures.

Consideration must also be given to the flux used. A flux of gallium of about 10^{14} atoms/cm^2-sec is comparable to the silicon flux. It also means higher oven temperatures and the effects associated with outgassing. Further, most of this flux is wasted. Gallium being a corrosive element, this is not a favorable solution.

We now specify the procedure for obtaining the flux required for a certain doping level. The temperature is first fixed. The consideration that governs temperature choice are related to the delay time effects and will be discussed later. Once this temperature is chosen, we need to see if the growth temperature-doping level (T_S, N_B) coordinate lies below the solid doping level curve indicated in figure 5.3. It may be possible to move the temperature coordinate to a level where the point does lie in the linear regime.

Once it has been ascertained that the temperature of operation lies within the linear regime, we proceed to determine the flux needed to achieve the required steady-state doping. We first determine how much below the maximum allowable doping curve for the linear regime our level is. We call the factor ℓ

$$\text{ie} \qquad \ell = \frac{\text{desired doping}}{\left(\begin{array}{l}\text{maximum allowable doping for linear}\\ \text{regime at growth temperature}\end{array}\right)}$$

We then proceed vertically till we intersect the flux curve. We call this flux F_{Dmax}, which is the flux required at the temperature of

growth to achieve the maximum doping in the linear. Then the required flux for the desired doping level is

$$F_{reqd} = \ell \cdot F_{Dmax}$$

We must clarify here that the above procedure does not include delay effects. This subject will be developed in detail later.

5.6 Saturation Effects

We have in previous chapters alluded to saturation effects in the dopant incorporation process in flux is increased beyond a certain limit. We now discuss this effect more completely.

As the flux increases, we find that a smaller and smaller fraction of the incident dopant atoms get incorporated into the growing silicon film. We do find that absolute number of dopant atoms incorporated does continue to increase, though at a lesser rate. The information is best understood by examining the behavior of the sticking coefficient with respect to flux. It is also clear that this information would give us clues on the microsteps involved in dopant incorporation, While we shall defer a more sophisticated discussion to the next chapter, we will present here a simple model to explain our saturation results. This simple analysis can be used in our design rates.

We have mentioned earlier that the incident gallium could behave in one of two ways:

(a) It could go down as a uniform layer with some sort of silicon-gallium phase on the surface to explain the persistence of the silicon auger signal after a considerable dose of gallium, or

(b) It could go down in the form of islands whose characteristic

dimension grew as more gallium was deposited, though exposing an appreciable amount of silicon throughout.

We must at this stage speculate on the microscopic steps involved in incorporation. There are a few different possibilities which we shall presently examine.

(a) The stationary step with a migratory dopant adatom

Here the adatoms are assumed to be sufficiently mobile so as to migrate to a nearby step, find an appropriate kink site and incorporate into it. The process of adatom migration is considered to be faster than that of step propogation - so much so that the steps can be considered stationary. We distinguish here that the adatom supply could be either dopant islands or randomly distributed adatoms.

(b) The stationary island with a moving step

Here the dopant adatoms are assumed to go into clusters which remain relatively stationary. Incorporation occurs as the step propogates across the island or possibly under it.

Let us now consider the migratory adatom case. Evidently here, if the gallium deposit forms islands, it will be the atoms on the perimeter of the base of these islands which will migrate first and more easily.

It is clear that incorporation will depend on the perimeter of these islands. Let us calculate first the behavior of the island size as the flux is increased. As before we assume first order kinetics. The number of adatoms on the surface is then

$$N_{DS} = \frac{F_D}{K_I + K_D} \qquad (5.1)$$

Let us assume for simplicity that these are distributed equally in α hemispherical islands per cm^2. Let β be the volume occupied by each atom. Then the number of atoms per hemispherical island is

$$N_{DS}'' = \frac{N_{DS}}{\alpha} = \frac{F_D}{\alpha(K_D + K_I)} \tag{5.2}$$

and the volume of each hemispherical island is

$$v_{hemi} = \beta N_{DS}'' = \frac{\beta F_D}{\alpha(K_D + K_I)} \tag{5.3}$$

We now compute the radius of the base of the hemisphere r_o

$$\frac{1}{2} \frac{4}{3} \pi r_o^3 = v_{hemi} \tag{5.4}$$

Therefore

$$r_o = \left(\frac{3}{2} \cdot \frac{v_{hemi}}{\pi}\right)^{1/3} \tag{5.5}$$

Substituting (5.3) gives

$$r_o = \left(\frac{3}{2\pi}\right)^{1/3} \left[\frac{\beta}{\alpha} \cdot \frac{1}{K_D + K_I} \right]^{1/3} \cdot F_D^{1/3} \tag{5.6}$$

The area of the base of the hemisphere is

$$A_h = \pi r_o^2 = \pi\left(\frac{3}{2\pi}\right)^{2/3} \cdot \left[\frac{\beta}{\alpha(K_D + K_I)}\right]^{2/3} \qquad (5.7)$$

While the perimeter is

$$P_h = 2\pi r_o = 2\pi\left(\frac{3}{2\pi}\right)^{1/3} \left[\frac{\beta}{\alpha(K_D + K_I)}\right]^{1/3} \cdot F_D^{1/3} \qquad (5.8)$$

Clearly then if incorporation is from the perimeter of the islands, the incorporation rate will be proportional to the perimeter of the islands and then we have the incorporation rate for perimeter incorporation

$$\left.\frac{d N_{inc}}{dt}\right|_P \qquad F_D^{1/3} \qquad (5.9)$$

In the case of incorporation via step propogation across an island, the incorporation rate will depend on the number of atoms intercepted on the base of these hemispheres or the basal area. Thus the rate of incorporation for areal incorporation will behave as

$$\left.\frac{d N_{inc}}{dt}\right|_A \alpha \quad F_D^{2/3} \qquad (5.10)$$

Let us now look at the sticking coefficient defined previously. We have

$$s = \left.\frac{d N_{inc}}{dt}\right|_{F_D} \qquad (5.11)$$

Putting in the variation of $\frac{dN_{ince}}{dt}$ for the two cases in question, we

$$S\Big|_P \alpha F_D^{-2/3} \tag{5.12}$$

$$S\Big|_P \alpha F_D^{-1/3} \tag{5.13}$$

Thus an examination of the saturation behavior of incorporation, in terms of falling sticking coefficient, might indicate the nature of incorporation.

Let us also consider the case where the gallium goes down as a uniform monolayer, with additional gallium going down as a second layer. Clearly incorporation will depend to a first order on the gallium in contact with the silicon. Thus, if this were the case, the second and third overlayer would not contribute appreciably to incorporation. This means that there would be no increase in doping levels after a monolayer of adatoms is formed. The sticking coefficient would demonstrate a linear drop off with flux, i.e. $S \alpha \frac{1}{F_D}$ and the incremental S would drop to zero after a single monolayer. Experimental evidence shows that doping levels continue to rise, thus contradicting the prediction of the uniform adlayer mechanism. We must not discount though that certain second order effects might set in, explaining the rise in doping level. For now we shall ignore this possibility.

It is also clear that if either perimetric or areal mechanisms are in operation, the point at which saturation effects set in will depend on when a certain definite number of adatoms accumulate on the surface.

This is the critical number of atoms required for nucleation of gallium on silicon and depends on the surface conditions. Obviously, this number will be reached for lower values of incident dopant flux at lower temperatures. Using the kinetic data, we have measured it should be possible to determine when this effect sets in, once sticking coefficient behavior with flux is established.

We mention here that both perimetric and areal incorporation may be in effect and it might not be possible to say definitely which is predominant.

Experimental Results

The sticking coefficient (from doping density measurements) were measured at different flux rates of dopant at different temperatures. These are shown in figures 5.4 and 5.5. Using our universal design chart (figure 5.3) we note that the saturation effects become pronounced after a fraction of a monolayer or so of dopant atoms have accumulated on the surface, no matter what the temperature. This suggests that we should normalize the flux to that flux required to produce a monolayer on the surface. This is shown in figure 5.6. We note that it seems possible to draw a universal curve. We also show the best fit ranges for the $\frac{-2}{3}$ power dependence with flux. While not totally unambiguous, we are inclined to believe that $\frac{-2}{3}$ dependence

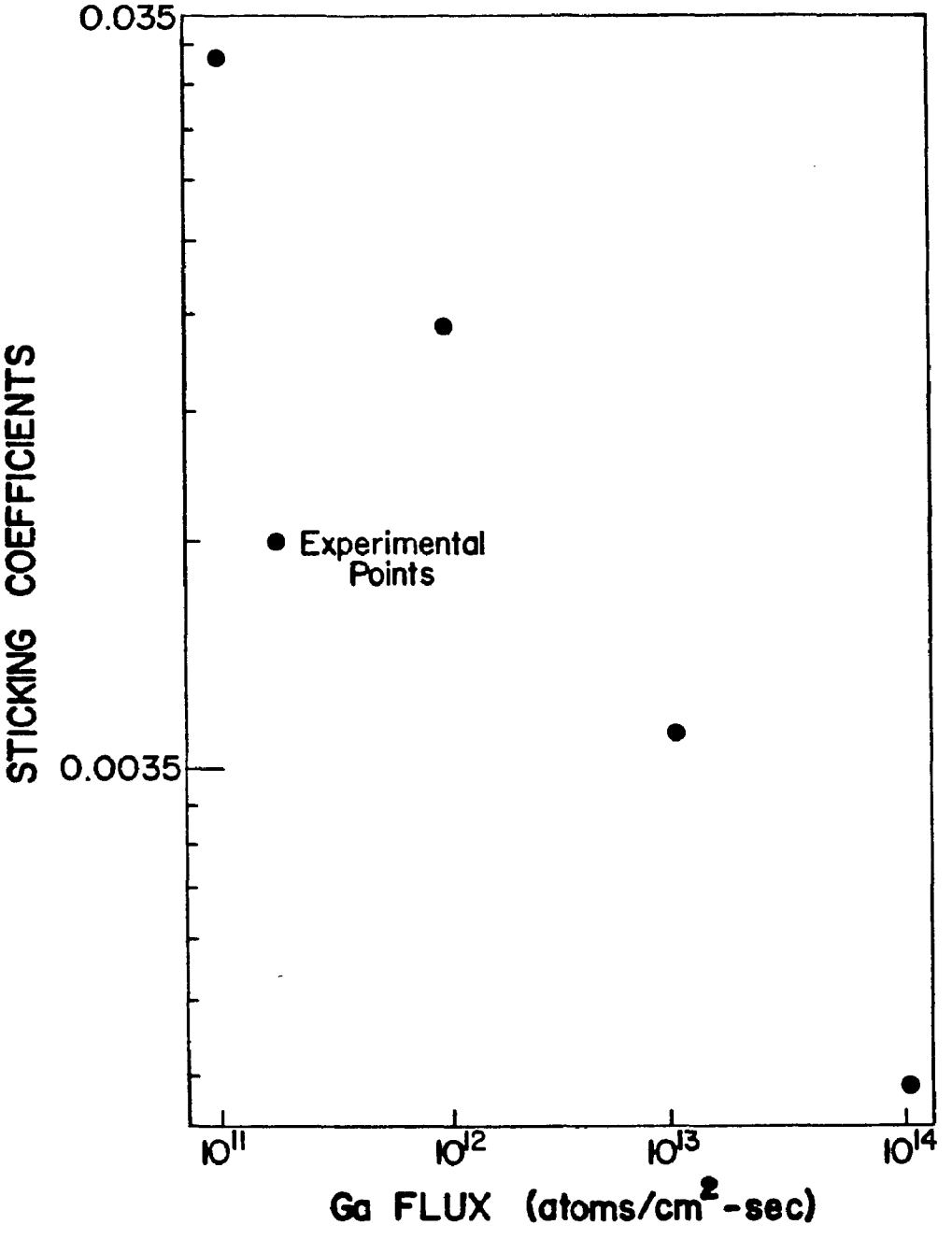

Figure 5.4 Saturation effects in Ga sticking coefficients with flux at 625 °C

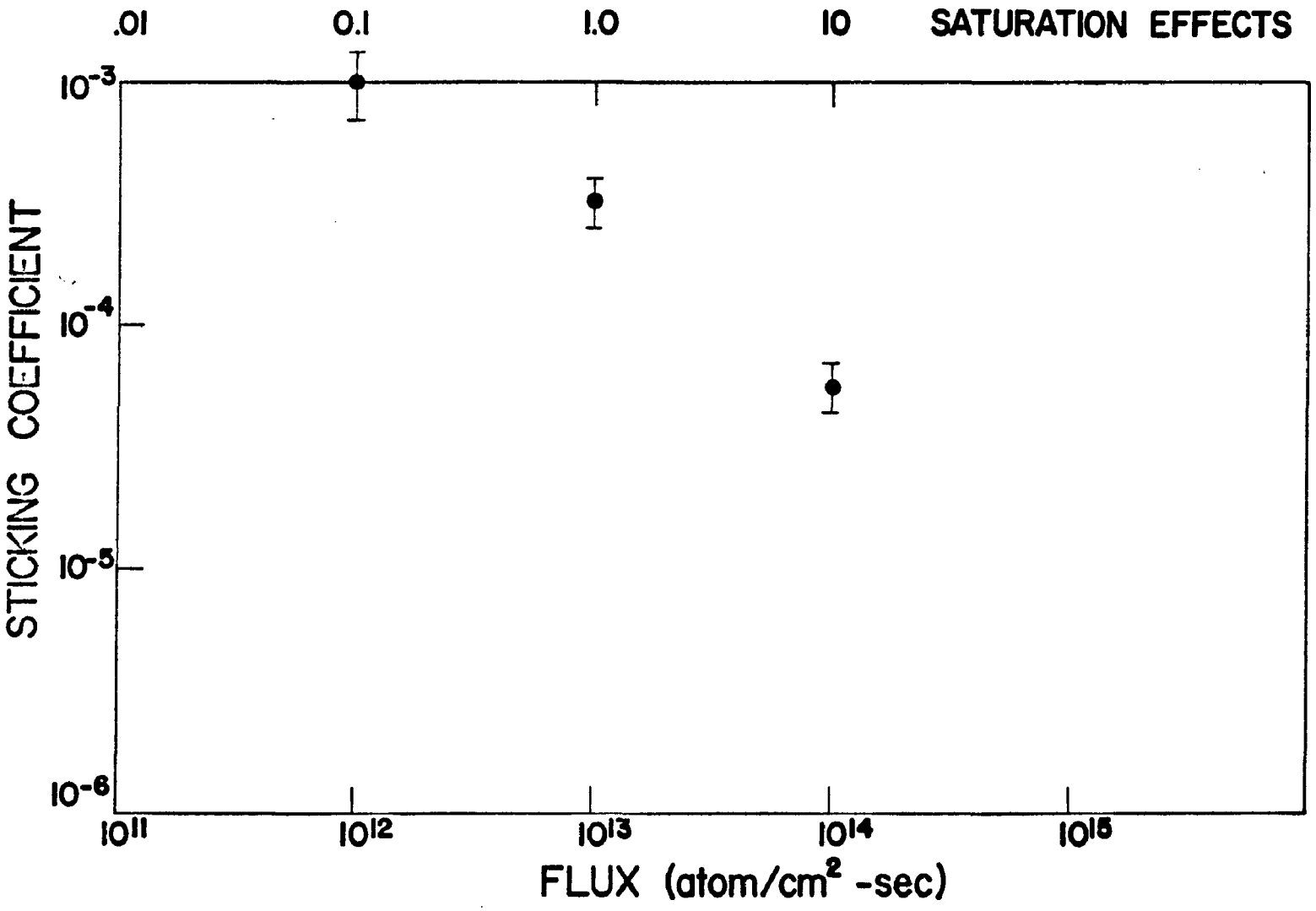

Figure 5.5 Gallium sticking coefficients with flux at 700 °C

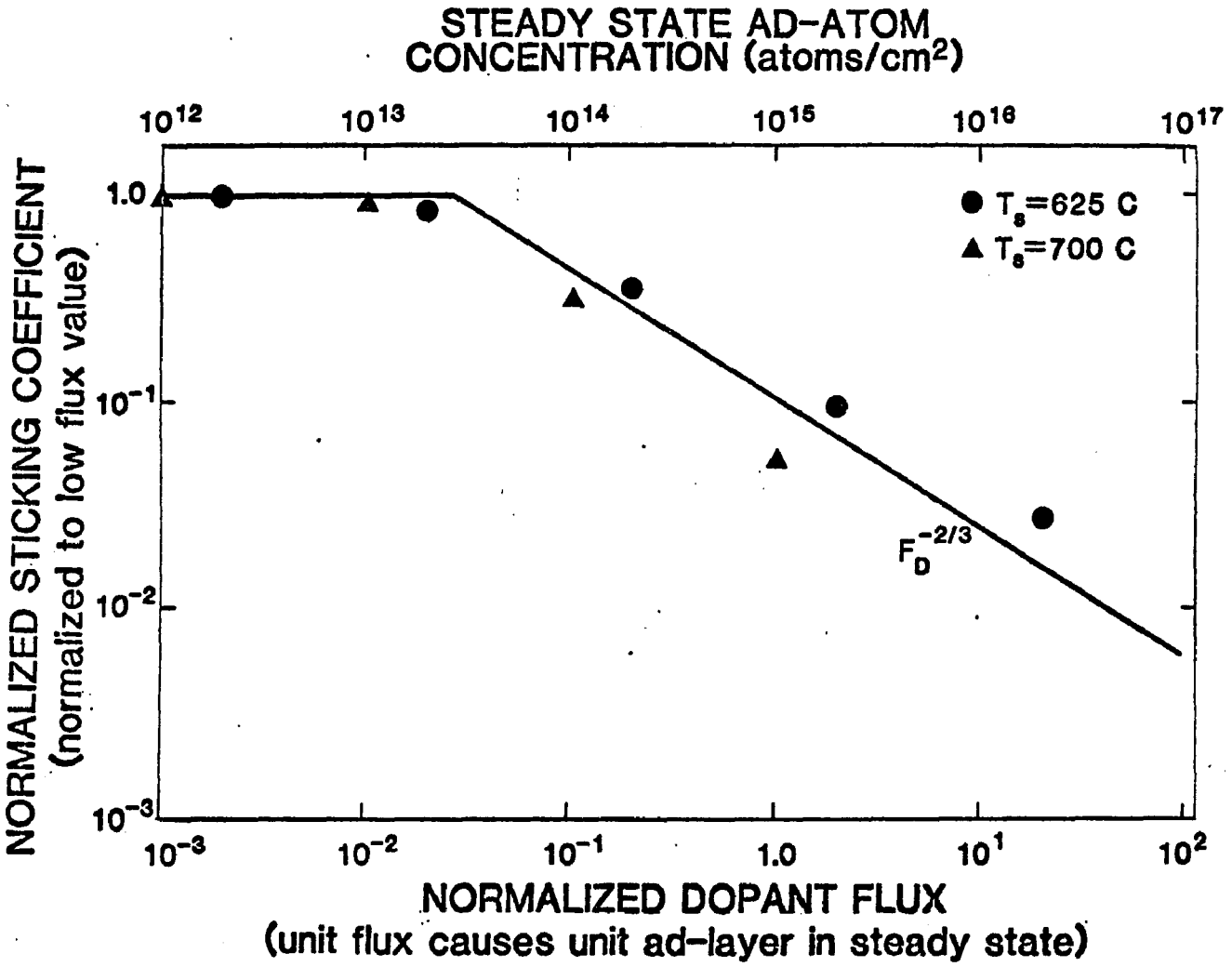

Figure 5.6 Saturation characteristics of sticking coefficient

provides a better fit to our data. In other words, perimetric incorporation is probably the dominant mechanism. We note that saturation begins to set in at fluxes required to sustain about a fraction of a monolayer, perhaps half to a tenth. We may thus write that in the saturation region, the sticking coefficient s^* is

$$s^* = s\left(\frac{F_D}{F_{DS}}\right)^{-2/3} \tag{5.14}$$

$$= s_o\left(\frac{F_D}{F_{DS}}\right)^{-2/3} \exp\left(\frac{E_D - E_S}{kT}\right) \tag{5.15}$$

where F_{DS} is the saturation flux.

5.7 Some Conjectures On The Details of Incorporation

We now wish to discuss the microscopic steps involved in the process of incorporation. This is very closely related to the manner in which the gallium distributes itself on the silicon surface. Our observation that the gallium continues to incorporate at larger absolute rates, as evidenced by increased doping with flux even at high fluxes, precludes the possibility that gallium is going down uniformly on the surface.

Evidence seems compelling that clustering of gallium on the silicon surface is occurring. There is then a question of what the distribution, size and shape of these clusters are. There is some evidence, though not conclusive, that the clusters are of irregular shape and randomly distributed. Typical sizes were estimated from very high (-50,000 X) SEM pictures to be of the order of 1000 Å across. It must however, be conceded that changes in the arrangement of gallium on the silicon surface could have occurred during the transfer to the SEM from the growth chamber. If the clusters showed a definite distribution in size and shape as well as spacing, we could conclude that neighboring gallium clusters were interacting. However, since this is not the case, it is likely that the clusters do not interact with other clusters. When the distance is small they probably coalesce, a phenomenon that might explain the irregular shape and size of the islands. In fact this could be the principle mode of their growth at high coverage. The mobilities of these clusters is expected to be low on account of their large mass and area of contact with the silicon. Coalescence may therefore involve distortion of the islands

as they approach one another. At low coverages, the principle growth mode of these islands would have to be by diffusion of individual gallium atoms to the clusters.

If in fact clustering is taking place, we need to re-examine the question of gallium desorption from the silicon surface. Table 4.3 shows the desorption energies for some elements from silicon and also the activation energy for vaporization from their elemental state. With the exception of phosphorous, there seems to be a very close agreement between the two values. This, in the light of the above discussion, would imply that the desorption of gallium from gallium islands on silicon could be an important factor. The differences in the two values could arise from the effect of the substrate if atoms desorb from close to the basal periphery of the islands. This could also explain the fact observed by other workers[65] and by us (see below) that the residence time is not such an intimate function of surface coverage.

The actual step of incorporation probably involves the breaking off of a gallium atom from the periphery of one of these islands and the subsequent migration of these atoms on the surface until a kink site is reached. The steps involved in this process would be:

(a) Ga atom attached to cluster $\rightarrow$ Ga atome released, this rate would depend on the number of atoms in the cluster available for release and also on the activation energy required for this release.

TABLE 5.1

Element	Desorption energy from Si (eV)	Vaporization energy (eV)
Silicon	4.52	4.52
Phosphorous	2.90[a]	0.284
Gallium	2.88	2.66
Indium	2.48	2.49
Gold	3.3	3.59
Silver	2.87	2.92

(b) Released gallium atom $\rightarrow$ gallium atom at kink site; this rate depends on how fast the gallium atom can migrate to the kink site. This is given by standard diffusion theory. Unfortunately, we have not any data on the surface diffusivity of gallium on silicon. We would expect however, that the temperature dependence of K_I and $D_{Ga/Si}$ be the same if the surface diffusion is a rate limiting step. In that case $Ediff_{Ga/Si} \simeq E_I$ where $Ediff_{Ga/Si}$ is the surface diffusion activation energy for gallium on silicon.

(c) Gallium atom at kink site $\rightarrow$ gallium atom incorporated; we expect this rate to be extremely fast. Thus the net rate would be

$$dN_{inc} = K_I''[Ga^+]\ [Kink]$$

where Ga^* is the species of gallium avaliable for release from the islands, and K_I' is different from K_{I_2} by a constant.

The distance moved by the gallium atom is

$$X_D = \sqrt{D_{Ga/Si}\tau_D} \qquad (5.16)$$

where τ_D is the residence time described earlier and $D_{Ga/Si}$ is the diffusivity of Ga atoms or silicon

The average speed is then

$$V_D = \sqrt{\frac{D_{Ga/Si}}{\tau_D}}$$

At low coverages the Ga* concentration would be approximately the net gallium concentration on the surface. At higher coverage, this must be more accurately measured as the atoms on the perphery of the gallium clusters.

We note from figure 5.2 that the sticking coefficient under saturated conditions has the same slope as under unsaturated conditions. We have drawn close fit lines for different coverages as shown. This has an important implication; the activation energy for the sticking coefficient is the same for all values of surface coverage. We have reason to believe on theoretical grounds (see chapter 4) and also based on experimental evidence (see below) that the residence time does not change much with coverage. Further the acitvation energy for desorption is fairly constant. These observations, coupled with the fact that the sticking coefficient activation energy does not change, leads us to believe that the activation energy for incorporation does not change much (although the pre-exponent does change).

We note that the accurate desorption of the incorporation rate would be

$$\frac{dN_{inc}}{dt} = K_I'[Ga^+]\ (Kink]$$

As long as the number of kink sites is large, they may be assumed to be constant. While at very low coverages $[Ga^+]$ may be assumed to be equal to N_{DS}, this assumption breaks down when more and more gallium atoms on the surface are not available for migration. In

this situation we must use the more accurate description of $[Ga^+]$ as the atoms on the periphery of the cluster.

We can see that the activation energy for incorporation, once these values are used remains the same for both the high and low coverage regimes. This means the process that requires activation is the same for both the high and low coverage regimes. This leads us to believe that surface diffusion of gallium atoms may be process that requires the activation energy.

To summarize: it seems very probable, from the evidence at hand that gallium atoms are clustering on the silicon surface and incorporation of gallium atoms proceeds by gallium atoms breaking away from the periphery of these clusters and subsequently surface diffusing to an available, nearby kink site.

5.8 Design Criteria for the Saturation Regime

We showed that the design rules for growth at a certain steady state level in the linear regime could be accomplished using figure 5.3. However, there is a limit to the maximum amount of doping achievable in this regime; it may not be advisable to grow at higher temperatures.

In order to achieve higher doping levels, we need to increase the dopant flux to regions where there may be up to several tens of monolayers of gallium on the surface. To compute the flux needed, we use the saturated sticking coefficient values. If F_{DS} is the saturating flux at the growth temperature (figure 5.6)

$$F_D = \left[\frac{1}{S} \frac{N_{DB}}{N_o} \frac{F_{Si}}{F_{DS}^{2/3}} \right]^3$$

where S is the low flux sticking coefficient. However, this expression is only approximate, and we use interpolation fluxes based on experimentally determined dopings for different fluxes.

5.9 Growth of Profiles Showing Time Delay

We have so far designed growth conditions only with respect to the steady state concentration, without any regard for the time required to reach this steady state. Figure 5.7 shows an application of this technique. An n substrate ($\sim 5 \times 10^{15}$ P atoms/cm^3) was cleaned and a silicon film grown on top. Throughout the substrate temperature was maintained at 625° C. The dopant flux was increased by factors of 10 from 10^{10} to 10^{14} ga atoms/cm^2-sec, for periods over which 0.5 μ of film were grown. We have shown the doping profile we might expect if (a) saturation does not set in and (b) if delay effects are neglected. We also show the actual profile abtained by anodic oxidation and 4-point probe measurements. Firstly, the saturation effect is clearly seen. More important is the delay effect. This is most apparent when the gallium beam is shut off in the region near the surface. We have tabulated these delay times in table 5.1. These are in close agreement with the value of $\tau = \frac{1}{K_D}$ at 625° C.

It is clear from this profile and others like it, that the time delay effects are quite drastic. We shall presently develop techniques to circumvent these problems.

5.10 Reducing Delay Effects - Flash-Off and Build-Up

The time delay seen above arises from the inherent delay involved in the process of equalibration of the concentration of the surface dopant species. We return to our original equation for N_{DS} (2.6)

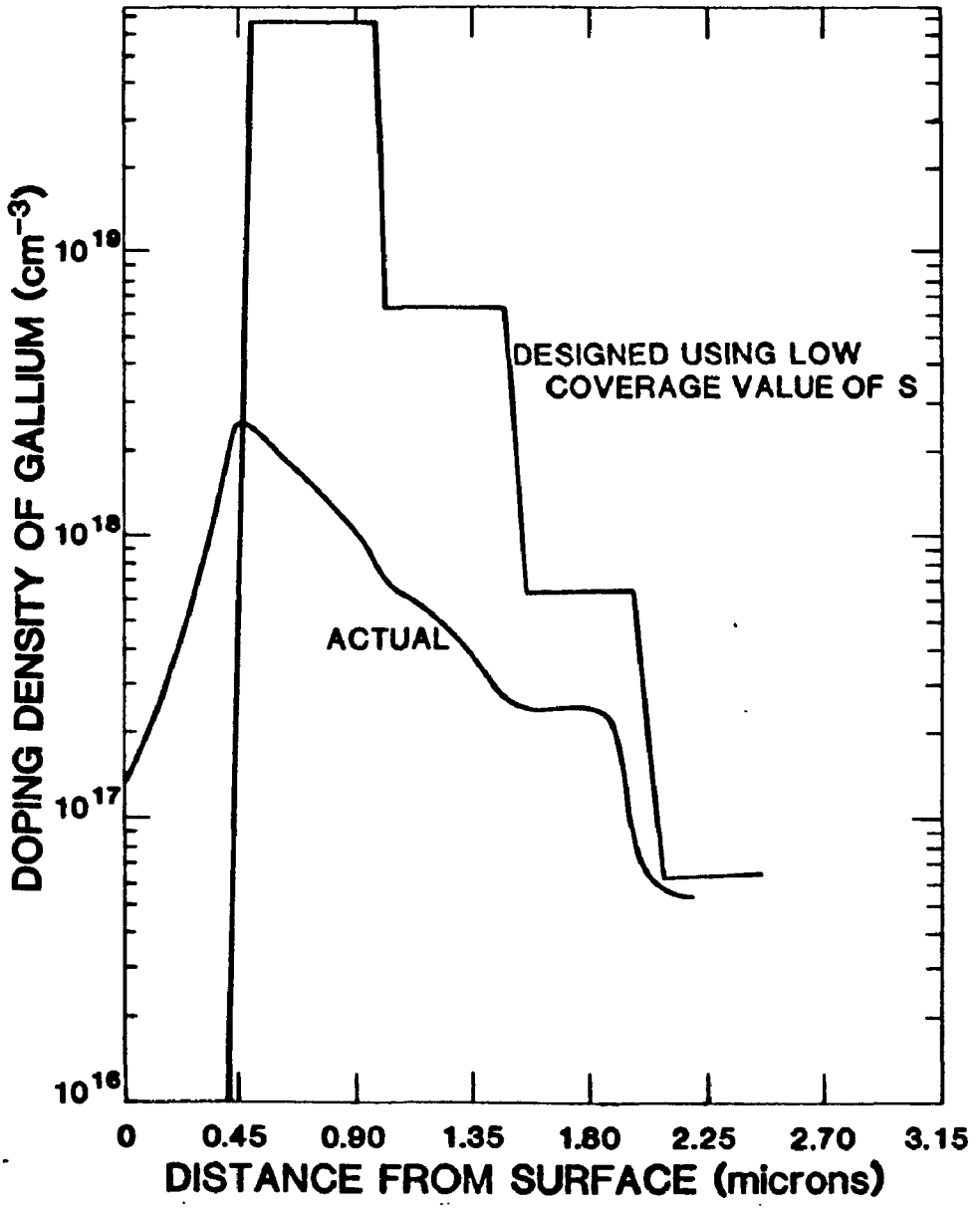

Figure 5.7 A profile showing intrinsic smearing effects due to time delay in reaching steady state

$$\frac{dN_{DS}}{dt} = F_D - K_D N_{DS} - K_I N_{DS}$$

The steady state value is $N_{DS_{ss}} = \frac{F_D}{K_D + K_I}$

Let us specify that growth occurs at t = 0. It is clear that if one could arrange that N_{DS} (t=0) = $N_{DS_{ss}}$, all of the grown film would be grown under steady-state conditions. This condition may be achieved in a number of ways; we discuss below some techniques that we have used to achieve this end.

5.10.1. Flash-Off

Consider the case where a high to low doping transition is to be achieved. Let us assume that we have achieved a steady state condition and are growing silicon doped at a high level of $2 \times 10^{18}/cm^3$ at a growth temperature of 625° C. Let us now desire to achieve an abrupt transition to a low value, say $N_A \sim <10^{15}/cm^3$ shutting off the gallium flux would cause a slow drop-off with a time constant equivalent to a few thousand angstroms of film grown. We desire greater abruptness.

In order to be doping at the high level, we need to have a surface concentration of gallium equivalent to several tens of monolayer. We therefore need to rid the surface of this large quantity of gallium before the next portion of the film is grown. This could be done by arresting growth for a period of several thousand seconds so that the gallium could desorb from the surface (which is the

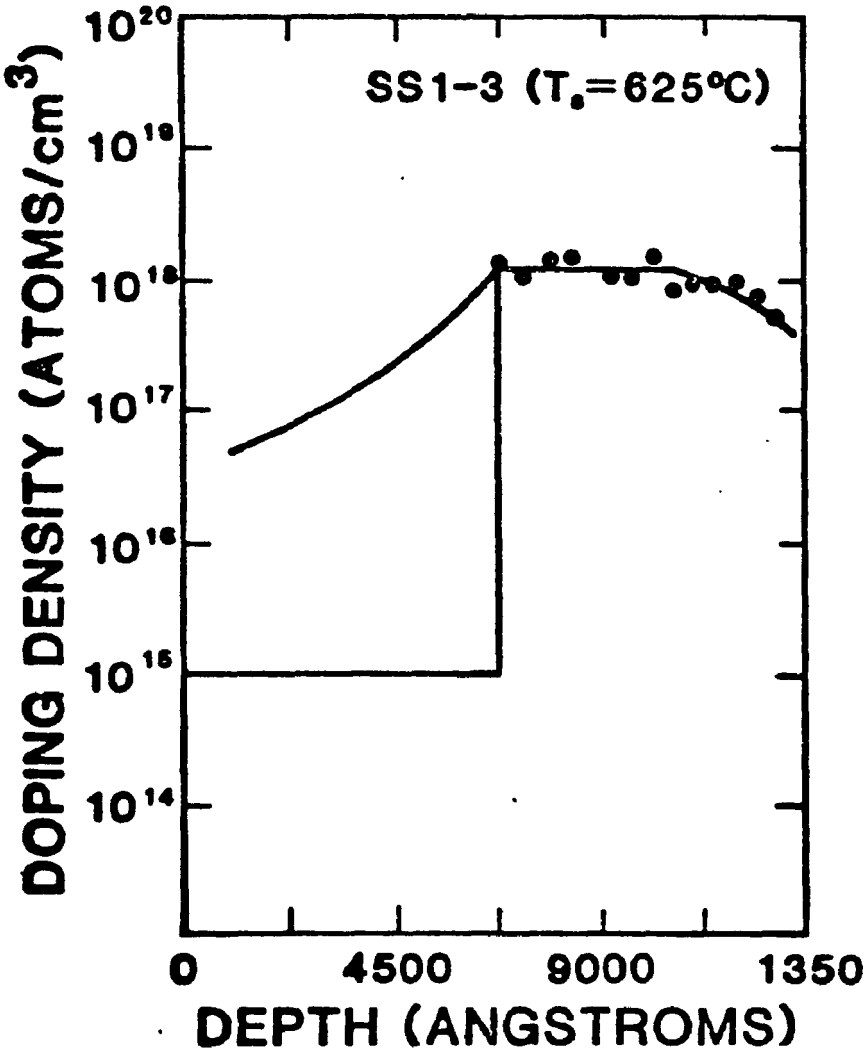

Figure 5.8 Illustrating "flash-off"

principal mode of its decay). This is a time consuming process, and also increases the risk of surface contamination by contaminants such as oxygen. Instead, if we increase the desorbtion rate by elevating substrate temperature briefly, we could get rid of this gallium much faster. Heating the substrate to 850° C for a few minutes would ensure that all the gallium is flashed off. Further, silicon growth could continue even during this phase as the gallium residence time at this high temperature is just a few seconds; most of the gallium would have been flashed off in the initial few seconds, and the thickness of film grown during that period would not be very significant. Even if growth arrest is required, the elevated sample temperature would ensure greater protection of the surface from contaminants.

This process is referred to as "flash-off". We have in fact verified its applicability, and figure 5.8 is a demonstration of its use. The profile was measured using anodic oxidation and resistivity measurements. The lower value is an upper limit and the actual concentration in the low region may be lower than $10^{15}/cm^3$.

5.10.2 (b) Build-Up

We may use dual techniques to cause an abrupt low-high transition. Consider the case where we wish to obtain a transition from a low value of about 10^{15} atoms/cm^3 to a high value at 10^{18} atoms/cm^3, with a growth temperature of 625° C. Ordinarily, merely increasing the flux from zero to the high value of 10^{14} atoms/cm^3-sec would cause the film to be doped to this level only after several thousands of angstroms have been grown. On the other hand, we could arrest growth for several minutes (about 15) and continue to dose the sample with gallium.

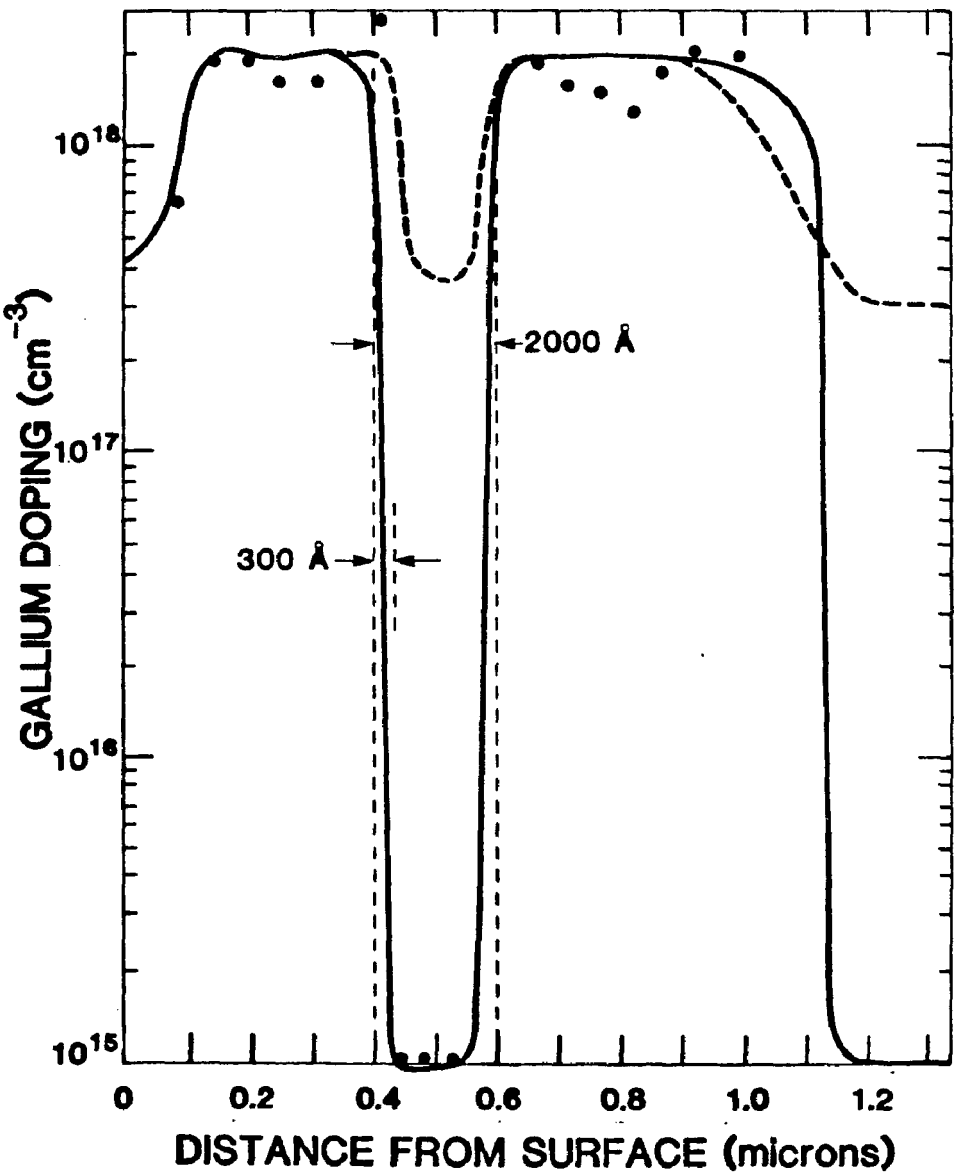

Figure 5.9 Illustrating "prebuild-up" and "flash-off"

During that time a surface concentration of gallium, sufficient to cause the needed doping, would have accumulated. Film growth may then be resumed. Figure 5.9 shows the profile obtained in the following way: An n-type substrate as before was used. A buffer layer with no intentional doping was grown for 5000 A^{o} at 800^{o} C gallium was then built up for 17 minutes at a substrate temperature of 625^{o} C with silicon growth arrested during this period. Growth was then resumed at this level for 5000 A^{o}. At this point, the growth was stopped and the gallium beam shuttered. The sample was flashed at 850^{o} C for 5 minutes and growth resumed for 2000 A^{o}. This corresponds to the low well in figure 5.9. At this stage, the pre-build up procedure was repeated and growth resumed resulting in the high level on the surface side of the well. After 3000 A^{o}, the gallium flux was shuttered off without interruption of growth and the gallium doping allowed to decay with its own time constant. This corresponds to the drop-off near the surface. This growth continued for 1000 A^{o}.

The profile shown in figure 5.9 is obtained from anodic sectioning with 4-point probe readings. Also shown are results of SIMS analysis for gallium. The anlysis (by C.A. Evans Assoc) was performed in a machine used primarily for GaAs and as a result, the gallium sensitivity was not very good. Further processes inherent in the sputter technique used limit the resolution of the method.

As can be seen in the curve, the 2000 A^{o} well with walls that make the transitions within 300 A^{o} are possible using flash-off and build-up methods.

5.11 Techniques to Obtain Dopings at Intermediate Levels:

The above techniques are adequate for making transitions from very high to very low levels. In order to obtain transitions from intermediate levels to other intermediate levels techniques based on similar but more quantitative principles are required.

In principle, we need to know how much time it takes to change the surface gallium concentration from that required for doping at the initial level to that required at the final level. Let us assume that we intend to make an abrupt transition from a level N_{DB_1} grown at temperature T_{S1} to another level N_{DB} grown at temperature.

We can calculate the steady state fluxes required for these two levels as outlined in previous sections. Let these be F_{D1} and F_{D2}. Let the characteristic time constant at temperature T_2 be τ_2 and at temperature T_1, let it be τ_1. Then the steady state surface concentrations are for segments 1 and 2 respectively.

$$N_{DS_1} = F_{D_1}\tau_1$$

$$N_{DS_2} = F_{D_2}\tau_2$$

We then need to arrest growth for a time period Δt in which this transition may be accomplished.

Consider first the case where $N_{DS2} > N_{DS1}$. Two options are available to us. We may merely increase (or decrease) the flux to F_{D2} for a period of time equal to about $\Delta t = 3\tau_2$ and resume growth or we may increase the flux to a level F_{D_3} for a shorter period of time Δt such that

$$\Delta t = -\tau_2 \ell n\left(1 - \frac{N_{DS_2}}{F_{D_3}\tau_3}\right) \qquad (5.18)$$

$$\simeq \frac{N_{DS_2}}{F_{D_3}} \quad \text{if} \quad \Delta t << \tau_3$$

i.e. if

$$F_{D_3} >> F_{D_2}$$

After this period Δt, the flux is returned to its normal value F_{D_2} and growth resumed. this technique is called poisecast control and is depicted in figure 5.10. The danger in using poisecast control lies in the fact that if the time Δt is not calculated correctly, over shoot is possible. This is shown in figure 5.10. Reducing the flux causes the value of N_{DS} to return to steady state but at the time constant τ_2. This may be unacceptable.

The advantage of using F_{D_2} is that there is no such effect. Since the process is first order, no overshoot is possible.

The next case is when $N_{DB2} < N_{DB1}$. The easiest technique to follow here is to flash-off all of the N_{DS1} atoms/cm^2 on the surface, change the sample temperature and flux to their new values while arresting growth for a period t = T. Other methods involving partial flash-off are difficult to control. Poisecast control may be used to establish the new level N_{DS2} with a higher initial flux FD_3 as before. We show in figure 5.11 a profile measured using anodic etching and four-point probe methods which illustrates the use of the above mentioned techniques to achieve various staircase-type structures. The structure has no specific use but was grown to demonstrate the great

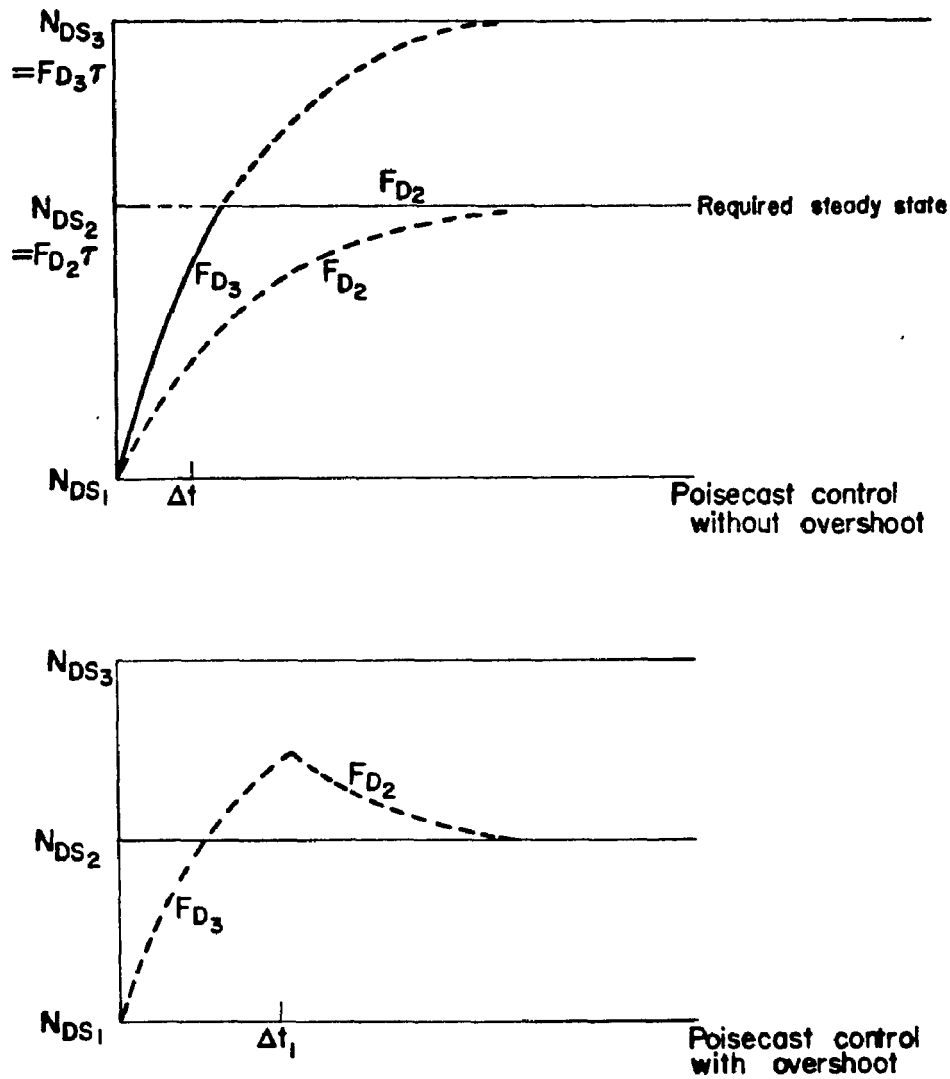

Figure 5.10 Illustrating poisecast control

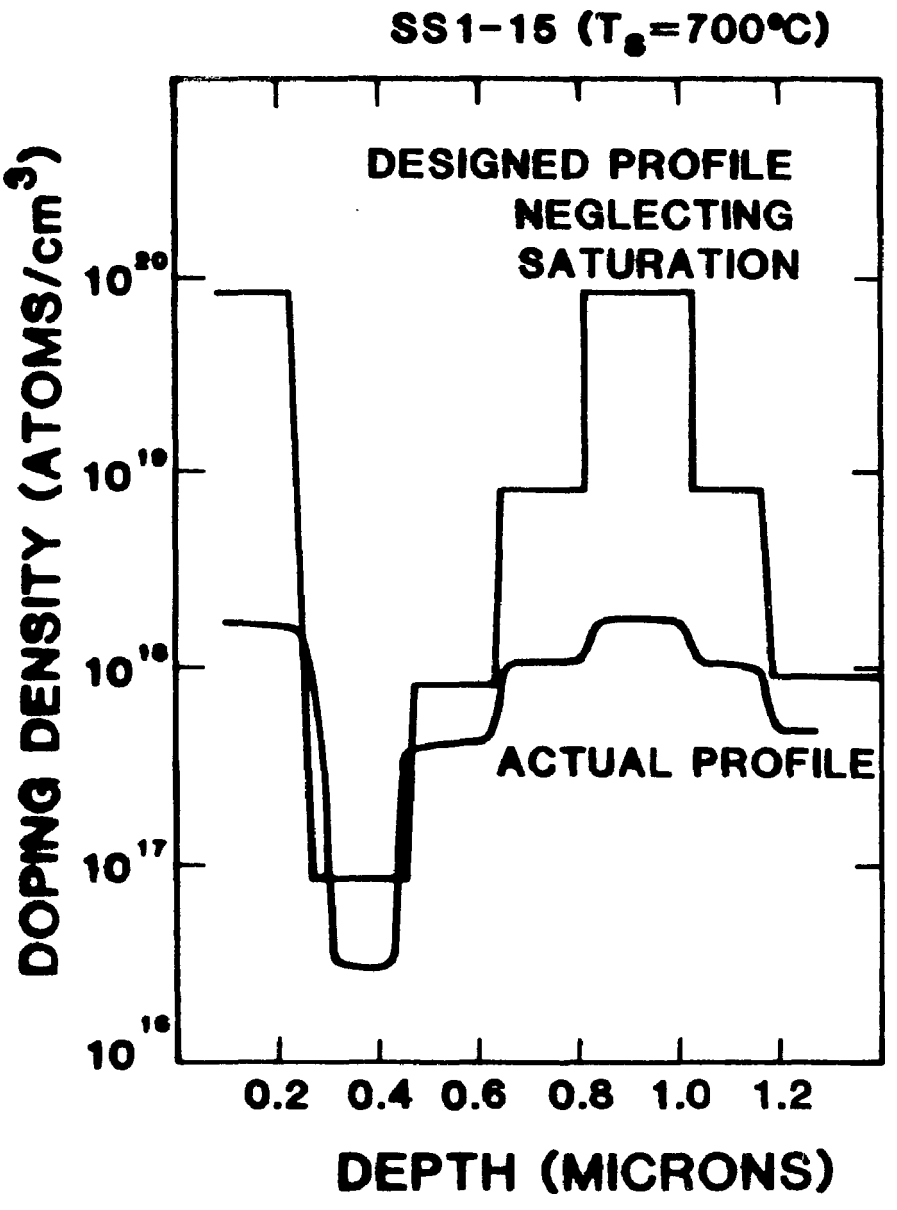

Figure 5.11 An arbitrary profile using our design techniques

versatility of the technique developed.

5.12 The Growth of Junctions

P-N junctions may be grown by MBE in one of 2 ways A P or n layer may be grown over an n or p substrate respectively. Usually for diagnostic purposes a relatively lightly doped epitaxial film is grown over a relatively heavily doped substrate. Alternatively, an n^+ layer may be grown over a lightly doped n substrate and a p film grown on top of this n layer. We have used both techniques.

5.12.1 MBE Defined Junction

Consider the profile shown in figure 5.12. We have found that p-n junctions show marginally less leakage currents when grown over lightly doped substrates. This may be due to the higher defect density associated with the heavier doped material. It also helps to grow the initial portion of the film at higher temperatures.
Apparently epitaxy proceeds better and carbon contamination does not out-diffuse. Hence a rather low doped buffer layer is first grown at a relatively high temperature (650-750° C). Thereafter a highly doped n layer is grown. This ensures that the reverse biased junction does not deplete into the substrate. Typically this is a few thousand angstroms and the doping level is about $10^{19}/cm^3$. The p layer is then grown at the required doping level for the required thickness and then capped by a thin ($\sim$ 1000 A°) p^+ layer which serves two functions; one to provide a stop for the depletion region so that reach through does not occur, and the other is to provide a low resistivity surface layer for better ohmic contacting.

We give below certain calculated parameters for this junction

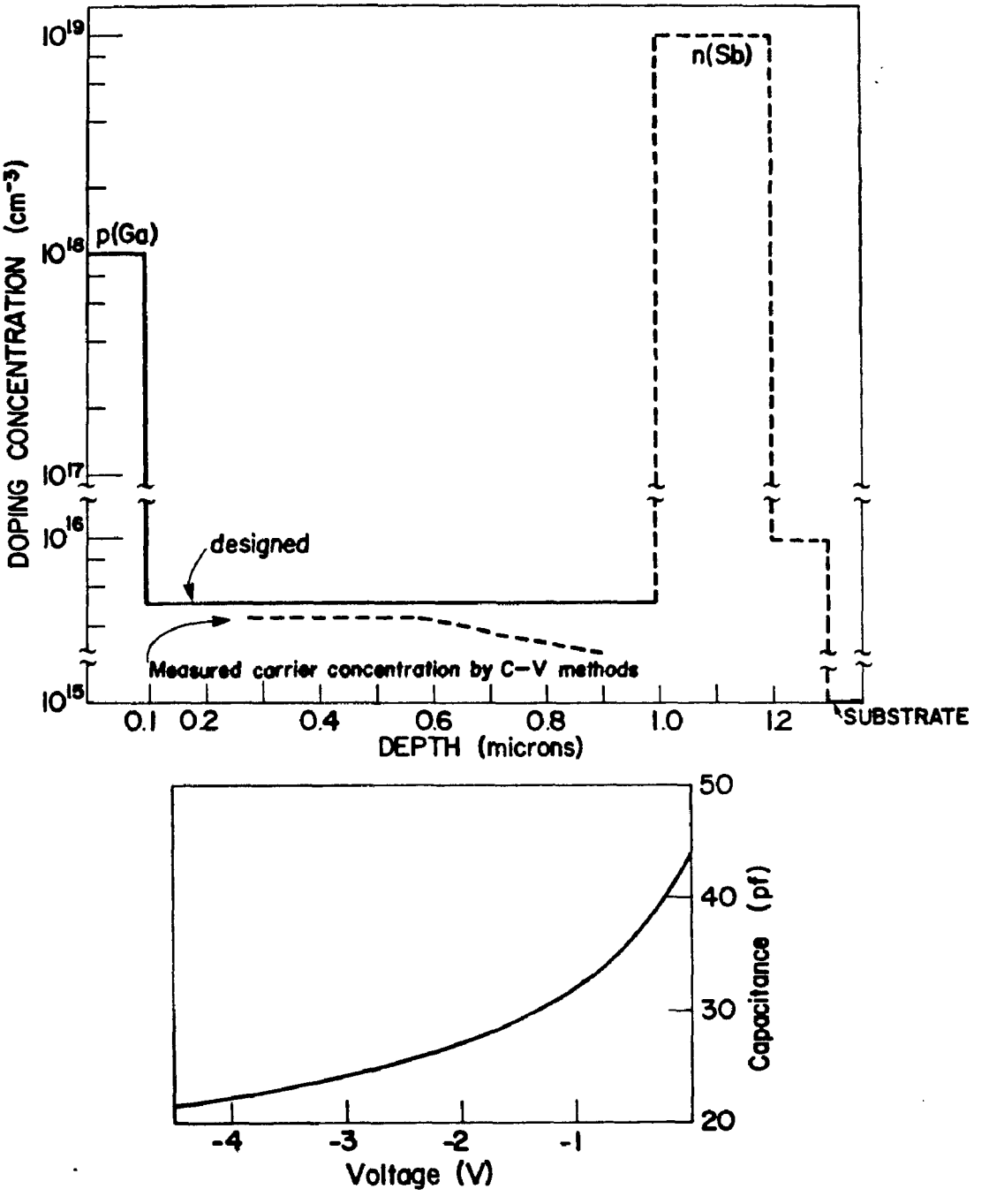

Figure 5.12 Profile for a measured p-n junction and measured C-V characterestics

(a) built in voltage: 0.92 V

(b) depletion at

0V is 0.35μ

3V is 0.7 μ

15V is 7.4 μ

(c) The avalanching field is 4×10^5 V . Hence if the breakdown mechanism is by pure avalanching, the breakdown voltage would be 28 volts. However, points of high electrical strain may develop causing premature breakdown.

The growth schedule followed was as given below.

(1) Clean substrate by galliation

(2) Look for LEED, RHEED patterns, Auger spectra to ensure clean surface

(3) Maintain sample at 900° C

(4) Get Sb oven to 300° C

(5) Begin growth, lowering substrate temperature to 700° C in the time taken to grow about 500 A°

(6) Lower T_S to 650° C

(7) Increase oven temperature to 367°C

(8) Arrest silicon growth and pre-build up Sb for 300 sec.

(9) Resume Si growth for 2000 A°

(10) Arrest Si growth. Flash-off at T_S = 900° C for 5 minutes, shutter off Sb oven and turn off. Ensure clean surface as in (2)

(11) Get Ga oven to 630° C

(12) Reduce T_S to 700° C and prebuild-up Ga for 300 sec.

(13) Grow 1.5μ under these conditions

(14) Lower T_S to 625° C arrest growth

(15) Increase Ga oven temperature to 905° C

(16) Prebuild up Ga for 300 sec.

(17) Resume growth for 1000 A°

(18) Flash sample at 900° C for 300 sec.

(19) Ensure clean surface as in (2).

The sample was then unloaded and etched using retangular aluminum area 1 x 10^{-3} in spots evaporated thereon as masks. No attempt was made to passivate the surface which produced a effect. As a result, there was a large shunt resistance across the junction (about 800 Ω). This softened the breakdown a bit. At 5 V, the leakage was 20 MA/cm ^{2} while at 25 V, it was 1 or A/cm^2. Breakdown seemed to set in here. Thus, except for the parallel resistance, the diode seemed to work as designed. The CV profile is shown in figure 5.12and the doping profile obtained, thus is also shown. The slight bump in the actual profile may be due to an inadvertant temperature fluctuation.

A DLTS run was done on this sample. It showed two t_2 lap levels (majority). These have not been identified as yet but have concentration of the order of $\sim 10^{14}/cm^3$. A detailed systematic study of the deep traps and the influence of growth conditions would be interesting but is beyond the scope of this work.

5.12.2 Junctions Grown Directly on Substrates:

Several junctions have been grown using the substrate as one side. One example is the profile shown in figure 5.7. The sample was

processed into mesa diodes as described earlier. Once again, no steps were taken to passivate the surface. A breakdown voltage of excess of 80 volts was demonstrated. This has been done quite routinely, and is interesting because the maximum field occurs at the interface between the substrate and film which would be expected to be of inferior electrical quality. Apparently, this is not the case. The experimentally observed breakdown voltages are compatable to that theoretically predicted for these doping levels. Further, the film does not breakdown prematurely for an entire range of doping levels.

Under illumination from the sides of the mesa along with a small microscope lamp i.e. defocussed a light current of about 1 A/cm^2 was produced with fill factors in excess of 50%. This indicates that the minority curves lifetime is quite good. A very rough estimate of this lifetime shows that it is less than microseconds.

5.13 Hall Mobility:

We have measured the room temperature mobility of a thin ($\sim 2\mu$) uniformly doped layer doped at about $1 \times 10^{16}/cm^3$ isolated from the junction by a p-n junction. The magnetic field strength was between 2 and 4 K gauss. The mobility (hole) measured using the Van der Pau technique was in the vicinity of 400 cm^2/v sec. This is about 60-80% of bulk silicon mobilities at this doping level. This is quite impressive considering that the surface and interface have a dominant scattering effect.

5.14 Growth of a TUNNETT Profile:

One of the applications of very high control of doping is in the area of microwave devices. We consider here a TUNNETT which a highly doped p - n junction that breaks down by a tunnelling mechanism.

(This is therefore a low voltage soft breakdown with a negative temperature coefficient). The junction is followed by a low doped segment called the drift region. Consider the profile described in figure 5.13. Holes get injected via tunnelling and drift through the lowly doped region. This causes an induced current in the external circuit. If an rf voltage is applied in phase opposition to this induced current, microwave power may be generated. A detailed analysis of this device is a complicated venture and will not be attempted here. However, certain pertinent points may be mentioned.

(a) The injection mechanism is tunnelling. Thus the highly doped layer must be made very small and the regions around the junction need to be highly doped. This is so that the field has a sufficiently high gradient to favor tunnelling. The distance of this region has been calculated to be less than 500 Å for GaAs, and less than 200 Å for silicon (owing to the indirect mechanism). The doping levels are typically in the 10^{19} range.

(b) The drift region must be sufficiently lowly doped so that the field is high enough to enable carriers to move at saturated drift velocities, but not high enough to initiate avalanche generation. The latter is a source of noise and detracts from a TUNNETT'S low noise performance (inherent in the tunnelling mechanism). The drift region contributes a phase difference of $\frac{3\pi}{2}$ radians. Thus for a 440 Ghz device in silicon the drift distance must be about 1700 Å , at a level of $10^{16}/cm^3$.

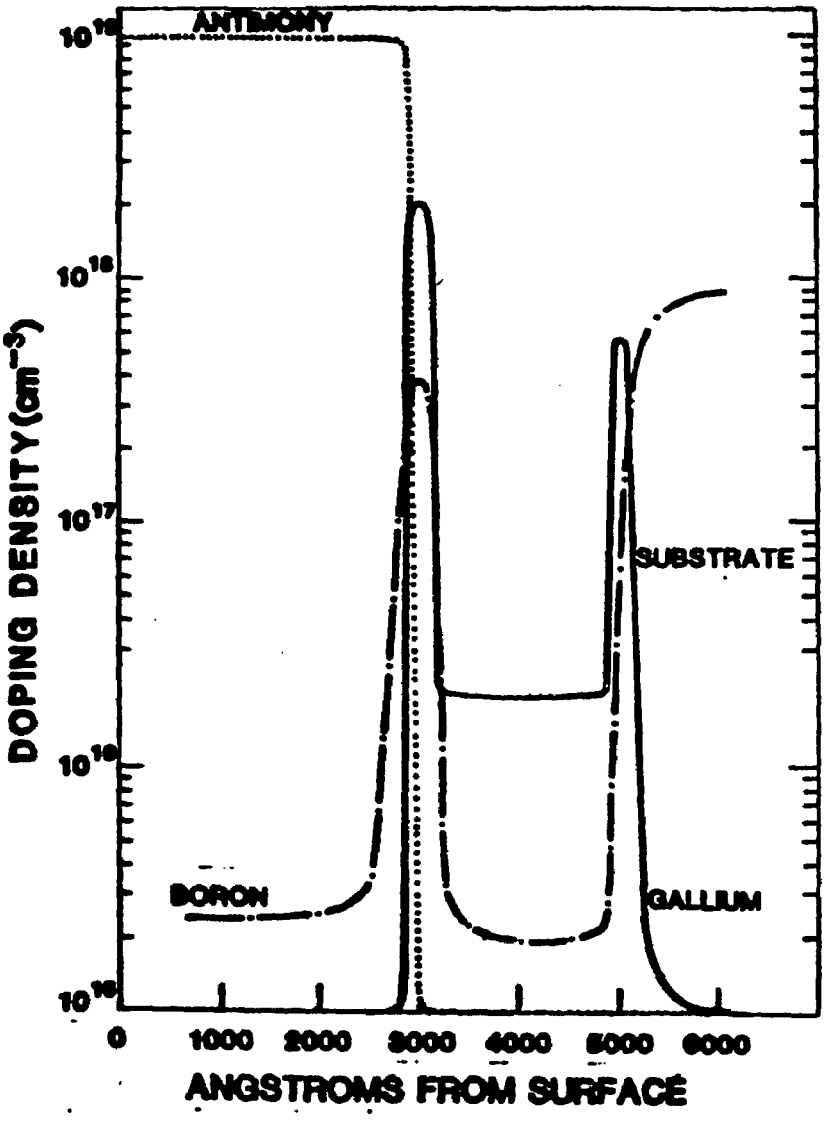

Figure 5.13 Profile for a "TUNNETT"

We can thus see that the depth and doping requirements are very stringent. TUNNETTS are probably the only solid state oscillator candidates at very high frequencies ($\sim 10^{12}$ Hz). At these freqencies dimensions become more critical and all conventional techniques of semiconductor processing fail. This doping profile may be obtained by MBE. We have done so and plotted the doping profile based on SIMS data. The junction had a soft breakdown in the region of 0.5 V. The temperature coefficient was measured to be negative, indicating that tunnelling with the predominant mechanism. The SIMS plot shows the presence of Boron, a point that will be discussed later. The doping profile is probably the best approximation to date. The ultimate test is of course the rf performance of the diode. At these high frequencies, preparing the device and packaging it present unique problems. Primarily this involves getting chips that are less than 10 μ across and also less than 10 μ in thickness. These technologies are not easily accessible right now by us but are being developed. Hence rf testing of these devices is beyond the scope of this work. Nevertheless, low frequency scaling of these devices may be possible.

The object of the above exercise is to show that devices that demand such stringent doping profiles are possible using MBE.

5.15 Boron as a Contaminant in Gallium Doped Films:

We have used Pyrolytic Boron Nitride (PBN) crucibles to hold our dopant sources. Although one of the most non-reactive compounds. PBN does seem to be attacked by gallium at very high temperatures. This is evidenced by a substantial level of Boron in gallium doped films. From our SIMS results, the Boron level seems to be an order of magni-

tude or more, less than the gallium level. We suspect that the gallium displaces the boron as follows

$$Ga + BN \rightleftarrows GaN + B$$

The boron could dissolve in the molten gallium.

Commercial gallium contains a fair amount of oxygen dissolved, due to the fact that oxygen is bubbled through it to remove aluminum traces.[87] Dissolved boron can react with the gallium oxide to form B_2O_3 which is quite volatile. This probably forms the source of boron in the grown films. The problem may be rectified by adding aluminum to better cut the oxygen.

5.16 Highest Level of Doping Reached

We mentioned earlier that since MBE was a kinetics dominated process, there should be, in principle, no limit to maximum amount of doping possible. Our results bear this out only partially. We do find that increasing the flux does increase the doping level. These levels may already be very close to or even in excess of the solid solubility limits for Ga and Sb in silicon. We have been able to obtain gallium levels of about $2 \times 10^{18}/cm^3$ at temperatures as low as 550°C which, based on recent data[105], may be above solid solubility limits. We have also been able to obtain Sb levels in excess of $10^{19}/cm^3$ at 625°C which again may be above solid solubility limits.

It is quite likely that these concentrations may be pushed up further at higher fluxes. We need also to caution here that solid solubility data is rather dubious at the low temperatures employed in Si MBE.

5.17 Conclusions:

This chapter has been concerned with the development of Si MBE as a tool for the growth of desired profiles hithertofore impossible. It represents a good deal of the results of this work. It presents a verification of the dopant incorporation kinetics model presented in chapter two and presents numbers that seem reasonable for the type of processes most favored to occur. We have carried things a step further and speculated on the microscopic details of incorporation. We concede that evidence for these conjectures are not indisputable, nevertheless, we need to point it out as a strong possibility.

CHAPTER 6

Future Directions in Si MBE

6.1 Introduction

This chapter is the concluding chapter of this dissertation. It summarizes the work done and lays emphasis on certain important points. In addition, it provides some clues for future and more widespread application of Si MBE using thermally generated dopant beams. Elaboration of the general formula to obtain any doping profile using the case of a cosine profile will be done. In addition, other techniques of dopant incorporation, such as ion beams and laser induced incorporation, will be pointed out.

6.2 Present Status of Si MBE

The simultaneous incorporation of dopant to any predetermined degree should make Si MBE an extremely versatile tool for novel device structures. There are several reasons for the present limited use of Si MBE. One is that it has to compete with established conventional techniques which are widely used in industry. Not withstanding its greater versatility, it cannot compete as far as economy and throughput are concerned. Secondly, there has been very little work done in this area and there needs to be a bigger thrust to make unconventional devices using this technique.

This particular thesis makes some contribution in that it provides a format by which systematic study of dopant incorporation may be made. As a result of this, one can establish a set of processing parameters that exploit the capabilities of the process to the maximum. These are points of a practical nature.

On a more philosophical plane, there has been some scientific value in that this study has provided experimental values of desorption and incorporation coefficients, especially the activation energies for these processes. We point out that the possibility of Ga island formation has regrettably not been established beyond doubt. However, some interesting possibilities emerge if one assumes that island formation is taking place. It is hoped that with more elaborate tools, this issue will be resolved.

6.3 Possible Application of Si MBE

Several applications of the MBE technique as developed are apparent. We list some of these here. The point to note is that we need no longer tailor doping profiles and device performance to fit the Gaussian or error function complement profiles that result from ion implantation and diffusion techniques. Instead, we need now to design the profiles for optimum device performance. Moreover we now have the capability of making any number of transitions from one type to another and from one level to another, in any sequence. Some possibilities are:

(a) Sophisticated microwave structures of the Read design.[107] These include TUNNETTS,[106] MITTATS, IMPATTS, and their double drift versions.

(b) n i p i type structures.[108] These superlattices can produce two-dimensional containment of free carriers leading to several interesting properties and applications.

(c) All conventional devices such as BJTs and JFETs may be grown with more optimal profiles. The elimination of repeated diffusions of opposite types implies less compensation, better crystal quality,

and consequently improved performance.

(d) Varactor diodes with tailor-made V-f characteristics for different applications.

(e) Buried channel structures with sharp wells as in charge coupled devices.

In addition, there are several miscellaneous applications such as the final shallow n diffusion in the standard N-MOS process where MBE may replace it, ensuring a high surface concentration and a rapid enough transition to a low level.

In fact, there probably is not an area where MBE cannot contribute to improved device performance in silicon devices.

Moreover, MBE remains the only hope for synthesis of new devices and investigation of effects that occur in very thin structures.

6.4 Obtaining the Cosine Profile

We shall now investigate in more detail the implacations of equation 2-26

$$F_D(x/\nu) = \frac{F_{Si}}{K_i N_o \tau}\left\{N_{DB}(x) + v\tau + \frac{dN_{DB}(x)}{dt}\right\} \qquad (6.1)$$

Consider the profile

$$N_{DB}(x) = N_{DBO} + N_{DB1} \cos \beta x \qquad (6.2)$$

Putting this in eqn 6.1 we get

$$F_D(x/\nu) = \frac{F_{Si}}{K_i N_o \tau}\left\{N_{DBO} + N_{DB1} \cos \beta x - v\tau\beta\, N_{DB1} \sin \beta x\right\} \qquad (6.3)$$

We need now to make some transformations. Eqn 6.3 as it stands is written in virtual time $t' = \frac{x}{v}$. Note that v and F_{Si} are related, and are not independent of each other. Let us assume for the time being that v is constant, then

$$F_D(t') = \left\{ \frac{F_{Si}}{K_I N_o T} \quad N_{DBO} + N_{DB1} \cos(\beta v t') - N_{DB1}.\, vt\beta \sin(\beta v t') \right\} \qquad (6.4)$$

Thus

$$F_D(t') = \frac{F_{Si} N_{DBO}}{K_I N_o T} + \frac{I_{Si} N_{DB1}}{K_I N_o T} \left(\cos(\beta v t') - \beta v t \sin(\beta v t') \right) \qquad (6.5)$$

In the above expressional $2\pi\beta^{-1}$ is the period of the doping profile. Further writing

$\Gamma = 2\pi\ \beta^{-1}$ and $\lambda = \nu T$ we get and $N_{DB1} = \gamma N_{DBO}$.

$$F_S(t') = \frac{F_{Si}\ N_{DBO}}{U_1\ No\tau}\left\{1 + \gamma\left\{\cos\ \beta\omega t' - \frac{2n\lambda}{\Gamma}\sin\ \beta\omega t'\right\}\right\} \qquad 6.6$$

The quantity $\frac{\lambda}{\Gamma}$ is the ratio of the characteristic distance to the period of the doping variation. In the case where the right side of eqn 6.6 is positive, (i.e. $\frac{\lambda}{\Gamma}$ is small) interpretation of the flux program is easy. Certain interesting things occur when $\frac{\lambda}{\Gamma}$ is large and γ is also large. This condition is best studied with $N_{DBO} \to 0$ and $\gamma = 0$ such that N_{DB1} is finite then

$$F_D(t') = \frac{F_{Si}\ N_{DB1}}{K_I\ NoT}\left\{\cos\ \beta\omega t' - \frac{2\pi\lambda}{\Gamma}\ \sin\ \beta\omega t'\right\} \qquad 6.7$$

It is possible that for $\frac{\lambda}{\Gamma} > \frac{1}{2\pi}$

$F_D(t')$ becomes negative!

This interesting situation is interpreted as there being a net desorbing flux. In other words, we may achieve this situation by programming the substrate temperature assuming a constant incident flux. such that the net flux is given by eqn 6.7. Needless to say, expansion of the time scale may be had by decreasing v the velocity of growth.

It is clear therefore that temperature fluctuations of the order of several degrees in a few seconds will permit growth of profiles with periods up to tens of angstroms. The important thing to note is that

in the case of small resistively, heated substrates with low thermal inertia as we have used this is quite easily possible.

6.5. Suggestions for Future Work

As mentioned earlier, there has been relatively speaking a rather small effort in Si MBE. Several aspects need more investigation. These include the study similar to this one on other dopants such as Aluminum, Antimony. Work needs to be done also in the area of captive sources for n type dopants. These are compound sources , (such as Ga Sb for Sb). The group V element that is preferentially released at more easily controllable temperatures is also easier to incorporate as the vapor is predominantly the dimer in this case. More work also needs to be done in correlating film quality with different growth programs especially the effect of flash-off and build-up methods.

From another aspect, silicon MBE systems should be developed to accept more varied types of wafers such as the popular circular ones, as well as larger wafers. This would involve surmounting the substrate temperature control and film uniformity problems.Greater throughout is also another objective.

Work needs to be done in silicon growth on heterogeneous substrates such as sapphire, spinel,ferrites and other interesting materials such as semiconducting alloys so that electronic devices may be conveniently integrated with other transducers. This would lead to a new generation of integrated system technology.

In a more radical investigative vein, new techniques of doping such as ion beam doping which might provide for better magnitude and depth control as well as well as the possibility of spatial resolution

need to be tried out. Low temperature incorporation in near amorphous layers coupled with surface laser induced recrystallization may provide another means of dopant control.

APPENDIX 1

Solution of the incorporation kinetics for a second order system.

In this case we assume $p = 2$ then

$$\frac{dN_{DS}}{dt} = F_D - K_D N_{DS}^2 - K_I N_{DS} \qquad \text{A1.1}$$

In steady state

$$N_{DS} = \frac{\frac{K_I}{K_D} \pm \sqrt{\left(\frac{K_I}{K_D}\right)^2 + 4\frac{F_D}{K_D}}}{2} \qquad \text{A1.2}$$

Since $N_{DS} > 0$ we neglect the negative sign to get

$$N_{DS} = \tfrac{1}{2}\left\{\frac{K_I}{K_D} + \sqrt{\left(\frac{K_I}{K_D}\right)^2 + 4\frac{F_D}{K_D}}\right\} \qquad \text{A1.3}$$

If $\frac{K_I}{K_D} \ll \frac{F_D}{K_D}$ we get

$$N_{DS} \simeq \sqrt{\frac{F_D}{K_D}} \qquad \text{A1.4}$$

This gives the bulk doping

$$N_{DB} \approx \frac{K_I}{\sqrt{K_D}} \cdot \frac{\sqrt{F_D}}{F_{si}} \cdot N_o \qquad \text{A1.5}$$

and the sticking coefficient

$$s \approx \frac{K_I}{\sqrt{K_D}} \cdot \frac{1}{\sqrt{F_D}} \qquad \text{A1.6}$$

Thus the sticking coefficient is flux dependent at all times.

To obtain an idea of what the delay time will be consider the case when the flux is suddenly shut off after steady state doping is reached.

Let the doping level correspond to a surface concentration N_{DSo} then

$$N_{DS}(t) = \frac{N_{DSo}}{1 - K_D N_{DSo} t} \qquad \text{A1.7}$$

The drop off is linear with time. This implies that characteristic time is surface concentration dependent i.e.,

$$\tau = \frac{1}{K_D N_{DSo}} \qquad \text{A1.8}$$

and

$$\frac{N_{DS}(t)}{N_{DSo}} = \frac{1}{1 - t/\tau} \qquad \text{A1.9}$$

Thus

$$N_{DB}(t) = \frac{K_I N_{DSo}}{1 - t/\tau} \qquad \text{A1.10}$$

or

$$N_{DB}(x) = \frac{K_I N_{DSo}}{1 - x/v\tau} \qquad \text{A1.11}$$

The rise time is more complex and depends on the flux.

It must be noted here that for a 4th order desorption system, things are far more complex and can not be handled analytically. In that case numerical solution of the differential equations involved is recommended.

APPENDIX 2.

The following is the flow chart used to calculate the Fermi level at the surface and the conductivity of the film when we have a step profile as shown in fig. 3.10. Surface state density is $N_{SS}/eVcm^2$.

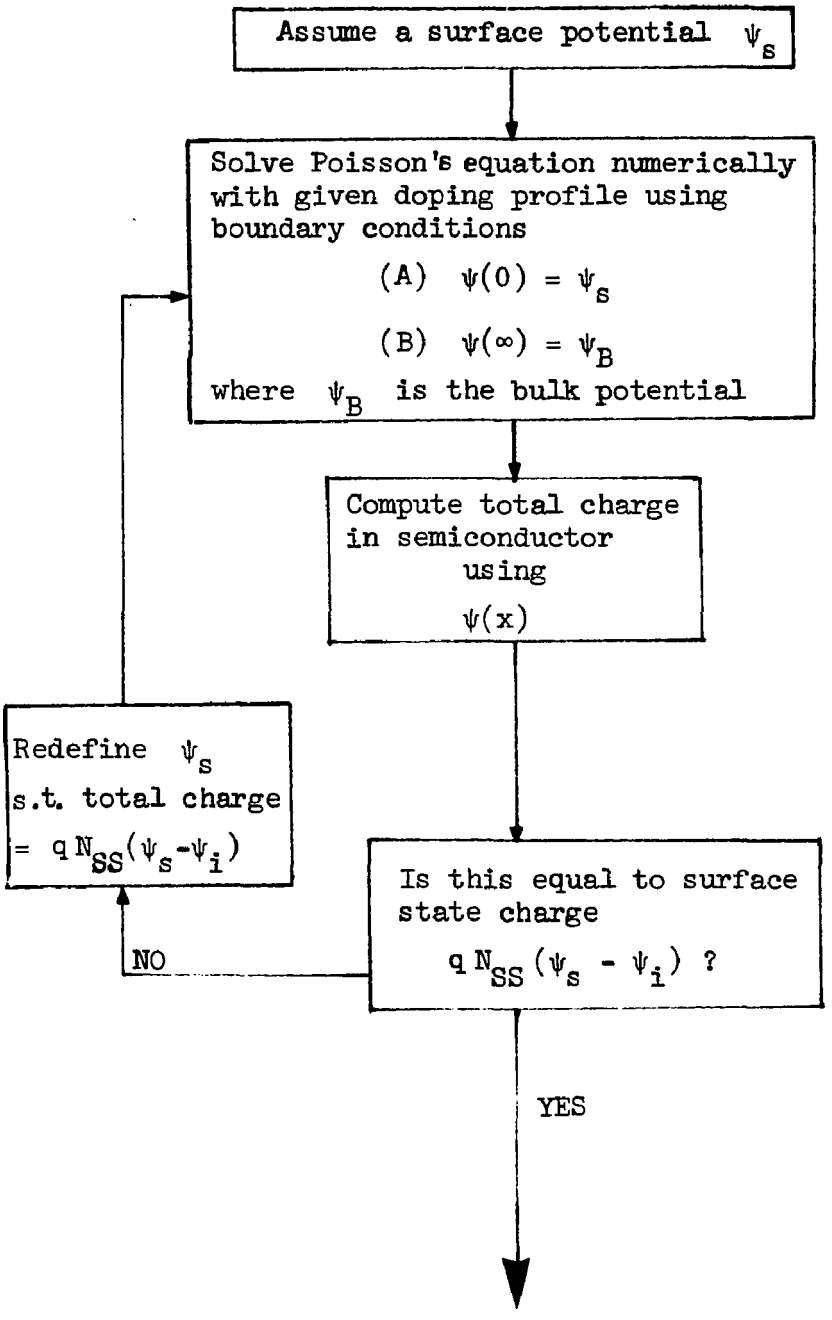

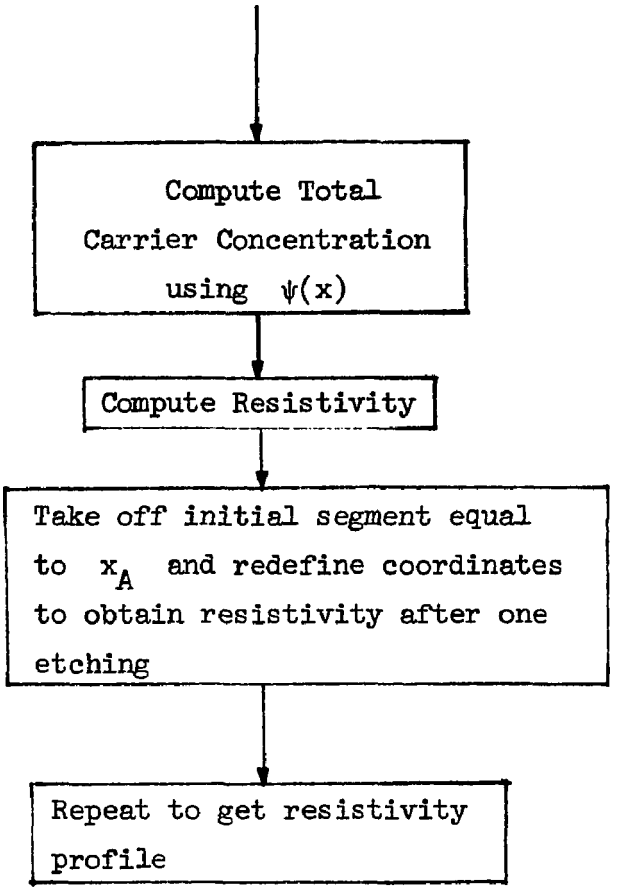

The Fortran listing of the program follows.

```
// QUICKRUN
$IGECFGAS,MATFIV
*JOB
      DIMENSION V(1001),AN(10001),P(1001),PI(1001),CAR(1001),CHG(1001)
CCC   V HOLDS  POTENTIAL MATRIXCCC
CCC   P HOLDS HOLE CARRIER MATRIXCCC
CCC   AN HOLDS DOPINGCCC
      JIJ=1
CCC   FIX SURFACE POTENTIALCCC
      VS = 0.5
CCC   FIX DOPINGCCC
      AN1=1.0E16
      AN2=AN1
      SSN=1.0E12
      I1=500
16    AN2=2.0E18
      SIG=0.0
      ASIG=0.0
      CALL DOPE(AN,AN1,AN2,I1)
CCC   FIX BULK POTENTIALCCC
      CN = 2.8E19
      VN = 1.04E19
      VF = 0.026*ALOG(VN/AN(1000))
      DATA NWIDE,TOL,W,H,EPS/1000,0.001,1.5,1.00E-7,1.01E-12/
      NWP1=NWIDE+1
      V(1)=VS
      V(NWP1)=VF
      DO 1 I=2,NWIDE
      AI=I
      V(I)=V(1)-(V(1)-VF)*I/1000+0.15*SIN(AI)
1     CONTINUE
      V(600)=VF/2
      V(700)=VF/2
      V(800)=VF /2
      V(900)=VF/2
CCC   SOLVE POISSONS EQUATIONCCC
15      CALL POIS (V,VS,VF,AN,CHGMAX,KNT,CN,VN,I1)
      WRITE (6,20) CHGMAX,KNT
20    FORMAT (1H ,10X,'CHGMAX= ',E11.4// 10X,'KNT= ',I6)
CCC   COMPUTE HOLE CONCENTRATIONCCC
25      DO 30 I=1,1000
      P(I) = VN*EXP(-V(I)/0.026)
      PN(I)=CN*EXP((V(I)-1.1)/0.026)
      CHG(I)=P(I)-PN(I)-AN(I)
30    CONTINUE
CCC   COMPUTE TOTAL CARRIERSCCC
      IJ=I1+500
      DO 40 I=1,IJ
      SIG = SIG + P(I) +PN(I)
      SIG=SIG*1.0E-7
      ASIG=ASIG+P(I)-PN(I)-AN(I)
      ASIG=ASIG*1.0E-7
40    CONTINUE
      WRITE (6,35)
35    FORMAT(1H1,5X,'DOPING',10X,'POTENTIAL',10X,'HOLE CONC',
     110X,'ELECTRON CONC.',10X,'NET CHARGE')
      WRITE(6,36)(AN(I),V(I),P(I),PN(I),CHG(I),I=1,1000,25)
36    FORMAT(1H ,5X,E13.6,3X,E13.6,6X,E13.6,4X,E13.6,2X,E13.6)
      WRITE (6,37)SIG ,ASIG
37    FORMAT(1H  //15X,'THE TOTAL NUMBER OF FREE CARRIERS IS ',E13.6,
     1//15X,'THE NET CHARGE IS ',E13.6)
      VSN=0.55+ASIG/SSN
      IF (ABS(VSN-VS).LT.0.001) GO TO 39
      VS=VSN
```

```
      GO TO 16
39    STOP
      STOP
      END
CCCCCCCCCCCCCCCCCCCCCCCCCCCCCCCCCCCCCCCCCCCCCCCCCCCCCCCCCCCCCCCCCCCCCCCCCCC
CCCCCCCCCCCCCCCCCCCCCCCCCCCCCCCCCCCCCCCCCCCCCCCCCCCCCCCCCCCCCCCCCCCCCCCCCCC
CCCCCCCCCCCCCCCCCCCCCCCCCCCCCCCCCCCCCCCCCCCCCCCCCCCCCCCCCCCCCCCCCCCCCCCCCCC
      SUBROUTINE POIS (V,VS,VF,AN,CHGMAX,KNT,CN,VN,I1)
      DIMENSION V(1001),AN(1001)
      DATA NWIDE,TOL,W,H,EPS/1000,0.001,1.5,1.00E-7, .01E-12/
      NWIDE=I1+500
      NWP1 = NWIDE + 1
      V(1) = VS
      V(NWP1) = VF
      DO 10 KNT = 1,50
      CHGMAX = 0.0
         DO 9 I = 2,NWIDE
      RESID=V(I+1)+V(I-1)-2.0*V(I)
      PAP=VN*(EXP(-V(I)*38.4))-CN*EXP((V(I)-1.1)*38.4)
      PAP=PAP-AN(I)
      RESID=RESID+1.584E-07*F**2*PAP
      RESID=RESID*W/2.0
         IF(CHGMAX.LT.ABS(RESID)) CHGMAX = ABS(RESID)
         V(I) = V(I) + RESID
9        CONTINUE
      IF (CHGMAX.LT.TOL) GO TO 20
10    CONTINUE
      RETURN
20    CONTINUE
      RETURN
      END
       SUBROUTINE DOPE(AN,AN1,AN2,I1)
      DIMENSION AN(1000)
      DO 10 I=1,I1
      AN(I)=AN1
10    CONTINUE
      J=I1+1
      DO 20 I=J  ,1000
      AN(I)=AN2
20    CONTINUE
      RETURN
      END
CCCCCCCCCCCCCCCCCCCCCCCCCCCCCCCCCCCCCCCCCCCCCCCCCCCCCCCCCCCCCCCCCCCCCCCCCCC
*RUN
//
```

REFERENCES

1. Cho, A. Y., Jour. Vac. Sci. Tech., 16, 275 (1975)
2. Unvala, B. A., Nature, 194, 966 (1962)
3. Hale, A. P., Vac., 13, 93 (1963)
4. Booker, G. R. and Unvala, B. A., Phil Mag., 8, 1997 (1963)
5. Unvala, B. A. and Booker, G. R., Phil. Mag., 9, 591 (1964)
6. Jona, F., IBM Jour. Res. Dev., 9, 375 (1965)
7. Booker, G. R. and Unvala, B. A., Phil. Mag., 11, 11 (1965)
8. Jona, F. Appl. Phy. Lett., 9, 235 (1966)
9. Joyce, B. A. and Bradely, R. R., Phil. Mag., 14, 289 (1966)
10. Booker, G. R. and Joyce, B. A. , Phil. Mag., 14, 301 (1966)
11. Booker, G. R., Jour. Appld. Phys., 37, 441 (1966)
12. Thomas, D. J. D., Phys. Stat. Solidi, 13, 359 (1966)
13. Thomas, R. N. and Francombe, M. H., Appld. Phys. Lett., 11, 108 (1967)
14. Thomas, R. N. and Francombe, M. H., Appld. Phys. Lett., 11, 139 (1967)
15. Watts, B. E., Bradely, R. R., Joyce, B. A. and Booker, G. R., Phil. Mag., 17, 1163 (1968)
16. Thomas, R. N. and Francombe, M. H., Appld. Phys. Lett., 13, 270 (1968)
17. Joyce, B. A., Neave, J. H. and Watts, B. E., Surf. Sci., 15, 1 (1969)
18. Cullis, A. G. and Booker, G. R., Jour. Crust. Growth, 9, 132 (1971)

19. Thomas, R. N. and Francombe, M. H., Surf. Sci., 25, 357 (1971)

20. Widmer, H., Appld. Phys. Lett., 5, 108 (1964)

21. Quesser, H. J. Finch, R. H. and Washburn, J., Jour. Appld. Phys., 33, 1536 (1962)

22. Finch, R. H., Quesser, H. J., Thomas, G. and Washburn, J., Jour. Appld. Phys., 34, 406 (1963)

23. Bean, J. C., in "Impurity Doping in Silicon", ed. Wang, F.F.Y., to be published by N. Holland (1981)

24. Ota, Y., Buchanan, W. L. and Peterson, O. G., IEDM Tech. Dig., 375 (1977)

25. Katayama, Y., Shiraki, Y., Kobayashi, K.L.I., Komatsubura, K. F. and Hashimoto, N., Appld. Phys. Lett., 34, 740 (1979)

26. Becker, G. E. and Bean, J. C., Jour. Appld. Phys., 48, 3395 (1977)

27. Bean, J. C., Appld. Phys. Lett., 33, 654 (1978)

28. Burton, W. K., Cabrera, N., and Frank, F. C., Phil. Trnas. Roy. Soc., 243A, 299 (1950)

29. Abbink, H. C., Broudy, R. M. and McCarthy, G. P., Jour. Appld. Phys., 39, 4673 (1968)

30 Chernov, A. A., Jour. Cryst. Growth, 42, 55 (1977)

31. Wood, C. E. C. and Joyce, B. A., Jour. Appld. Phys. 49, (1978)

32. Nguyen, T. T. A., Surf. Sci., 43, 562 (1974)

33. Frenkel, J.,Z. Phys., 26, 117 (1924)

34. Alexandre, F., Raisin, C., Abdalla, M. I., Brenae, A. and Masson, J. M., Jour. Appld. Phys., 51, 4296 (1980)

35. Chatterjee, D., "Theory of Auger Transitions", pub. by Academic

Press (1976)

36. Semiconductor International, November 1980, Pub. by Milton Kiver Publications.

37. Wright, S. and Kroemer, H.,Appld. Phys. Lett. 36, 210 (1980)

38, Ueda, R., private communication.

39. Honig, R. E. and Kramer, D. A., RCA Rev., 30, 285 (1969)

40. McHugh, J. A., in "Methods of Surface Analysis", ed. Czanderna, A. W., 273, Pub. by Elsevier (1979)

41. C. A. Evans and associates.

42. Werner, H. W., Surf. Sci., 47, 301 (1975)

43. Smith, D. P., Surf. Sci., 25, 171 (1971)

44. Phillips, B. F., Jour. Vac. Sci. Tech.,

45. Miller, G. L., IEEE Trans., ED-22, 265 (1975)

46. Wiley, J. D. and Miller, G. L., IEEE Trans., ED-22, 265 (1975)

47. Kennedy, D. P., Murley, P. C., and Kleinfelder, W., IBM Jour. Res. Dev., 12, 399 (1968)

48. Johnson, W. C. and Panousis, P. T., IEEE Trnas., ED-18, 965 (1971)

49. Wilson, C. L., IEEE Trnas., ED-27, 2262 (1980)

50. Metzger, R. A., M.S. Thesis, Univ. of Calif., Los Angeles, (1980)

51. Sze, S. M., "Physics of Semiconductor Devices", 430, Adison Wesley (1969)

52. Lang, D. V., Jour. Appld. Phys., 45, 3023 (1974)

53. Lang, D. V., Jour. Appld. Phys., 45, 3014 (1974)

54. Van der Pau, L. J., Philips Tech. Jour., 20, 220 (196)

55. Saito, Y., Kawazu, A. and Tominaga, G., Surf. Sci., 103, 563(1981)

56. Kawazu, A., Otsuki, T. and Tominaga, G., Jpn. Jour. Appld. Phys., 20, 553 (1981)

57. Kawazu, A., Saito, Y., Oqiwara, N., Otsuki, T. and Tominaga, G., Sur. Sci., 86, 108 (1979)

58. Oyama, T., Ohi, S., Kawazu, A. and Tominaga, G., to be published in Surf. Sci. (1981)

59. Levine, J. D. and Gyftpolous, G. P., Surf. Sci., 1, 171 (1964)

60. Ponec, V., Knor, Z., and Cerny, S., in "Adsorption on Solids", 200, pub. CRC Press (1974)

61. Gyftpolous, E. P. and Levine, J. D., Jour. Appld. Phys., 33, 67 (1972)

62. Redhead, P. A., Vac., 12, 203 (1962)

63. Nguyen, T. T. A., Chakraverty, B. K. and Cinti, R., Surf. Sci., 43, 577 (1974)

64. Arthur, J. R., Jour. Appld. Phys., 39, 4032 (1968)

65. Nguyen, T. T. A., Surf. Sci., 43, 562 (1974)

66. Florio, J. V. and Robinson, W. D., Surf. Sci., 18, 399 (1969)

67. Davis, L. E., Levenson, L. L., Miller, J. J., Jour. Cryst. growth, 17, 354 (1972)

68. Sewell, P. B. and Cohen, M., Appld. Phys. Lett., 11, 298 (1967)

69. Palmberg, D. W. and Rhodin, T. N., Jour. Appld. Phys., 39 2425 (1968)

70. Vaidya, S. and Murarka, S. P., Appld. Phys. Lett., 37, 51 (1980)

71. Bean, J. C., Appld. Phys. Lett., 36, 741 (1980)

72. Knuth, E. L., Jour. Chem. Phys., 69, 5073 (1978)

73. Jona, F., Proc. 13th Sagamore Army Materials Conf., 399, pub.

Syracuse Univ. Press (1966)

74. Pendry, J. B., "Low Energy Electron Diffraction", pub. Academic Press (1974)

75. Bauer, E., Tech. of Materials Research, 2, 501, ed. R. Bunshah (1969)

76. Allen, F. G., Jour. Appld. Phys., 30, 1563 (1959)

77. Based on a design by Bell Telephone Laboratories, Murray Hill, New Jersey, U.S.A.

78. Shokley, W., Bell Syst. Tech. Jour., , 101 (1949)

79. Geus, J. W., Nederlands Tidschrift Voor Vacuum Techniek, 10, 59 (1972)

80. Konig, U., Kasper, E. and Herzog, H. J., Jour. Cryst. Growth, 52, 151 (1981)

81. Ploog, K. and Fischer, A., Jour. Vac. Sci. Tech., 15, 255 (1978)

82. Wood, C.E.C., Jour. Appld. Phys., 51, (1980)

83. Wright, S. private communication.

84. Wood, C.E.C., Desimone, D., Judapravira, S., Jour. Appld. Phys., 51, 2074 (1980)

85. Lelay, G., Manneville, M. and Kern, R., Surf. Sci., 65, 261 (1977)

86. Lelay, G., Manneville, M. and Kern, R., Surf. Sci., 72, 405 (1978)

87. Udall, J., Private communication.

88. Kilgore, B. F. and Roberts, R. W., Rev. Sci. Instr., 34, 11 (1963)

89. Sakamoto, T., Takahashi, T., Suzuki, E., Shoji, A., Kawanami, H.,

Komiya, Y. and Tauri, Y., Surf. Sci., 86, 102 (1979)

90. Yamada, I., Saris, F. W., Takagi, T., Matsubara, K., Takaoka, M. and Ishiyama, S., Jpn. Jour. Appld. Phys. 19, L181 (1981)

91. Bennet, R. J. and Parrish, C., Solid State Elect., 16, 497 (1973)

92. Tabe, M., Arai, K. and Nakamura, H., Jpn. Jour. Appld. Phys., 20, 703 (1981)

93. Bennet, R. J. and Parrish, C., Solid State Elec., 18, 833 (1975)

94. Kuznetsov, V. P., Tolomasov, V. A. and Tumanova, A. N. Sov. Phys. Crystallogr., 24, 588 (1979)

95. Kuznetsov, V. P., Rubtsova, R. A., Sergievskya, and Postinikov, V. V., Sov. Phys. Crystallogr., 16, 356 (1971)

96. Tolomosov, V. A., Abrosmova, L. N. and Gorshenin, G. N., Sov. Phys. Crystallogr., 15, 1076 (1971)

97. Goodwin, C. A. and Ota, Y. IEEE Trans., Ed-26, 1796 (1979)

98. Sugiara, H. and Yamaguchi, M., Jpn. Jour. Appld. Phys., 19, 583 (1980)

99. Itoh, T., Nakamura, T. and Muromachi, M. and Sugiyama, T., Jpn. Jour. Appl. Phys., 16, 553 (1977)

100. Konig, U., Kibbel, H. and Kasper, E., Jour. Vac. Sci. Tech., 16, 985 (1979)

101. Katayama, Y., Shiraki, Y., Kobayashi, K. L. I., Komatsubura, N. and Hashimoto, N., Appld. Phys. Lett. 34, 740 (1979)

102. Goodwin, C. A. and Ota, Y., IEEE Trans., ED-26, 1796 (1979)

103. Gadzuk, J. W., Surf. Sci., 5, 159 (1967)

104. Valdes, L. B., Proc. I.R.E., 42, 420 (1954)

105. Haridoss, S., Beniere, F., Gauneau, M. and Rupert, A., Jour. Appld. Phys. 51, 5833 (1981)

106. Elta, M. E. and Haddad, G. I., IEEE Trans. MTT-27, 442 (1979)

107. Read, W. T., Bell Syst. Tech. Jour., 47, 369 (1964)

108. Dohler, G. H., Jour. Vac. Sci. Tech., 16, 851 (1979)